2014

Synthesis of Fluorescent Molecules and their Applications as Viscosity Sensors, Metal Ion Indicators, and Near-Infrared Probes

Mengyuan Wang
University of Central Florida

SYNTHESIS OF FLUORESCENT MOLECULES AND THEIR APPLICATIONS AS VISCOSITY SENSORS, METAL ION INDICATORS, AND NEAR-INFRARED PROBES

by

MENGYUAN WANG
B.S. Nanjing University of Technology, 2010

A dissertation submitted in partial fulfillment of the requirements
for the degree of Doctor of Philosophy
in the Department of Chemistry
in the College of Sciences
at the University of Central Florida
Orlando, Florida

Fall Term
2014

Major Professor: Kevin D. Belfield

ABSTRACT

The primary focus of this dissertation is the development of novel fluorescent near-infrared molecules for various applications. In Chapter 1, a compound **dU-BZ** synthesized via Sonogashira coupling reaction methodology is described. A deoxyuridine building block was introduced to enhance hydrophilic properties and reduce toxicity, while an alkynylated benzothiazolium dye was incorporated for near-IR emission and reduce photodamage and phototoxicity that is characteristic of common fluorphores that are excited by UV or visible light. A 30-fold enhancement of fluorescence intensity of **dU-BZ** was achieved in a viscous environment. Values of fluorescence quantum yields in 99% glycerol/1% methanol (v/v) of varying temperature from 293 K to 343 K, together with fluorescence quantum yields, radiative and nonradiative rate constants and fluorescence lifetimes in glycerol/methanol solutions of varying viscosities from 4.8 to 950 cP were determined. It was found that both fluorescence quantum yields and fluorescence lifetimes increased with increasing viscosity, which is consistent with results predicted by theory. This suggests that the newly designed compound **dU-BZ** is capable of functioning as a probe of local microviscosity, and was later confirmed by *in vitro* bioimaging experiments.

In Chapter 2, a new BAPTA (O,O'-bis(2-aminophenyl)ethyleneglycol-N,N,N',N'-tetra acetic acid) and BODIPY (4,4-difluoro-4-bora-3a,4a-diaza-s-indacene)-based calcium indicator, **BAPBO-3**, is reported. A new synthetic route was employed to simplify both synthesis and purification, which tend to be low yielding and cumbersome for BAPTA derivatives. Upon excitation, a 1.5-fold increase in fluorescence intensity in buffer containing 39 μM Ca^{2+} and a 3-

fold increase in fluorescence intensity in buffer containing 1 M Ca^{2+} was observed; modest but promising fluorescence turn-on enhancements.

In Chapter 3, a newly-designed unsymmetrical squaraine dye, **SQ3**, was synthesized. A one-pot synthesis was employed resulting in a 10% yield, a result that is generally quite favorable for the creation of unsymmetrical squaraines Photophysical and photochemical characterization was conducted in various solvents, and a 678 nm absorption maximum and a 692 nm emission maximum were recorded in DMSO solution with a fluorescence quantum yield of 0.32. *In vitro* cell studies demonstrated that **SQ3** can be used as a near-IR probe for bioimaging.

To my parents and family

ACKNOWLEDGMENTS

As a member of Dr. Kevin D. Belfield's research group, valuable experience I have gained makes me always being grateful. In the past four years, insightful guidance, unconditional support, and endless encouragement from Dr. Belfield installed in me the qualities of being a scientist and a chemist. Dr. Belfield exceptional enthusiasm and positive attitude towards research were driving forces of my graduate career at University of Central Florida.

As an effort of team work, this dissertation would not reach any accomplishment without the members of Dr. Belfield's research group. I would like to thank my colleagues for their help and friendship. Specials thanks to Dr. Sheng Yao, Dr. Alma Morales, Dr. Andrew Frazer and Dr. Yuanwei Zhang, their expert advice on organic synthesis inspired me so much along the way. I would like to express my appreciation to Dr. Mykhailo Bondar and Mr. Adam Woodward for their patient guidance on photophysical characterizations. Many thanks also to Ms. Xiling Yue for her suggestions on cell-related work. Thank you to assistance on NMR analysis from Dr. David Richardson, and support from Dr. Maria Christina A. Dancel at the University of Florida with MS measurements.

At last, I would like to give my deepest gratitude to my parents for their love and confidence in me while pursuing my doctoral degree.

TABLE OF CONTENTS

LIST OF FIGURES

LIST OF TABLES

LIST OF SCHEMES

CHAPTER 1. A DEOXYURIDINE-BASED VISCOSITY SENSOR FOR *IN VITRO* APPLICATION

1.1 Introduction

Information such as physiological composition can be reflected by microenvironments in cellular compartments.[1] For example, an increase in mitochondrial membrane viscosity was discovered after exposure to β-amyloid, which is essentially involved in Alzheimer's disease.[2] Mechanical methods [3, 4] have been universally applied to measure the viscosity of bulk liquids. However, viscosity on the microscopic scale may differ largely. It is a significant challenge to use techniques to measure microviscosity on the order of micrometers so that intracellular viscosity can be probed.

One method to monitor viscosity changes at the single cell level is the use of fluorescence imaging with molecular rotors.[5, 6] Molecular rotors are fluorophores whose fluorescence intensity is affected by intramolecular rotation that can be greatly affected by the viscosity of its surrounding environment. This can be accomplished via an intramolecular charge transfer (ICT) mechanism by molecular twisting in the excited state. A local excited (LE) state and a twisted intramolecular charge transfer (TICT) state are involved,[7] and de-excitation to the ground state can occur from both states. With different conformations of the two excited states, the energy gap between the LE and TICT states leads to different intensities of radiative decay, and this energy gap is caused by nonradiative deactivation from LE state to a dark, non-emissive TICT

state. In viscous media, the rate constant of nonradiative relaxation is reduced, and the radiative decay of LE state occurs, resulting in higher fluorescence quantum yield and longer fluorescence lifetime.[8] A qualitative sketch of the energy levels of a TICT molecule is shown in Figure 1. Upon excitation of the planar configuration, the molecule elevates to the LE state, with the angle of intramolecular rotation close to zero (φ_0). From the LE state, the molecule can return to the ground state with rate constant k_f, or it undergoes intramolecular rotation to TICT state with a rate constant k_a and obtains a 90° intramolecular rotation angle φ_1. From the TICT state, the molecule can return to the ground state with a rate constant k_f' or it returns to the LE state with a rate constant k_d (k_d is usually very small). In the twisted conformation, the ground state energy level is higher and the molecule has a tendency to return to the planar ground state conformation. Even though the TICT state has a lower energy than the LE state, it is difficult for a molecule to return back to the LE state from the TICT state, since it has to overcome several small energy maxima.

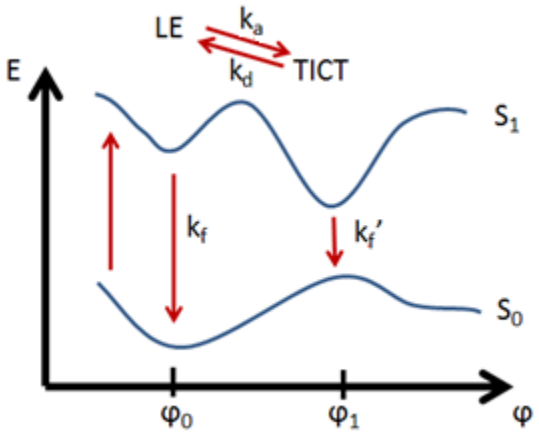

Figure 1. Ground state and excited state energies in the planar and twisted conformations of a TICT molecule.

A TICT rotor usually employs a donor group, an acceptor group, and a π-conjugation system between them for electron transfer. An alkylated nitrogen atom is universally applied as a donor group, and acceptor groups vary from nitriles and carboxylic esters to aromatic rings. Extension of π-conjugation system usually brings changes in the fluorescence spectrum. These changes are significant, especially in consideration of designing a probe with emission maxima at specific wavelengths. A representative TICT rotor DMABN (1,4-dimethylaminobenzonitrile) (Figure 2a) has been extensively studied[9, 10]. However, short excitation wavelengths (ca. 290 nm) and emission ranges (from 340 nm, LE state to 460 nm, TICT state) hinder further development of this compound for biological environments and other applications due to detrimental effects of UV irradiation. To solve the problem, julolidines (Figure 2b and 2c) have emerged. With extended conjugation system, 9-(dicyanovinyl)julolidine (DCVJ) and 9-(2-carboxy-2-cyanovinyl) julolidine (CCVJ) exhibits excitation of 470-480 nm and emission at > 500 nm [6]. In fact, both TICT and photoisomerisation causing a zwitterion intermediate[11, 12] have been proposed to explain the photophysical behavior upon viscosity change. In addition, extended conjugation is also reflected in stilbene motif based molecular rotors, e.g. *p*-DASPMI (trans-4-(4-dimethylaminostyryl)-1-methylpyridiniumiodide)[13] (Figure 2d). This type of molecular rotor has a larger number of bonds that allow twisting, so that more complex solvent interactions are involved.[14, 15]

Another important subclass of fluorescent probes is produced by replacing acceptor groups with benzothiazole derivatives, represented by thioflavin T (4-(3,6-dimethyl-1,3-benzothiazol-3-ium-2-yl)-N,N-dimethylaniline) (Figure 2e), which has been applied to visualize and quantify the presence of amyloid. [16, 17]. The photophysical chatacteristics of this probe has been attributed

to not only dimer, excimer[18], and micelle[19, 20] formation but also de-excitation due to intramolecular rotation. Although the nature of the dark state that causes the viscosity dependence is not as clear as for the case of DMABN, a remarkable fluorescence intensity increase and red shift has been observed for these dyes[6] (Figure 2b-2e), suggesting possible applications in various fields, such as in biological imaging. It has been experimentally confirmed that one can probe the viscosity in cellular membranes[21] and model phospholipid bilayers.[22, 23] These compounds can also function as markers for monitoring physiological changes in cells[24, 25].

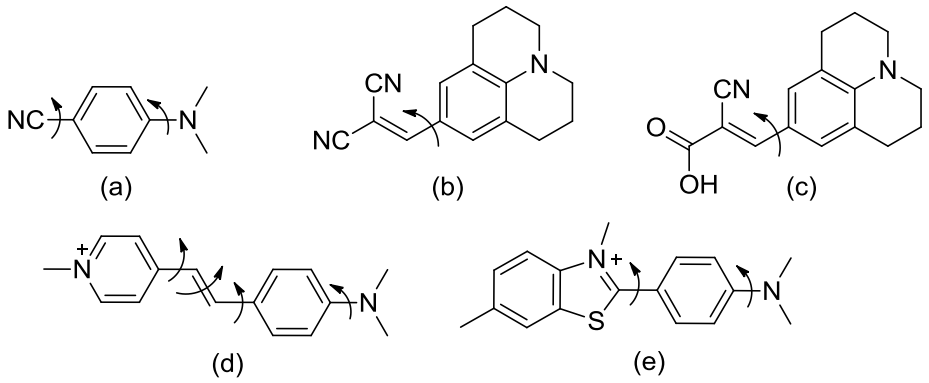

Figure 2. The structures of TICT molecular rotors: (a) 1,4-dimethylaminobenzonitrile (DMABN), (b) 9-(dicyanovinyl)julolidine (DCVJ), (c) 9-(2-carboxy-2-cyanovinyl)julolidine (CCVJ), (d) 4-(4-dimethylaminostyryl)-1-methylpyridiniumiodide (*p*-DASPMI), and (e) 4-(3,6-dimethyl-1,3-benzothiazol-3-ium-2-yl)-N,N-dimethylaniline (thioflavin T)

Molecular rotors have been proposed over decades for measurement of local viscosity by tracking the change of fluorescence quantum yield.[6, 26] A challenge in this approach is separating influences on fluorescence intensity caused by viscosity from other factors, such as

local concentration of fluorophores and specific solvent effects. A ratiometric approach was applied to address this problem.[5, 27-29] By conjugating the molecular rotor to a fluorescent label whose quantum yield is not affected by viscosity, the concentration can be determined in different viscous environments.[30, 31] An example of a ratiometric viscosity sensor was reported by Haidekker and Theodorakis based on a resonance energy transfer (RET) pair (Figure 3). With varied viscosity, the coumarin chromophore (shown in blue) functions as a viscosity independent indicator while the amino cinnamonitrile moiety (shown in red) serves as a viscosity sensitive rotor. However, a relatively low excitation wavelength (365 nm) restricted biological applications of this RET pair, since this wavelength is very close to the absorption range of biofluids (280 nm for Trp) and autofluorescence of the fluid. [27]

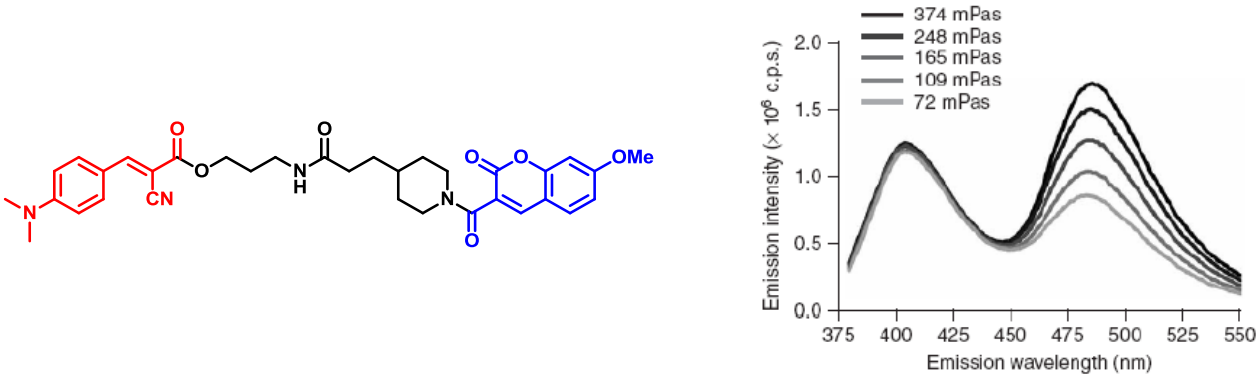

Figure 3. Structure of RET pair based fluorescent viscosity sensor (red part: rotor; blue part: fluorescent label) and emission spectrum upon changing viscosity in glycerol/ethylene glycol mixed solvent. Ref. 27, copyright 2007 Nature Publishing Group.

In consideration of developing a fluorescent viscosity sensor with longer absorption and emission wavelengths, Kuimova and Ogilby introduced a porphyrin dimer-based compound.

Without significant changes observed in the absorption spectrum by varying viscosity, the authors assigned two well resolved bands in the emission spectrum located at 710 and 780 nm, corresponding to twisted and planar conformations of the dimer, respectively, providing convenient means for monitoring dynamic processes at the cellular level.[5]

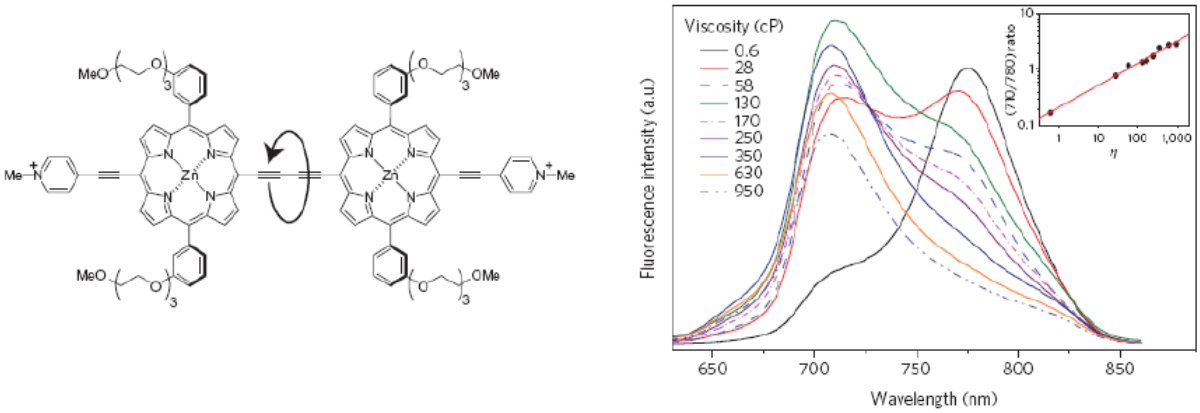

Figure 4. Porphyrin dimer-based fluorescent viscosity sensor and its viscosity dependent emission in glycerol/methanol solutions. Ref. 5, copyright 2009 Nature Publishing Group.

Another reported ratiometric viscosity sensor is based on cyanine dyes, and Peng *et al.* suggested that viscosity dependent emission was achieved by rotating the aldehyde group in the structure. And indeed, a 12-fold of enhancement in fluorescence intensity was obtained upon increasing viscosity. This probe was also shown to work at the cellular level through visualizing intracellular viscosity differences.[32]

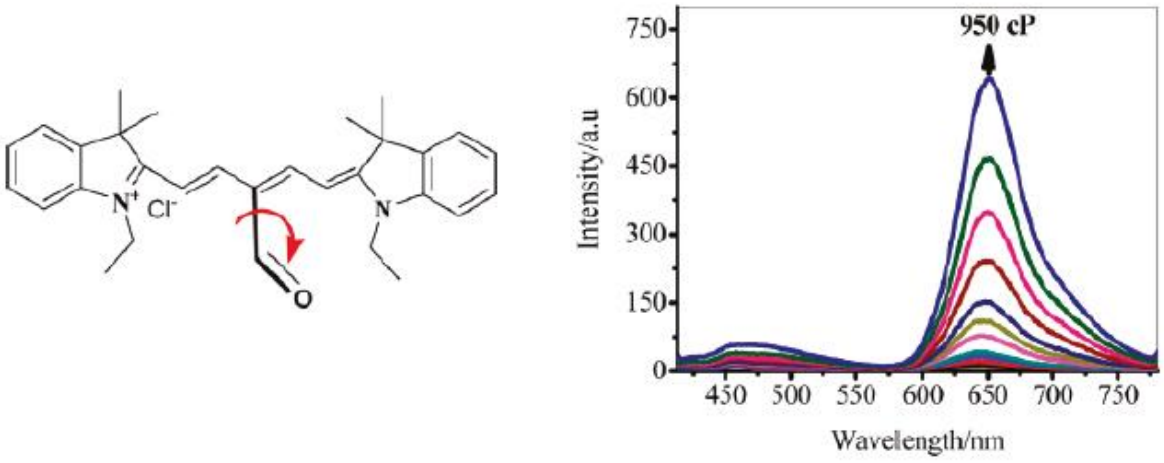

Figure 5. Cyanine dye based viscosity sensor with hypothetical rotation of the aldehyde group and viscosity dependent emission spectrum in glycerol/water mixed solvent. Ref.32, copyright 2011 American Chemistry Society.

An alternative method to determine viscosity by molecular rotors is the application of fluorescence lifetime imaging microscopy, since the fluorescence lifetime of molecular rotors does not change with the concentration of the fluorophore but changes with fluorescence quantum yield as a function of viscosity.[32, 33] In addition, conjugation of molecular rotors to another fluorophore can be omitted, which, in general, simplifies the synthesis and leaves possibility for further functionalization of the probe's structure.

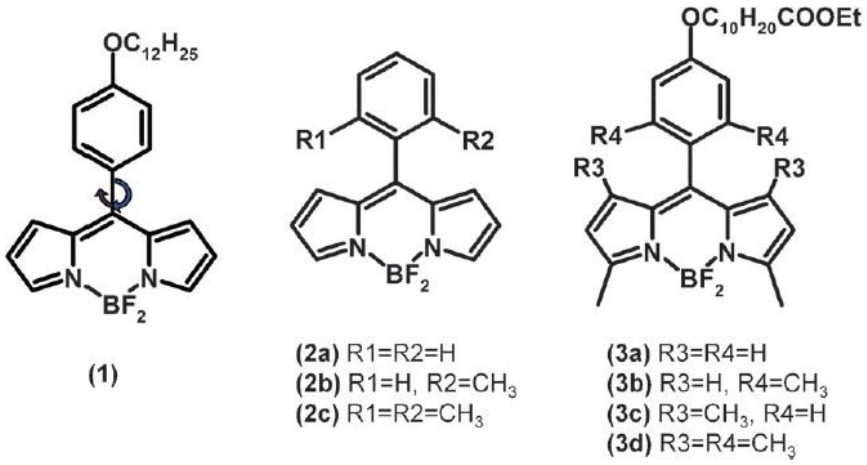

Figure 6. The structures of BODIPY based molecular rotors. Ref.34, Copyright 2008 American Chemical Society.

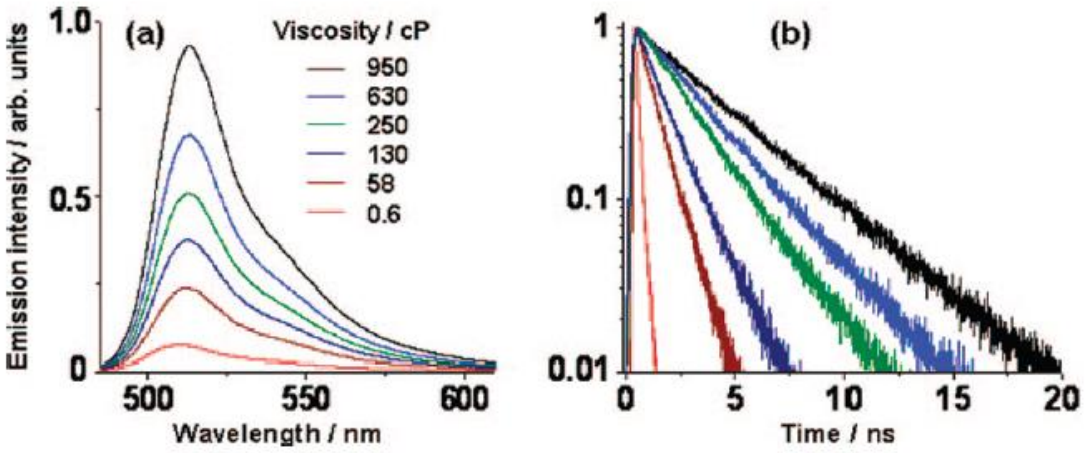

Figure 7. Fluorescence spectra (a) and decay (b) recorded for molecular rotor BODIPY-phenyl-C12 in methanol–glycerol mixtures of increasing viscosity. Ref.34, Copyright 2008 American Chemical Society.

Based on this design strategy, a series of 4,4’-difluoro-4-bora-3a,4a-diaza-s-indacene (BODIPY) based viscosity sensors were reported by Suhling’s group (Figure 6).[34] Different conformations were proposed to be generated due to rotation around the single bond between phenyl ring and BODIPY core, resulting in fluorescence intensity changes. In Figure 7, a significant increase in fluorescence intensity was observed for BODIPY-phenyl-C12 in solutions of different viscosities, together with increased fluorescence quantum yield and lifetime.

Our interest is to design and synthesize a dye emitting in the near-infrared region for bioimaging, [35-37] involving cyanine dyes, a class of materials that have been explored for some time. Absorption and emission maxima in the far red or near-IR can be achieved by extending their conjugation. In addition, moderate fluorescent quantum yields of cyanine dyes are sensitive to environmental conditions such as temperature and viscosity.

Improving the properties of fluorophores with biomolecules, especially the use of nucleosides is quite interesting.[38-41] Conjugation of fluorophores as side chains to DNA nucleosides is favorable because modified nucleosides can be paired with the complementary strand without radically altering the structure.[42] Also, requirements such as reduced toxicity and enhanced hydrophilicity can be fulfilled by modifying the compound with biocompatible nucleoside building blocks, and live cell uptake suggests that these nucleoside-modified fluorophores can function as biological probes.[43] Usually carried out by Sonogashira coupling to conjugate nucledosides and fluorophores, our aim was to introduce an acetylene linker between them, and this linker can avoid steric hindrance that accompanies by direct coupling.[44] A squaraine and

deoxyuridine based viscosity sensor **dU-SQ** was reported by our group exhibiting a 300-fold fluorescence increase.[43] Optimizing reaction conditions for Sonagashira coupling has been carefully studied, and by utilizing amberlite IRA-67, a milder base when compared to some conventional bases such as DIPEA and TEA, much cleaner reactions were yielded. Although this great increase in fluorescence intensity was due to not only TICT but also caused by the aggregation nature of squaraine dyes (Figure 8), this new compound supported that intercellular viscosity is dependent on microtubules (MTs) cross-linking and density, and cell images were captured during different stages of mitosis.

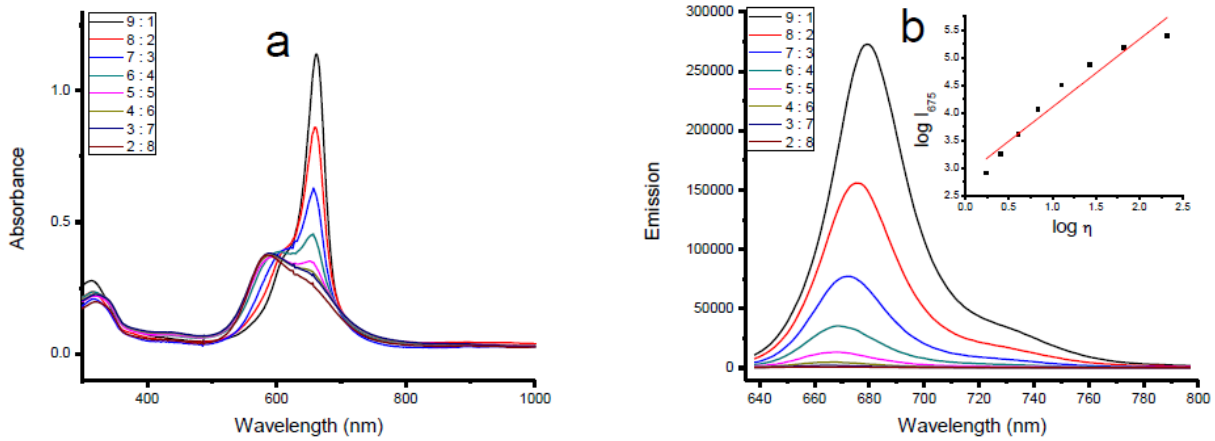

Figure 8. Absorption (a) and emission (b) spectrum of **dU-SQ** in glycerol/water solutions. Insert of (b) shows the linearity of log I (emission intensity at 675 nm) vs. log η (viscosity, cP) of **dU-SQ** in glycerol/water solutions. Excitation wavelength of 625 nm. Ref.43, copyright 2014 Wiley-VCH Verlag GmbH & Co. kGaA, Weinheim.

Herein, we report a newly designed molecular rotor **dU-BZ**, which undergoes a Sonogashira coupling for covalently linking cyanine chromophore to deoxyuridine through an acetylene linker. Linear absorption, emission spectra, and fluorescence quantum yields of **dU-BZ** in

glycerol/methanol solutions were obtained, and a 30-fold fluorescence enhancement was realized on a purely viscosity-dependent manner (no aggregation effects were observed that contributed to the 300-fold increase reported previously). Near-IR excitation and emission wavelengths ensure lower risks of photodamage and phototoxicity. *In vitro* fluorescence microscopy was conducted to demonstrate that the new compound is an effective microviscosity probe at the cellular level.

1.2 Theoretical Background

Free-volume concepts[45] can be described by fluorescence quantum yield, Φ_f, viscosity, η, and temperature,T[26]

$$\boldsymbol{\Phi_f = B(\eta/T)^x} \quad (1)$$

where $B = (k_r / k_{nr}^0)$ $(T/A)^x$, k_{nr}^0 is the free-rotor reorientation rate, A is a constant, and x is a medium-dependent constant ranging between 0 and 1. When Φ_f is linearly related to η/T (x=1), the bulk viscosity of solvent can accurately indicate the friction experienced by molecular rotor. Normally, faster rotational diffusion is expected because the fluorophore can occupy certain free volume within the solvent, in which case x<1. If plotting log Φ_f verses log (η/T), a straight line will be yielded together with the exponent x as its slope, due to eq. 2.

$$\boldsymbol{\log \Phi_f = x \log\left(\frac{\eta}{T}\right) + x \log B} \quad (2)$$

The Förster-Hoffmann equation[46] can be used to describe Φ_f, and fluorescent lifetime, τ_f, of molecular rotors as a function of η

$$\boldsymbol{\Phi_f = z\eta^\alpha} \quad (3)$$

where

$$\boldsymbol{\Phi_f} = \frac{\boldsymbol{k_r}}{\boldsymbol{k_r} + \boldsymbol{k_{nr}}} \tag{4}$$

$$\boldsymbol{\tau_f} = \frac{\mathbf{1}}{\boldsymbol{k_r} + \boldsymbol{k_{nr}}} \tag{5}$$

then

$$\boldsymbol{\tau_f} = \boldsymbol{z k_r^{-1} \eta^{\alpha}} \tag{6}$$

where z and α are constants, the value of 2/3 for α is predicted by Förster and Hoffmann, and k_r and k_{nr} are radiative and nonradiative rate constants.[47] In a photon counting confocal FLIM experiment, after scanning the sample by the radiation from a pulsed light, varied arrival times of fluorescence photon are collected by time-correlated single-photon counting (TCSPC).[48, 49] An image is produced based on the differences in the exponential decay rate of the fluorescence, from which a value for τ_f can be extracted. According to eq 6, a straight line with a slope of α will be yielded after plotting log τ_f verses log η, since

$$\boldsymbol{\log \tau_f = \alpha \log \eta + \log\left(\frac{z}{k_r}\right)} \tag{7}$$

Excited by a linearly polarized light source, depolarization of the fluorescence occurs due to rotational diffusion of the fluorophore.[47, 50] Time-resolved fluorescence anisotropy imaging measures fluorescence intensity decays parallel and perpendicular to the polarization vector of the exciting light. The time-resolved fluorescence anisotropy, $r(t)$, is obtained:

$$\boldsymbol{r(t) = \frac{I_{\parallel}(t) - G\, I_{\perp}(t)}{I_{\parallel}(t) + 2G\, I_{\perp}(t)}} \tag{8}$$

where $I_{\perp}$ and $I_{||}$ are the fluorescence intensity decays parallel and perpendicular to the polarization vector of the exciting light, respectively. The measured intensity ratio is different from the true value by a factor *G*.

For a single-exponential intensity decay, *r (t)* is related to the rotational correlation time, θ, and the initial anisotropy, r_0.

$$\boldsymbol{r(t) = \frac{r_0}{1 + \frac{\tau}{\theta}}} \tag{9}$$

When taking into consideration the isotropic medium, θ is proportional to the viscosity, η, and the molecular hydrodynamic volume, υ:

$$\boldsymbol{\theta = (6D)^{-1} = \frac{\eta v}{RT}} \tag{10}$$

where *D* is the rotational diffusion coefficient, *R* is the Boltzmann constant, and *T* is the absolute temperature.

One should note that eq 3 only can be applied over a limited range of viscosities. According to the Förster-Hoffmann theory, Φ_f is solvent-independent at low viscosities, whereas at relatively high viscosities, a strong dependence on viscosity of Φ_f is expected, since radiative processes predominates over non-radiative relaxation. This very range of viscosities is determined by the properties of the particular molecular rotor and the mechanism of viscosity-dependent photophysical behavior.

1.3 Materials & Methods

1.3.1 Synthesis

Synthetic reagents and solvents were used as received from commercial suppliers. 5-Bromo-2-methylbenzothiazole was purchased from TCI. Iodoethane and (+)-5-iodo-2'-deoxyuridine were purchased from Alfa Aesar. ^{1}H and ^{13}C NMR spectra were recorded on a Bruker Avance 400 NMR spectrometer at 400 and 101 MHz, respectively. High-resolution mass spectrometry analysis was performed in the Department of Chemistry, University of Florida. Uncorrected melting points were collected using a Laboratory Devices Meltemp.

2-Methyl-5-((trimethylsilyl)ethynyl)benzothiazole (1). Under an argon atmosphere 5-bromo-2-methylbenzothiazole (1.5 g, 6.30 mmol), bis(triphenylphosphine)palladium(II) dichloride (442 mg, 0.63 mmol), copper iodide (144 mg, 0.75 mmol) were mixed in 30 mL of degassed acetonitrile and triethyl amine solution (1 : 1, v/v). Trimethylsilylacetylene (4.50 mL) was added before stirring at room temperature for 10 min. Pyridine (3 mL) was added, and the resulting mixture was first stirred at room temperature for 30 min, then at 50 ˚C for 18 h. After being cooled to room temperature, solvent was removed under reduced pressure and the solid residue was purified by column chromatography (silica gel, degrade elution hexanes/ethyl acetate from 10:1 to 7:1), resulting in 1.50 g of white solid (93% yield), m.p.: 126–127.5 ˚C. ^{1}H NMR (400 MHz, $CDCl_3$) δ: 8.02 (d, J = 1 Hz, 1H), 7.72 (d, J = 8.3 Hz, 1H), 7.43 (dd, J = 8.3, 1.5 Hz, 1H), 2.82 (s, 3H), 0.28 (s, 9H). ^{13}C NMR (101 Hz, $CDCl_3$) δ: 167.91, 153.25, 138.06, 128.31, 125.83,

121.04, 104.77, 94.38, 20.21 ppm. HR-MS (ESI) theoretical $[M+H]^+$ = 246.0767, found $[M+H]^+$ = 246.0777.

5-Ethynyl-2-methylbenzothiazole (2). 2-Methyl-6-((trimethylsilyl)ethynyl)benzothiazole (1 g, 4.07mmol) was dissolved in 15 mL of dichloromethane, and 15 mL of methanol/NaOH solution (3%, w/w) was added dropwise. The mixture was allowed to stir at room temperature for 2 h, followed by the removing the organic solvent *in vacuo*. The solid residue was further purified by column chromatography (silica gel, hexanes/ethyl acetate 10:1), affording 0.54 g of pale yellow crystal (77% yield), m.p.: 66–67 ˚C. ^{1}H NMR (400 MHz, $CDCl_3$) δ: 8.07 (d, J = 1.5 Hz, 1H), 7.75 (d, J = 8.3 Hz, 1H), 7.45 (dd, J = 8.1, 1.7 Hz, 1H), 3.12 (s, 1H), 2.82 (s, 3H). ^{13}C NMR (101 Hz, $CDCl_3$) δ: 168.12, 153.21, 136.39, 128.26, 126.09, 126.08, 121.33, 119.79, 83.38, 21.08 ppm. HR-MS (ESI) theoretical $[M+H]^+$ = 174.0372, found $[M+H]^+$ = 174.0378.

5-Ethynyl-3-ethyl-2-methylbenzothiazolium iodide (3). 5-Ethynyl-2-methylbenzothiazole (1 g, 5.78 mmol) was mixed with 2 mL of iodoethane in 1.5 mL of degassed acetonitrile. The mixture was heated in a microwave reactor (CEM, discover) at 150 ˚C for 20 min. Precipitate was collected by filtration and washed with diethyl ether to afford 1.06 g of grey powder, (91% yield), m.p.: 267 ˚C (dec.). ^{1}H NMR (400 MHz, DMSO-d_6) δ: 8.54 (d, J = 1.1 Hz, 1H), 8.43 (dd, J = 8.5, 1.5 Hz, 1H), 7.86 (dd, J = 8.4, 1.3 Hz, 1H), 4.78 (q, J = 7.2 Hz, 2H), 4.60 (s, 1H), 3.21 (s, 3H), 1.44 (m, 3H). ^{13}C NMR (101 Hz, DMSO-d_6) δ: 178.89, 141.14, 131.39, 130.18, 125.65, 123.20, 120.19, 84.29, 82.36, 45.36, 17.47, 13.74 ppm. HR-MS (ESI) theoretical $[M]^+$ = 202.0685, found $[M]^+$ = 202.0692.

2-(4-(Dimethylamino)styryl)-3-ethyl-5-ethynylbenzothiazolium iodide (4). 5-eEhynyl-3-ethyl-2-methylbenzothiazolium iodide (1.5 g, 7.42 mmol) and 2-methyl-N-benzaldehyde (1.33 g, 8.90 mmol) were mixed with 126 mL of acetic anhydride. The mixture was refluxed at 150 ˚C for 20 min and then the hot solution was poured into 200 mL of warm KI solution. After cooling to room temperature, precipitate was filtered and washed with water and a large amount of diethyl ether, yielding 1.81 g of purple solid (73% yield), m.p.: 256 ˚C (dec.). ^{1}H NMR (400 MHz, DMSO-d6) δ: ppm 1.37 - 1.44 (m, 3 H) 3.04 (s, 1 H) 3.13 (s, 6 H) 4.54 (s, 1 H) 4.78 - 4.85 (m, 2 H) 6.86 (d, J=9.05 Hz, 2 H) 7.59 (d, J=15.16 Hz, 1 H) 7.73 (d, J=8.31 Hz, 1 H) 7.94 (d, J=9.05 Hz, 2 H) 8.11 (d, J=14.92 Hz, 1 H) 8.27 - 8.31 (m, 2 H). ^{13}C NMR (101 MHz, DMSO-d6) δ 14.62, 40.54, 44.29, 83.01, 84.10, 100.30, 106.04, 112.74, 119.21, 122.23, 123.03, 125.12, 128.64, 134.07, 141.85, 152.08, 154.50, 172.35. HR-MS (ESI) theoretical $[M]^+$ = 333.1420, found $[M]^+$ = 333.1416.

Synthesis of dU-BZ (5). Under an argon atmosphere a mixture of 5-iodo-2'-deoxyuridine (425 mg, 1.2 mmol), **4** (1.2 g, 3.60 mmol), $Pd(PPh_3)_4$ (139 mg, 0.12 mmol), CuI (47 mg, 0.24 mmol), and 550 mg of Amberlite IRA-67 in 11.3 mL of degassed DMF was stirred at 55 ˚C for 48 h. The Amberlite IRA-67 beads were excluded by filtration first, and to the DMF solution diethyl ether was added,. The resulting precipitate was collected by filtration. Further purification was carried out by column chromatography (silica gel, dichloromethane/methanol 10:1), resulting in 141 mg of purple solid (21% yield), m.p.: 249 ˚C (dec.). ^{1}H NMR (400 MHz, DMSO-d6) δ: ppm 1.38 - 1.45 (m, 3 H) 2.20 (d, J=6.11 Hz, 2 H) 3.13 (s, 6 H) 3.84 (q, J=3.18 Hz, 1 H) 4.25 - 4.31 (m, 1 H)

4.80 - 4.90 (m, 2 H) 5.23 - 5.37 (m, 2 H) 6.14 (t, J=6.36 Hz, 1 H) 6.86 (d, J=9.05 Hz, 2 H) 7.62 (d, J=15.16 Hz, 1 H) 7.73 (dd, J=8.44, 1.34 Hz, 1 H) 7.95 (d, J=9.05 Hz, 2 H) 8.12 (d, J=15.16 Hz, 1 H) 8.23 (s, 1 H) 8.32 (d, J=8.31 Hz, 1 H) 8.50 (s, 1 H) 11.78 (br. s., 1 H). ^{13}C NMR (101 MHz, DMSO-d6) δ 14.62, 31.15, 51.96, 61.57, 70.65, 85.15, 85.83, 88.37, 88.43, 98.29, 106.15, 112.82, 118.24, 122.31, 123.83, 125.13, 128.22, 128.95, 129.31, 130.83, 134.07,150.18, 152.04, 154.53, 158.08, 172.37. HR-MS (ESI) theoretical $[M]^+$ = 559.2010, found $[M]^+$ = 559.2006.

1.3.2 Viscosity Values

Viscosities of pure glycerol at different temperature were employed to approximate the viscosity of 99% glycerol/1% methanol solution. Reported values[51] were directly used as viscosities of solutions with glycerol percentages ranging from 10% to 95%.

1.3.3 Linear Photophysical and Photochemical Characterization

The linear absorption spectra were obtained using an Agilent 8453 UV−vis spectrophotometer in 10 mm path length quartz cuvettes in solvents with different glycerol/methanol ratios, with molar concentration C =1 × 10^{-5} M. The steady-state fluorescence was measured with a PTI QuantaMaster spectrofluorimeter using 10 mm spectrofluorometric quartz cuvettes with C = 1 × 10^{-5} M. The correction for the spectral response of the PTI detection system was performed for all fluorescence spectra. The fluorescence quantum yields, Φ_f, were obtained by a standard method [47] relative to cresyl violet in methanol.

1.3.4 Fluorescence Lifetimes

Fluorescence lifetimes, τ_f, were measured using a PicoQuant PicoHarp 300 time-correlated single photon-counting system with time resolution ≈ 80 ps, a Coherent Mira 900 fs laser system was used for excitation, linearly polarized at the magic angle.

1.3.5 *In Vitro* Bioimaging

3T3 cells (ATCC®) were seeded on poly-D-lysine coated coverslips at a concentration of 5×10^4 cells/ mL and incubated for 48 h. A **dU-BZ** stock solution in DMSO (dimethyl sulfoxide) was then diluted to 15 μM with DMEM medium (Corning, Cellgro®) and added to the cells. Cells were co-incubated with diluted **dU-BZ** for 30 min and then fixed with 4% formaldehyde. $NaBH_4$ was added twice at 1mg/ mL for 5 min to reduce auto-fluorescence. Cells were then permeabilized with 0.1% Triton-X. 1% BSA was applied to block non-specific binding. Hoechst 33258 (Invitrogen™) was added in to cell for 5 min to visualize cell nuclei. Coverslips were then washed with PBS (phosphate buffer saline, Corning, Cellgro®) and mounted on slides with ProLong Gold® antifade reagent (Invitrogen™).

Cell slides were imaged with an Olympus IX70 DSU microscope. A Texas Red filter cube (562/40 ex., 593, 624/40 em.) was employed to excite **dU-BZ** and collect the fluorescence at the optimize wavelength range.

1.4 Results & Discussion

1.4.1 Synthesis

The synthesis of molecular rotor **dU-BZ** is illustrated in Scheme 1. Intermediate compound **3** was synthesized according to the literature[43], and the resulting NMR matched the reported data. Next, compound **4** was synthesized by condensation of intermediate **3** with dimethylamino benzaldehyde via a Knoevenagel reaction; acetic anhydride was employed as both base and solvent.

The following procedure was used for the conjugation of a deoxyuridine analog and compound **4** through a triple bond. Rather than directly using deoxyuridine, a modified form, idoxuridine was exploiting not only due to the iodo group provided for conjugation, but also its similar enough structure can be incorporated into DNA/RNA strands for future study. Hydroxyl groups of idoxuridine are all unprotected in order to avoid possible low overall yield. Although protected hydroxyl groups possess enhanced water solubility when compared to unprotected ones, in consideration of the overall yield of the reaction, protected nucleosides were not pursued.

dU-BZ was obtained via a Sonogashira coupling between (+)-5-iodo-2'-deoxyuridine and compound **4** in 21% yield after purification by column chromatography. After conjugation with the deoxyuridine analog, **dU-BZ** exhibited enhanced water solubility when compared to compound 4. The ^{1}H NMR, ^{13}C NMR, and HR-MS spectra were in good accordance with the chemical structure as expected.

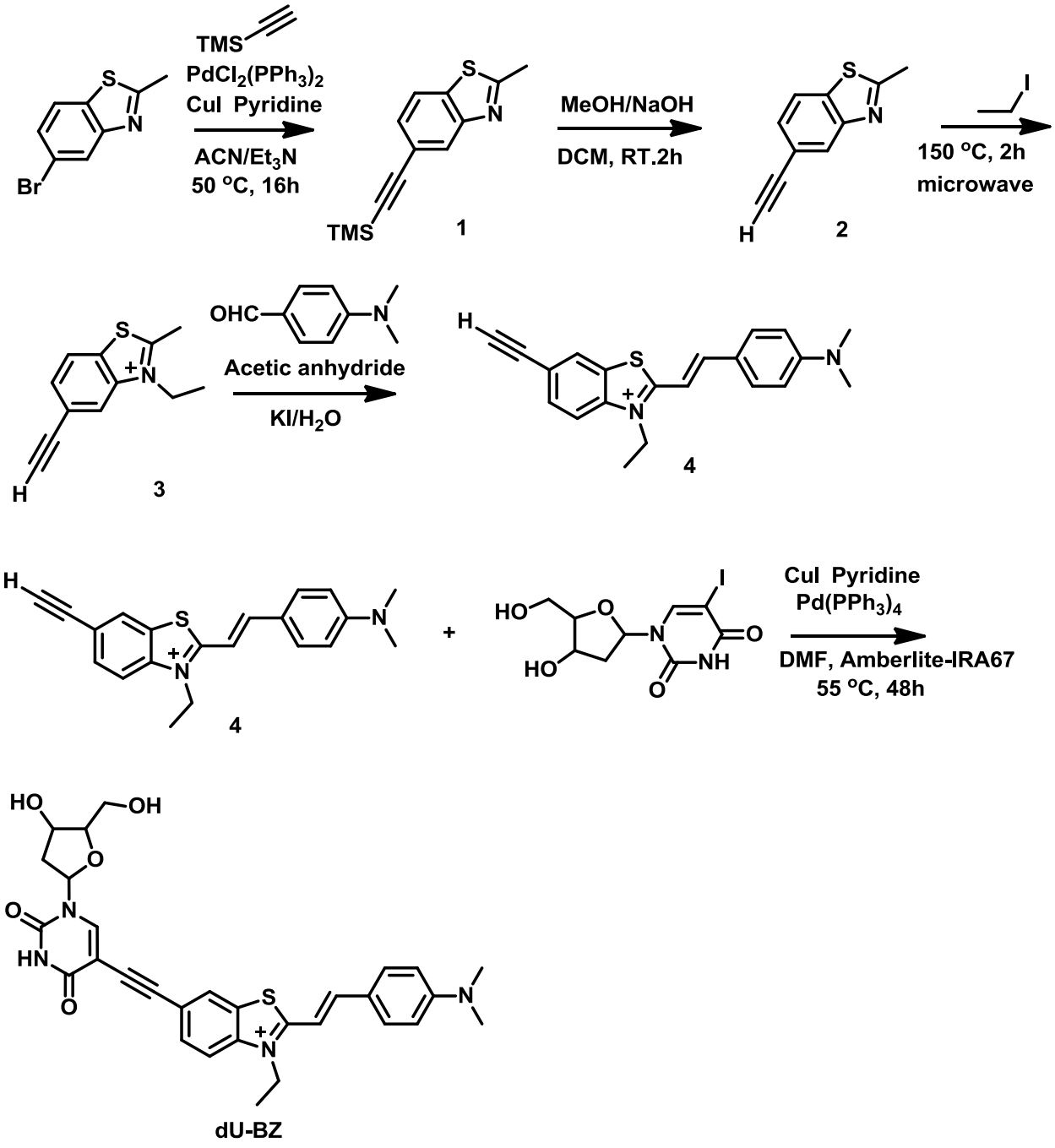

Scheme 1. Synthetic route of molecular rotor **dU-BZ**

1.4.2 Photophsical Characterization

The Φ_f of *dU-BZ* was measured in 99% glycerol/1% methanol (v/v) solution at various temperatures, ranging from 343 to 293K, with viscosity ranging from 50.6 to 1412 cP (Table 1). According to Figures 9a and 9b, no significant shifts were observed in absorption and emission spectra, but an increase in the fluorescence intensity was obtained with decreasing temperature when excited at 551 nm, and Φ_f increased from 0.04 to 0.34.

Table 1. Fluorescence Quantum Yield (Φ_f) of dU-BZ and Viscosity (η) as a Function of Temperature (T) in 99% Glycerol/1% Methanol (v/v) Solution.

Temperature (T)/K	Viscosity (η)/cP	Fluorescence quantum yield (Φ_f)
343	50.6	0.04 ± 2.4E-03
333	81.3	0.07 ± 3.5E-03
323	142	0.10 ± 5.3E-03
313	284	0.17 ± 8.5E-03
303	612	0.24 ± 1.2E-02
293	1412	0.34 ± 1.7E-02

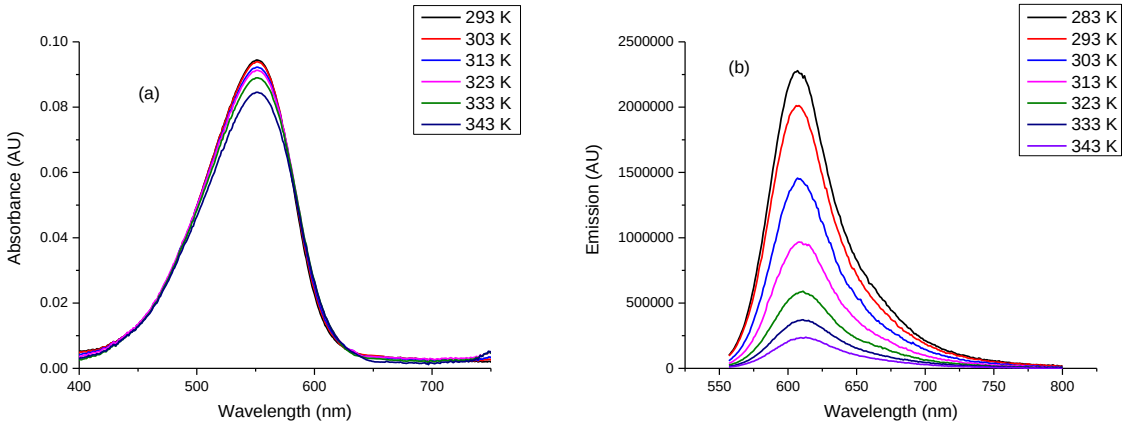

Figure 9. Absorption (a) and emission (b) spectra of **dU-BZ** recorded as a function of temperature in 99% glycerol/1% methanol (v/v) solution.

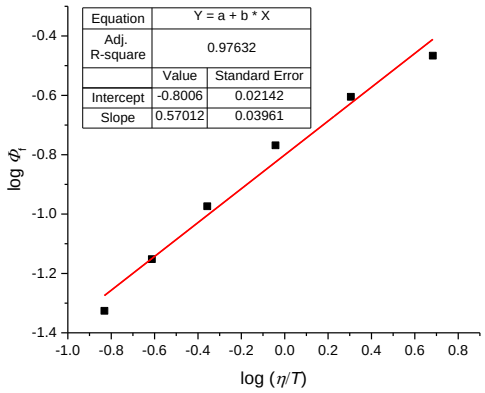

Figure 10. Plot of log Φ_f vs. log (η/T) for **dU-BZ** in 99% glycerol/1% methanol (v/v) solution.

From eq 2, a linear behavior will be observed when plotting log Φ_f vs. log (η/T). These results are shown in Figure 10. The slope of this plot provided the exponent x, 0.57 $\pm$ 0.04, with a R^2

value of 0.98. Due to increased viscosity and decreased free volume, a decreased nonradiative rate constant is expected, and this prediction will be described in the following experiments.

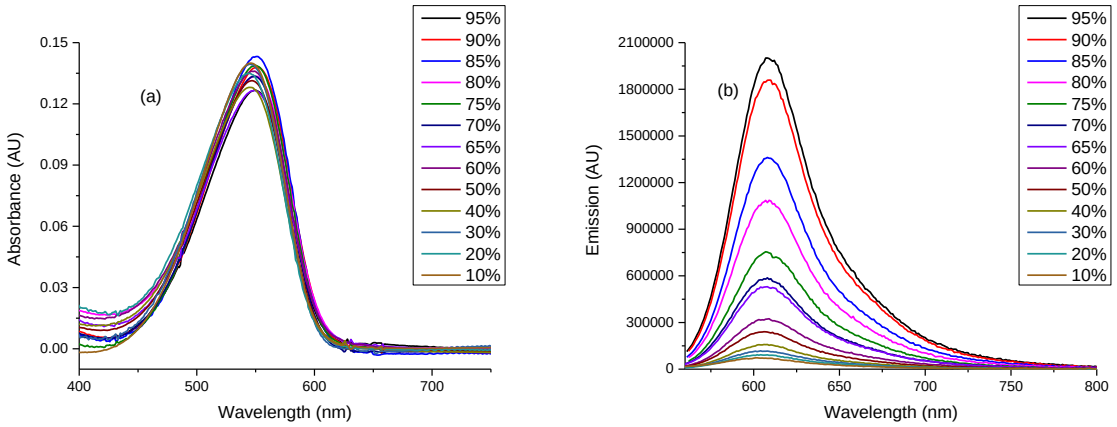

Figure 11. Absorption (a) and emission (b) spectra of **dU-BZ** obtained as a function of viscosity in glycerol/methanol (v/v) solutions, percentage indicated is the glycerol content of the solution.

At the same concentration, there was no obvious change observed in the absorption spectra for **dU-BZ** by varying the ratio of glycerol and methanol in solution. However, without any changes in shape of the emission spectrum or the peak emission wavelength, a 30-fold increase in fluorescence intensity appeared at 608 nm by increasing viscosity from 1.8 cP to 950 cP. This result is consistent with the Förester-Hoffmann equation (Figure 11).

Measured values, Φ_f and τ_f, were used to calculate the rate constants via eqs 2 and 3. Plotted in Figure 12, with viscosity increasing from 58 cP to 950 cP (Table 2), Φ_f shows significantly increased values as expected. It is worth noting that k_r remained constant but k_{nr} decreased

largely as a function of viscosity. These data suggest that the main contribution to the increase of Φ_f is via suppression of the nonradiative process.[3] In a highly viscous environment, because of the intramolecular rotation hindrance, the torsion angle between the benzothiazole and aminobenzene rings is close to zero, which yields the most stable conformation of the molecule in the LE state. At the same time, nonradiative relaxation to the TICT state, which has a conformation angle value close to 90°, is deactivated, and radiative decay from LE state to ground state starts to take place instead of de-excitation from the TICT state.

Table 2. Fluorescence Quantum Yield (Φ_f), Fluorescence Lifetime (τ_f)*, Radiative (k_r) and Nonradiative (k_{nr}) Rate Constants of dU-BZ as a Function of Viscosities (η) in Glycerol/Methanol Solutions.

% glycerol	Viscosity (η)/cP	Fluorescence quantum yield (Φ_f)	Fluorescence lifetime (τ_f)/ns	k_r/ns^{-1}	k_{nr}/ns^{-1}
95	950	0.26 ± 0.01	1.07	0.243	0.692
90	630	0.19 ± 9.5E-03	0.87	0.218	0.931
85	350	0.13 ± 6.5E-03	0.59	0.220	1.475
80	250	0.11 ± 5.5E-03	0.57	0.193	1.561
75	170	0.07 ± 3.5E-03	0.40	0.175	2.325
70	130	0.06 ± 3.0E-03	0.30	0.200	3.133
65	70	0.06 ± 2.9E-03	0.28	0.179	3.393
60	58	0.03 ± 1.5E-03	0.19	0.158	5.105
50	28	0.02 ± 1.0E-03	0.10	0.200	9.800
40	13	0.015 ± 7.5E-04	0.06	0.250	16.417
30	7.7	0.010 ± 5.0E-04	0.05	0.200	19.800
20	4.8	0.008 ± 4.0E-04	0.04	0.200	24.800
10	1.8	0.006 ± 3.2E-04	0.05	0.120	19.880

* Values of lifetime less than 0.2 ns are not reliable due to the resolution of the experimental system.

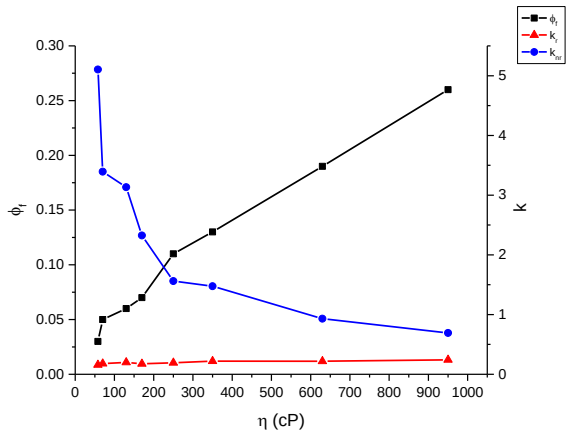

Figure 12. Fluorescence quantum yield (Φ_f), radiative (k_r), and nonradiative (k_{nr}) rate constants of **dU-BZ** obtained as a function of viscosity in glycerol/methanol solutions.

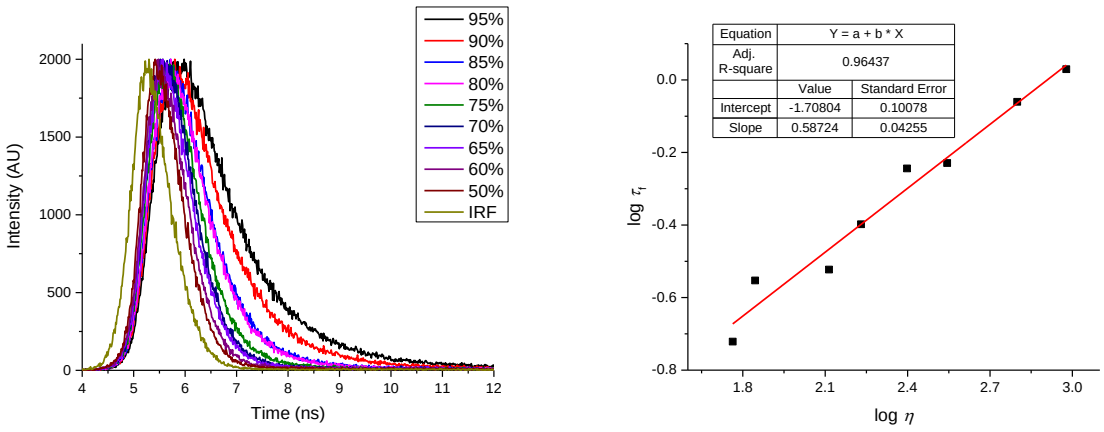

Figure 13. (a) Fluorescence decay of **dU-BZ** recorded as a function of viscosity in glycerol/methanol solutions, percentage indicated the content of glycerol in solution. (b) log τ_f vs. log η for **dU-BZ**.

1.4.3 Fluoresence Lifetime of **dU-BZ** in Glycerol/Methanol Solutions

Figure 13(a) shows fluorescence lifetime decay of **dU-BZ** with decreasing viscosity in glycerol/methanol solutions. As a function of viscosity, the fluorescence lifetime varied markedly from 0.19 ns at 58 cP to 1.07 ns at 950 cP. From eq 7, a straight line will be yielded if plotting log τ_f vs. log η, and as expected, a linear behavior showed in Figure 13(b), with a slope, α, of 0.59 ± 0.04, consistent with the value predicted by Förster-Hoffmann equation, and a R^2 value of 0.96 for **dU-BZ**. It was also found that plots below 58 cP fit in the same straight line, but lifetime values lower than 0.2 ns were not reliable due to the resolution of the experimental system (Table 2). Only plots from 58 cP to 950 cP are shown in the figure.

1.4.4 *In Vitro* Bioimaging of **dU-BZ**

Highly viscous, up to 400 cP, intra- and intercellular environments[32] have been reported. Taking into consideration **dU-BZ**, *in vitro* fluorescence enhancement by using **dU-BZ** is expected, and indeed, after incubation with 3T3 cells (mouse embryonic fibroblast cells) for 30 min, **dU-BZ** appeared to readily enter the cells and remarkably clear fluorescence images were obtained (Figure 14, Hoechst stained cell nuclei as reference). These results demonstrate that compound **dU-BZ** is able to visulaize microviscosity at the cellular level.

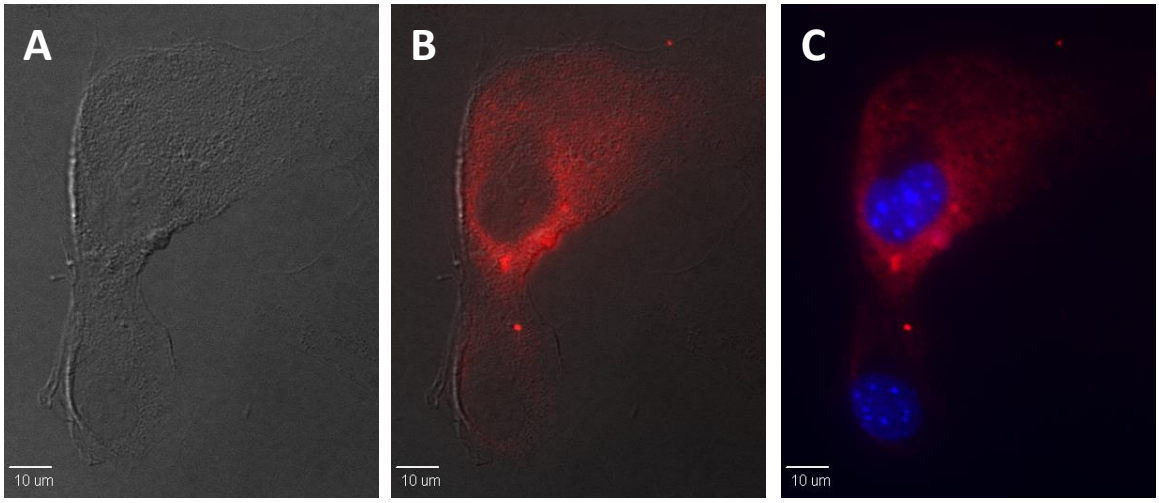

Figure 14. 3T3 cells were incubated with **dU-BZ** (15 μM, 30 min). DIC image (A) indicates healthy morphology of 3T3 cells. Overlay image of **dU-BZ** fluorescence and DIC (B) indicates effective uptake of **dU-BZ**. C shows overlay image of Hoechst and **dU-BZ** fluorescence. Scale bar shows 10 μM.

1.5 Conclusion and Future Work

A deoxyribonucleoside-modified cyanine dye was prepared and characterized. Near-IR absorption and emission were obtained, which are favorable for *in vitro* and *in vivo* imaging. Viscosity-dependent studies, including fluorescence quantum yields, fluorescence lifetimes, and nonradiative rate constants were determineed, and results were in accordance with that predicted by theory for molecular rotors. A 30-fold enhancement in fluorescence intensity in homogenous glycerol/methanol solutions was obtained, and fluorescence lifetime increased from 0.19 to 1.07 ns with increasing viscosity from 58 cP to 950 cP. Significantly, *in vitro* investigations suggest that **dU-BZ** is capable of functioning as a microviscosity sensor at cellular and subcellular levels.

Thus, the newly designed deoxyribonucleoside-modified cyanine dye is a promising candidate as a near-IR viscosity sensor for bioimaging.

Future work regarding optimizing this new molecular rotor **dU-BZ** can go in several directions. Since all three parts in the D-π-A (donor- π conjugation-acceptor) system are available for chemical modification, tuned photophysical properties, such as longer lifetime and higher quantum yield are conceivable. In addition, fluorescence anisotropy is powerful technique for microviscosity measurements in cells. As mentioned previously, with initial anisotropy, rotational correlation time θ can be obtained.

Monitoring viscoelastic change of cell membranes can provide information in various states of disease since the viscosity of cell membrane has great influence on the activities of membrane bound proteins[52-56]. Hydrocarbon chains are known to improve membrane localization, and Levitt[57] has reported living cell membrane detection of viscosity probes that utilize BODIPY core and a long alkyl chain. This suggests that increasing the length of the alkyl chain or replacing it with a farnesyl substituent on the donor moiety of **dU-BZ** may also yield a membrane-targeted viscosity sensor. In addition, DCVJ has been demonstrated to be a cell membrane-specific viscosity probe[58]. However, certain cytotoxicity was revealed, a strong reminder that the toxicity of a probe needs to be considered while developing the structure. Beyond this, **dU-BZ** can also be functionalized by attaching recognition groups for specific protein binding.[59]

Since deoxyribonucleoside analogs have been introduced as a building block for **dU-BZ**, another aspect for developing this new viscosity probe is RNA binding. Upon effective binding, e.g., binding to mRNA, one may be able to monitor viscosity changes during protein synthesis processes, which is significant for further development of RNA therapeutics.

CHAPTER 2. A NEW FLUORESCENT CALCIUM ION INDICATOR BASED ON BAPTA AND BODIPY DERIVATIVES

2.1 Introduction

Functioning as an intracellular second messenger, calcium ion (Ca^{2+}) plays a very important role by precisely controlling temporal and spatial fluctuations of its concentrations.[60, 61] Approaches to determine intracellular Ca^{2+} are accomplished using fluorescence indicators. Since Ca^{2+} chelator BAPTA (O,O'-bis(2-aminophenyl)ethyleneglycol-N,N,N',N'-tetra acetic acid)[62] appeared, numerous BAPTA based Ca^{2+} indicators have been designed and synthesized over decades, such as Indo-1,[63] Quin-2,[64] and Fura-2[65, 66] (Figure 15). However, photodamage and phototoxicity caused by UV-light excitation, shallow penetration, and photobleaching of fluorophores make it difficult for these probes to be applied in biological samples.[67, 68]

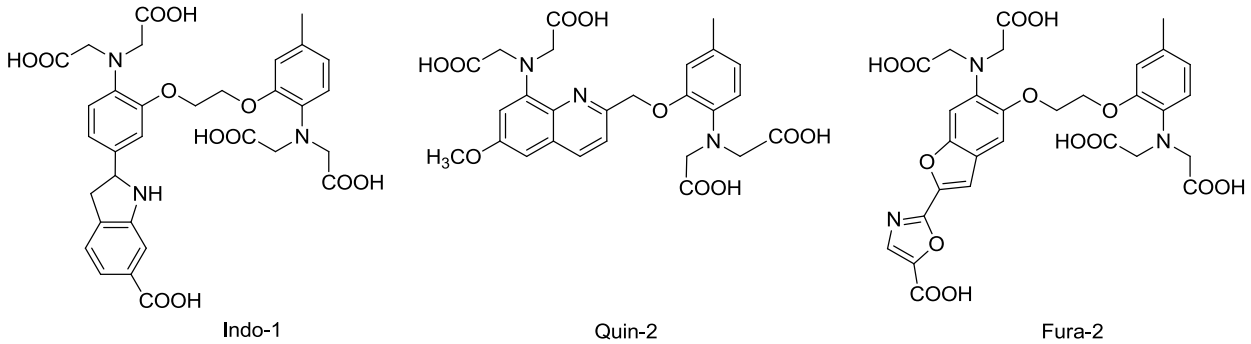

Figure 15. Indo-1, Quin-2, and Fura-2.

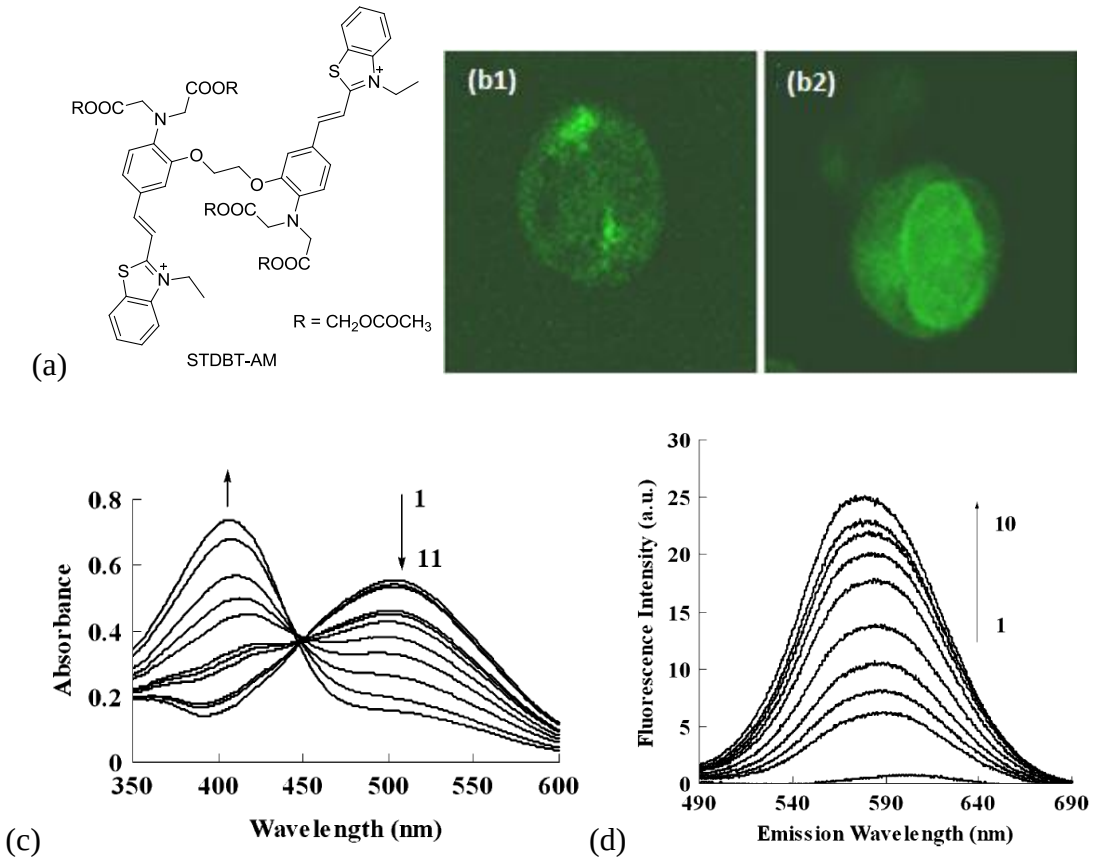

Figure 16. (a) Structure of STDBT-AM, (b1) *in vitro* cell image of Fluo-3 (b2) *in vitro* cell image of STDBT-AM, absorption (c) and emission (d) spectra of STDBT-AM. Ref.72, copyright 2010 Springer.

To overcome these obstacles, near-IR fluorescent calcium probes have drawn more and more attention. Ca^{2+} indicators based on cyanine[69, 70] or squaraine[71] dyes have been reported. A representative compound, STDBT-AM, demonstrated a fluorescence intensity increase upon Ca^{2+} binding together with significant intracellular localization (Figure 16).[72] When compared to the fluorescence image of Fluo-3, rather than distributing throughout the entire cell, the image of STDBT-AM showed a clear boundary between the nucleus and cytosol. But limitations such as low fluorescence quantum yield and/or poor ion sensitivity hinder further development of this

type of Ca^{2+} probe. In addition, aggregation behavior evident in Figure 16(c) is usually observed from cyanine and squaraine dyes, which makes factors causing the fluorescence increase more complicated.

Growing interest in 4,4-difluoro-4-bora-3a,4a-diaza-s-indacene (BODIPY) derivatives is due to its excellent features such as good solubility and low self-aggregation in various solvents, relative insensitive to solvent polarity and pH, good photostability, narrow emission bandwidths, high fluorescence quantum yield, relatively long fluorescence lifetime (in the nanosecond range), and near-IR excitation/emission wavelengths.[73-75] In addition, tuned photophysical properties are achievable by attachment of specific residues at appropriate positions of the BODIPY core.

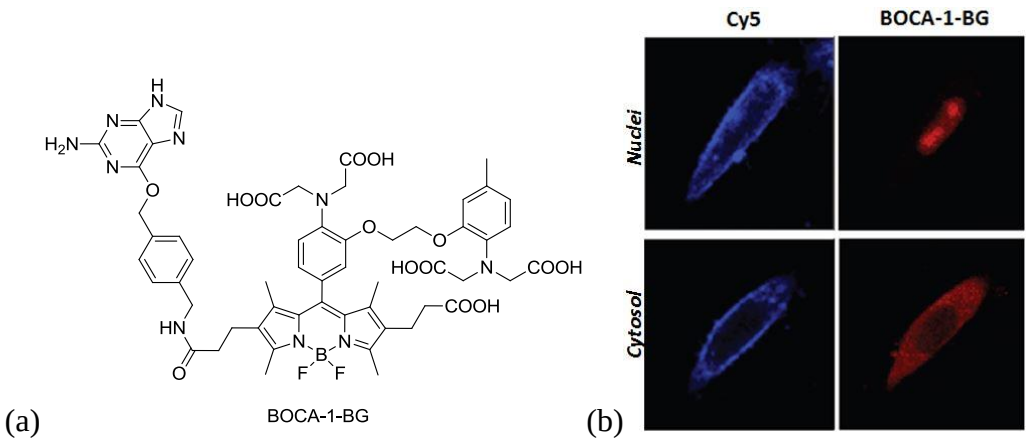

Figure 17. (a) Structure of BOCA-1-BG and (b) images of cell expressing SNAP-tag in nuclei or in cytosol after culturing with BOCA-1-BG with cell images of Cy5 in nuclei or in cytosol as control. Images were taken during the ATP stimulation to induce a Ca^{2+} signal. Ref. 79, copyright 2010 American Chemical Society.

BODIPY-based Ca^{2+} probes have been reported previously[76-78] but relatively modest fluorescence intensity increase upon binding Ca^{2+} (< 40 fold) hindered their further development.

A combination of a BAPTA chelator and a BODIPY core is an intriguing possibility. The resulting structure may not only possess high-affinity of Ca^{2+} but also possess the advantages brought by BODIPY. Based on this design theory, BOCA-1-BG (Figure 17a) was created by Kamiya and co-workers[79], and a 250-fold increase in fluorescence intensity upon Ca^{2+} binding was obtained. Furthermore, BOCA-1-BG is a targeted calcium probe with a residue O^6-benzylguanine which can selectively couple to SNAP-tag (The **S**oluble ***N***-ethylmaleimide sensitive fusion **A**ttachment **P**rotein), a human DNA repair protein. A SNAP-tag can localize in living cells during its fusion with selected proteins so that a targeted probe is achievable. *In vitro* cell images showed that BOCA-1-BG is more targeted in both nucleus and cytosol when compared to Cy5 (Figure 17b).

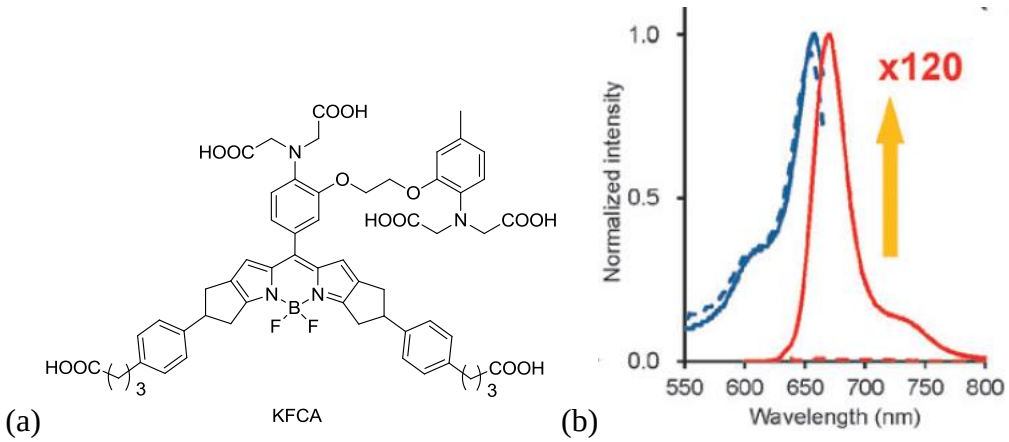

Figure 18. (a) Structure of KFCA (b) absorption and emission spectra in the absence (dotted line) and presence (solid line) of Ca^{2+}. Ref. 80, copyright 2011 Royal Society of Chemistry.

Although it doesn't possess as much increase in fluorescence intensity as BOCA-1-BG, longer absorption and emission maximum (655 nm and 670 nm, respectively) were observed for compound KFCA (Figure 18).[80] Additionally most BODIPY-based probes are less soluble in

water due to their hydrophobic BODIPY core, but KFCA showed relatively high water solubility (> 1 mM without addition of a co-solvent).

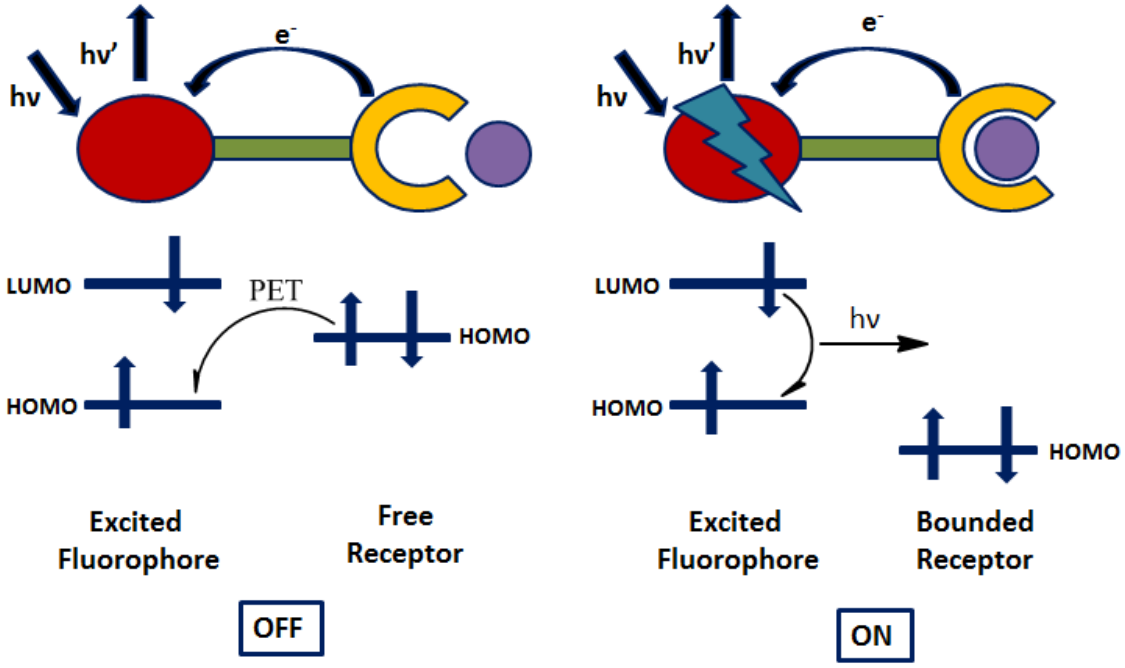

Figure 19. Left: mechanism of photoinduced electron transfer (PET). Right: no PET due to lower HOMO of the quencher.

Photoinduced electron transfer (PET) can be applied to explain the phenomenon of increased fluorescence intensity after Ca^{2+} binding. Serving as an electron donator, upon excitation, BAPTA transfers its electron to BODIPY. In an analyte free situation, PET opens a nonluminescent deactivation path to the ground state so that fluorescence of the BODIPY core is largely quenched via PET, resulting in a weak fluorescent or even nonfluorecent probe. Upon coordination of Ca^{2+}, the electron-donating ability of BAPTA is weakened and the energy level

of the donor orbital is lowered resulting in electron transfer to BODIPY being switched off, which leads to suppression of PET and emission recovery (Figure 19).

Although BAPTA and BODIPY-based calcium sensors exhibit superior chemical and photophysical properties, unfortunately, these types of probes have not been fully explored due to their inefficient synthesis and purification. Herein, we report a calcium sensor with two moieties, BAPTA and BODIPY, conjugated with an alkene linker via a Knoevenagel condensation. A new synthetic route was applied to simplify the rather inefficient and cumbersome purification procedure. Upon excitation, in buffer containing 39 μM Ca^{2+} and 1 M Ca^{2+}, 1.5-fold and 3-fold increases in fluorescence intensity were observed, respectively.

2.2 Materials and Methods

2.2.1 Synthesis

Synthetic reagents and solvents were used as received from commercial suppliers. All chemicals were purchased from Sigma-Aldrich or Fisher. ^{1}H and ^{13}C NMR spectra were recorded on a Bruker Avance 400 NMR spectrometer at 400 and 101 MHz, respectively. High-resolution mass spectrometry analysis was performed in the Department of Chemistry, University of Florida.

2-(2-Bromoethoxy)-4-methyl-1-nitrobenzene. 2-Nitro-5-methylphenoxide (4.59 g, 0.03 mol), DMF (2 mL) and K_2CO_3 (4.14 g, 0.03 mol) were mixed in and 1,2-dibromoethane (45 mL, 0.1 mol). The resulting mixture was refluxed while stirring at 120 ℃ for 4 h and the color of solution changed from orange to pale yellow. Followed by vacuum filtration and filtrate was

diluted with 40 mL DCM and washed 3 times with 70 mL water each time. Then organic layer was washed with 1 mol/L NaOH, until no color observed from NaOH layer. Organic layer was collected and dried over Na_2SO_4 and solvent was evaporated under vacuum. No further purification was performed and 7.80 g of pale yellow product was obtained (71% yield). ^{1}H NMR (400 MHz, $CDCl_3$) δ: 2.35 (s, 3H), 3.59-3.64 (m, 2H), 4.33-4.37 (t, 3H), 6.79-6.84 (dd, 2H), 7.68-7.71 (d, 1H). ^{13}C NMR (101 MHz, $CDCl_3$) δ: 21.83, 28.51, 29.87, 69.52, 115.84, 121.98, 125.73, 137.78, 146.04, 151.53. Ref. 83.

4-Methyl-1-nitro-2-(2-(2-nitrophenoxy)ethoxy)benzene. 2-(2-Bromoethoxy)-4-methyl-1-nitrobenzene (4.32 g, 16.61 mmol), 2-nitrophenol (2.50 g, 18 mmol) and K_2CO_3 (2.49 g, 18 mol) were mixed in DMF (10 mL). The resulting mixture was refluxed while stirring at 130 ℃ for 2 h before adding water to a 100 mL volume. Followed by vacuum filtration and the precipitate was washed with aqueous Na_2CO_3 until no color was observed from filtrate. After washing with water, recrystallization was performed to crude product with 1 L 95% ethanol, and 20 mL water was added to the solution after cooling down. The precipitate was collected and dried under vacuum, and 4.30 g of pale yellow powder resulted (81% yield). ^{1}H NMR (400 MHz, $CDCl_3$) δ: 2.44 (s, 3H), 4.51-4.55 (m, 4H), 6.86-6.88 (ddd, 1H), 7.02-7.09 (m, 2H), 7.24-7.26 (m, 1H), 7.55-7.58 (ddd, 1H), 7.76-7.78 (d, 1H), 7.81-7.83 (dd, 1H). ^{13}C NMR (101 MHz, $CDCl_3$) δ: 21.84, 21.86, 68.64, 68.71, 115.82, 121.98, 116.45, 121.29, 122.07, 125.53, 12575, 134.27, 137.91, 125.73, 134.27, 137.91, 140.28, 146.16, 151.89, 152.10. Ref. 83.

2-(2-(2-Aminophenoxy)ethoxy)-4-methylaniline. 4-Methyl-1-nitro-2-(2-(2-nitrophenoxy)ethoxy)benzene (3 g, 9.43 mmol) was dissolved in THF/ethanol (50 mL/50 mL), 10% Pd/C (2.13 g) was added to the solution and the resulting mixture was degassed for 20 min. After bringing temperature to 70 ℃, hydrazine hydrate (5.86 mL, 188.6 mmol) was added dropwise and reaction was refluxed while stirring for 12 h. After catalyst and solvent being removed, 1.80 g of white crystal was obtained as product without further purification (74% yield). ^{1}H NMR (400 MHz, $CDCl_3$) δ: 2.25 (s, 3H), 3.65 (NH_2, 4H), 4.31-4.37 (m, 4H), 6.62-6.63 (d, 2H), 6.68-6.73 (m, 3H), 6.80-6.86 (m, 2H). ^{13}C NMR (101 MHz, $CDCl_3$) δ: 20.89, 67.48, 112.52, 113.53, 115.39, 118.37, 121.88, 122.07, 128.03, 134.07, 136.81, 146.24. Ref. 83.

Dimethyl 2,2'-((2-(2-(2-(bis(2-methoxy-2-oxoethyl)amino)-5-methylphenoxy)ethoxy)phenyl)azanediyl)diacetate. 2-(2-(2-Aminophenoxy)ethoxy)-4-methylaniline (1.80 g, 7.0 mmol), methyl 2-bromoacetate (6 mL, 38.78 mmol), dry Na_2HPO_4 (4.2 g, 3.5 mmol) and NaI (0.42 g, 2.8 mmol) were mixed in dry acetonitrile (20 mL). The resulting mixture was first degased for 20 min then refluxed for 18 h while stirring. Upon completion, the reaction was first diluted with toluene and washed with water. The organic phase was dried over $MgSO_4$ and solvent was removed. Column chromatography was performed (hexanes:ethyl acetate = 2:1) and 3.10 g of yellow crystal was isolated (79% yield). ^{1}H NMR (400 MHz, $CDCl_3$) δ: 2.27 (s, 3H), 3.56-3.59 (m, 12H), 4.12-4.16 (dd, 8H), 4.27 (d, 4H) 6.66-6.76 (m, 3H), 6.82-6.83 (m, 4H), 6.86-6.92 (m, 2H). ^{13}C NMR (101 MHz, $CDCl_3$) δ: 0.36, 21.31, 51.89, 51.94, 53.79, 67.44, 67.54, 113.65, 114.58, 119.47, 119.65, 121.87, 122.14, 122.70, 132.58, 137.13, 139.66, 150.76, 172.36. Ref. 83.

Dimethyl 2,2'-((2-(2-(2-(bis(2-methoxy-2-oxoethyl)amino)-5-formylphenoxy)ethoxy)-4-methylphenyl)azanediyl)diacetate (BAPTA). Dimethyl 2,2'-((2-(2-(2-(bis(2-methoxy-2-oxoethyl)amino)-5-methylphenoxy)ethoxy)phenyl)azanediyl)diacetate (1.11 g, 2.03 mmol) was added in dry DMF (2.03 mL), the solution was cooled in ice after adding of pyridine (0.2 mL, 2.52 mmol), after being degassed with argon for 20 min, $POCl_3$ was added dropwise while stirring and the reaction immediately turned black. The reaction was brought to room temperature after stirring for 30 min, followed by heating to 60 ℃ for 1 h and stirred overnight at room temperature. 60 mL DCM was added, the diluted solution was poured into crushed ice and pH was adjusted to ~7 with aqueous NaOH. After extraction with DCM, organic layer was dried over $MgSO_4$ then solvent was removed. 15 mL isopropyl alcohol was added to wash and 0.73 g precipitate was collected (62% yield). ^{1}H NMR (400 MHz, $CDCl_3$) δ: 2.27 (s, 3H), 3.58-3.59 (m, 12H), 4.12 (d, 4H), 4.24-4.26 (dd, 6H), 4.31-4.33 (d, 2H), 6.66-6.69 (m, 2H), 6.74-6.77 (m, 2H), 7.37-7.39 (m, 2H), 9.80 (S, 1H). ^{13}C NMR (101 MHz, $CDCl_3$) δ: 0.34, 21.28, 51.91, 52.22, 53.93, 67.18, 67.82, 111.42, 114.75, 117.08, 119.79, 122.38, 126.94, 130.38, 132.53, 137.29, 145.44, 150.11, 150.64, 171.59, 172.31, 190.83. Ref. 83.

2,2'-((2-(2-(2-(Bis(carboxymethyl)amino)-5-formylphenoxy)ethoxy)-4-methylphenyl)azanediyl)diacetic acid (BAP-HY). BAPTA (1 g, 1.74 mmol) was added in 30 mL 1 M NaOH solution. The mixture was refluxed at 100 ℃ until the reaction mixture turned clear. After cooling in ice bath, concentrated HCl was added dropwise while stirring. The precipitate that formed was collected by vacuum filtration then washed with saturated NaCl

solution and dichloromethane, and dried under vacuum, resulting in 0.80 g product (89% yield). ^{1}H NMR (400 MHz, CDCl3) δ: 2.21 (s, 3H), 4.00 (dd, 4H), 4.18-4.28 (ddd, 8H), 6.66-6.80 (m, 4H), 7.40(m, 2H), 9.74(1H, s), 12.71 (COOH, 4H); ^{13}C NMR (101 MHz, $CDCl_3$) δ: 191.31, 173.50, 172.82, 150.31, 149.10, 145.64, 137.56, 131.21, 129.07, 126.33, 122.48, 119.30, 116.54, 116.24, 113.62, 68.26, 67.63, 54.63, 31.48, 21.25. Ref. 81.

4,4-Difluoro-3,5,8-trimethyl-4-bora-3a,4a-diaza-s-indacene (BO-3). To a solution of 2-methylpyrrole (500 mg, 6.15 mmol) in dry DCM (15 mL) was added acetyl chloride (0.2 mL, 3 mmol) and the mixture was refluxed for 2 h. Triethylamine (3 mL, 15 mmol) was added, followed by an addition of BF_3 Ɛt$_2$O (3 mL, 15 mmol) and stirring was continued for 30 min at rt. The reaction mixture was quenched with 10% aq HCl and extracted with EtOAc. The organic extracts were washed with water, dried over $MgSO_4$, filtered and evaporated to dryness. Flash chromatography on silica gel using hexane/DCM (2:1) afforded product (150 mg, 43% yield) as red solid. ^{1}H NMR (400 MHz, $CDCl_3$) δ: 6.93 (d, J = 3.9 Hz, 2H), 6.10 (d, J = 3.9 Hz, 2H), 2.48 (s, 6H), 2.27 (s, 3H); ^{13}C NMR (101 MHz, $CDCl_3$) δ: 155.57, 140.20, 134.98, 126.93, 118.67, 15.13, 14.72. Ref. 82.

Synthesis of BAPBO-3. **BO-3** (90 mg, 0.39 mmol) and 200 mg **BAP-HY** (0.39 mmol) were mixed in 13 mL dry toluene and 5 mL DMF, the resulting mixture was argon degased for 15 min, followed by adding of 0.93 mL glacial acetic acid and 0.74 mL piperidine, and refluxed with Dean-Stark apparatus for 3 h under argon. After the solvent was removed under vacuum, the crude product was washed with hexane and ether. The resulting solid was then washed with 0.02

M HCl. After filtration, the solid was dissolved in 0.02 M NaOH and the pH adjusted to 3-4 with 0.02 M HCl. After collection of the formed precipitate, 40 mg purple solid was afforded (14% yield). ^{1}H NMR (400 MHz, MeOD) δ: 2.37 (s, 3H), 2.48 (s, 3H), 2.54 (s, 3H), 4.15 (dd, 4H), 4.51 (ddd, 8H), 6.20-6.30 (m, 2H), 6.99-6.98 (m, 3H), 7.14-7.21 (m, 2H), 7.31-7.46 (m, 5H); ^{13}C NMR (101 MHz, MeOD) δ: 13.77, 20.59, 29.64, 54.37, 56.78, 67.65, 112.33, 118.23, 118.52, 119.11, 121.99, 127.61, 127.93, 133.50, 135.21, 140.22, 142.59, 150.71, 155.76, 157.16, 173.64. HR-MS (ESI) theoretical $[M]^+$ = 733.2505, found $[M]^+$ = 733.2515.

2.2.2 Linear Photophysical and Photochemical Characterization

A 200 μM stock solution of **BAPBO-3** in MeOH was prepared, and 75 μL was added to a cuvette containing 2.925 mL of buffer (Calcium Calibration Buffer Kit #1, which contains 30 mM MOPS/KOH, pH 7.2, 100 mM KCl and 10 mM EGTA or 10 mM CaEGTA) at Ca^{2+} concentrations (0 and 39 μM). The linear absorption spectra were obtained using an Agilent 8453 UV−vis spectrophotometer in 10 mm path length quartz cuvettes in buffers containing different concentrations of Ca^{2+}, with a C = 1.0 μM molar concentration of **BAPBO-3**. The steady-state fluorescence was measured with a PTI QuantaMaster spectrofluorimeter using 10 mm spectrofluorometric quartz cuvettes in buffers containing different concentrations of Ca^{2+}, with a C = 1.0 μM molar concentration of *BAPBO-3*. The correction for the spectral response of the PTI detection system was performed for all fluorescence spectra.

2.3 Results and Discussion

2.3.1 Synthesis

BAPTA, **BAP-HY**, and **BO-3** were prepared according to literature[81-83] and the resulting NMR spectra were consistent with the reported data. A Knoevenagel condensation was applied to produce **BAPBO-3** by conjugation of **BAP-HY** and **BO-3** via an alkene linker. DMF/toluene solution was employed as the solvent to ensure the solubility of **BAP-HY** (Scheme 2).

Hydrolysis was performed before condensation rather than enrolled as a last step to avoid possible breakage of a C=C (double bond). Actually, there are few BAPTA and BODIPY-based compounds with acetylene or alkene linkers reported so far, since the hydrolysis process of BAPTA was usually accomplished with bases like NaOH or K_2CO_3, which may cause bond breakage in most cases. A 14% yield was achieved after purification and the ^{1}H NMR, ^{13}C NMR, and HR-MS spectra were in good accordance with the chemical structure.

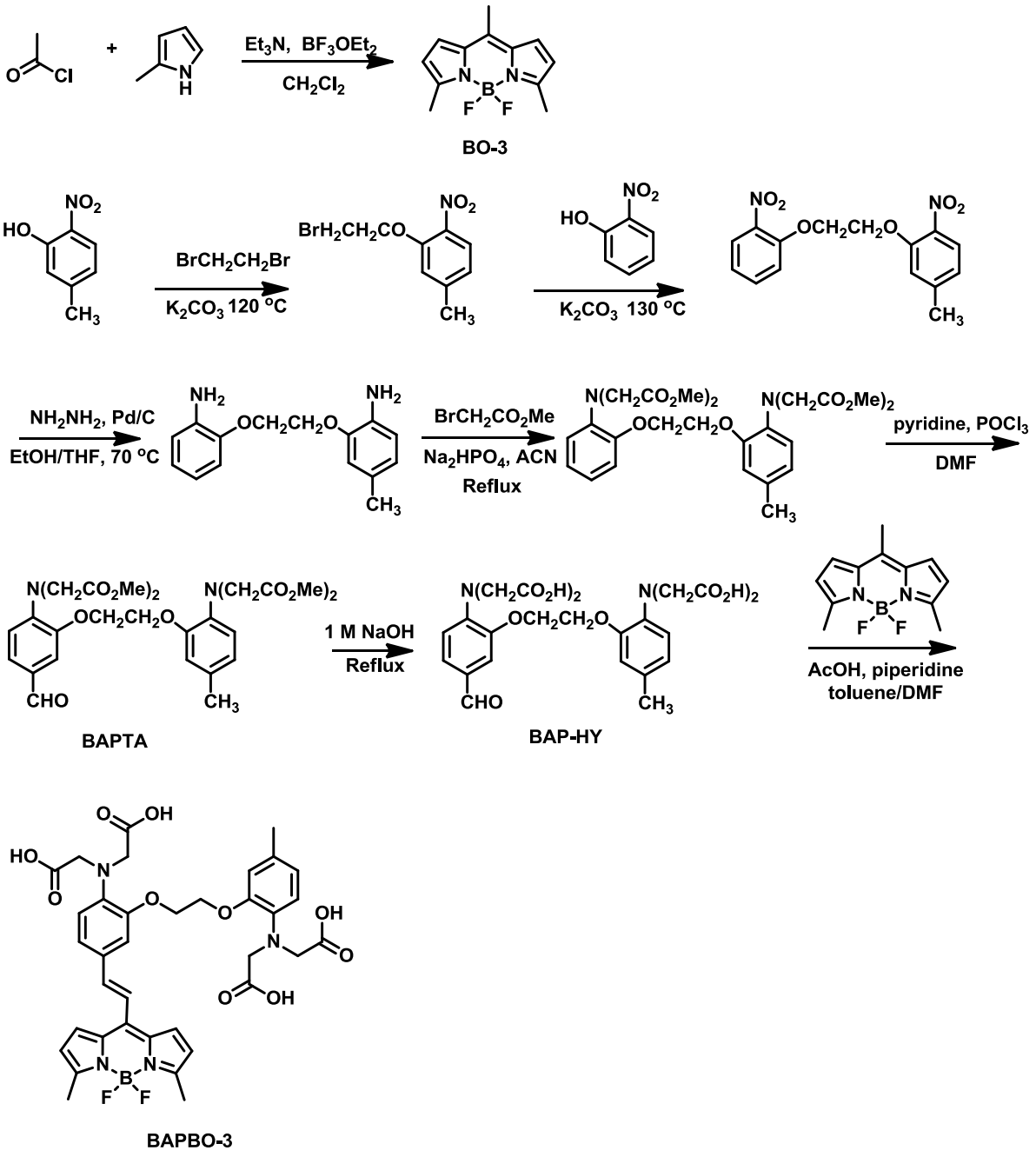

Scheme 2. Synthetic route of **BAPBO-3**

2.3.2 Linear Photophysical and Photochemical Properties

Upon excitation at 475 nm, the emission maximum of **BAPBO-3** was determined to be 527 nm, and 1.5-fold fluorescence enhancement upon Ca^{2+} binding (in solution containig 39 μM free Ca^{2+}) was observed without any significant changes in the absorption spectrum. The fluorescence quantum yield, Φ_f, was calculated to be $0.04 \pm 2.22 \times 10^{-3}$. However, when the buffer solution contained 1 M Ca^{2+}, a 3-fold fluorescence enhancement was observed together with a Φ_f of $0.07 \pm 3 \times 10^{-3}$. Apparently with a higher concentration of Ca^{2+}, increased Φ_f can be obtained.

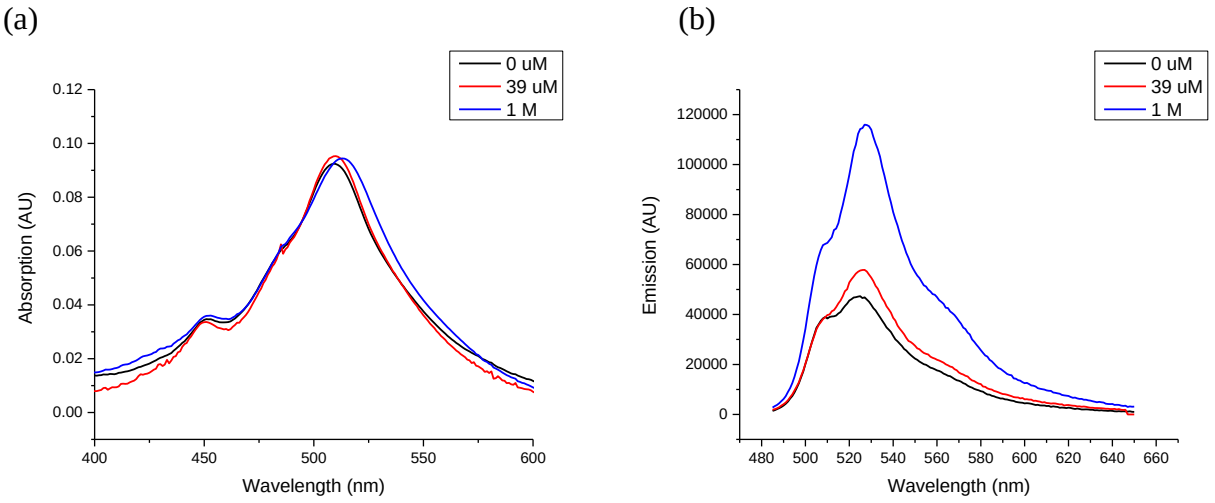

Figure 20. Absorption (a) and emission (b) spectra of **BAPBO-3** in buffers (30 mM MOPS/KOH, pH 7.2, 100 mM KCl and 10 mM EGTA or 10 mM CaEGTA) at different Ca^{2+} concentrations (0, 39 μM and 1 M).

2.4 Conclusion and Future Work

In summary, a new BAPTA and BODIPY based Ca^{2+} probe, **BAPBO-3** was prepared via Knoevenagel condensation. Synthesis and purification were simplified by a new synthetic route.

Upon excitation, a 1.5-fold fluorescence enhancement was obtained for **BAPBO-3** in buffer containing 39 μM Ca^{2+} together with a Φ_f of 0.04, while a 3-fold fluorescence enhancement was observed in buffer containing 1 M Ca^{2+} with a Φ_f of 0.07.

The fluorescence enhancement upon Ca^{2+} binding and overall fluorescence were modest. Thus, to work towards a more practical probe, modification of the molecular structure should be pursued. One possibility is introducing bulky groups to the BODIPY chromophore, by which the phenyl ring can be twisted out of the BODIPY plane, attenutaing fluorescence quenching that occurs through nonradiative pathways.[84] Second, the hydrophilicity needs to be considered after introducing such bulky groups, so that the stacking (aggregation) of the fluorophore can be avoided [85] and the original fluorescence of the compound can be preserved. Third, the PET process is not only affected by the electron-donating ability of receptor sites (binding form of BAPTA in this case), but also the reduction potential and excitation energy of the fluorophore. Attaching various substituents at the 2- and 6-positions of the BODIPY core to make the reduction potential more negative and lower the excitation energy can be considered. Although a certain amount of substituents is required to test for preferred features, it is still worth trying. Additional synthetic possibilities for chemical modification mentioned above are available. One strategy involves performing iodination of the 2- and 6-positions of the BOIDPY core, followed by a Heck reaction or a Sonogashira cross-coupling to conjugate specific groups to the structure.

Since longer absorption and emission wavelengths are preferred and water-soluble probes are attractive, designing an unsymmetrical probe is quite interesting. By conjugating hydrophilic

derivatives at one side of the BODIPY core and the other side functionalized by a chromophore that shifts absorption and emission spectra to longer wavelengths, the requirements mentioned above may be fulfilled.

Not only a water-soluble compound is needed, a cell membrane-permeable probe is also required for most biological applications. At the same time, good retention inside cells also needs to be considered. This may be accomplished by utilizing BAP-AM (1,2-bis(2-aminophenoxy)ethane-N,N,N′,N′-tetraacetic acid tetrakis(acetoxymethyl ester)). The acetoxymethyl ester groups of BAP-AM can help probes diffuse into cells and then these ester groups can be hydrolyzed by an enzyme, esterase, inside cells preventing diffusion back out of the cell. Even though purification and characterization is more difficult for compounds based on BAP-AM when compared to the one based on BAPTA with methyl or ethyl esters, from cell membrane penetration considerations to achieve better *in vitro* images, BAP-AM is worth investigating.

The ground state dissociation constant K_d is another value that can be calculated for a calcium sensor. K_d can be determined via direct fluorometric titration. For the complex PX_n, steady-state fluorescence intensity F recorded as a function of concentration of analyte [X] yields eq 1[86],

$$\boldsymbol{F} = \frac{\boldsymbol{F}_{\mathbf{min}}\boldsymbol{K}_{\mathbf{d}} + \boldsymbol{F}_{\mathbf{max}}[\boldsymbol{X}]^{\mathbf{n}}}{\boldsymbol{K}_{\mathbf{d}} + [\boldsymbol{X}]^{\mathbf{n}}} \quad (1)$$

where F stands for the fluorescence intensity at [X], while F_{min} and F_{max} are the fluorescence intensities at minimal [X] (in the absence of analyte X) and maximal [X] (in the presence of an excess of X).

After rearranging eq 1 in the form of log-log plot, an equation for a Hill plot[87] is given below:

$$\log \frac{F - F_{min}}{F_{max} - F} = n \log[X] - \log K_d \quad (2)$$

and linear behavior is expected with binding n, as its slope, and intercept of -log K_d. The corresponding K_d can then be calculated.

Another aspect for further development of **BAPBO-3** is attaching a protein specific tag so that a targeted calcium indicator can be formed. Compounds conjugating RGD peptide for deep *ex vivo* imaging of tumor vasculature have been reported by our research group previously.[59] With a targeted calcium indicator, molecular imaging of nerve morphology and calcium transients should be more easily obtained.

CHAPTER 3. A NEAR-INFRARED SQUARAINE DYE FOR *IN VITRO* APPLICATION

3.1 Introduction

Interesting squaraine dyes were extensively studied after being first synthesized in the 1960s.[88, 89]. With two donor groups conjugated to an oxocyclobutenolate acceptor core (D−A−D), a highly resonance stabilized zwitterionic structure is yielded. Excellent visible red and/or near-IR absorption and emission wavelengths facilitate applications covering various fields.[90-92] Since this long-wavelength region can avoid the self-absorption and self-fluorescence region of biological media, squaraine dyes can serve as bioimaging materials,[93-99] biomolecule labels,[93, 100-106] and photosensitizers for photodynamic therapy (PDT).[96, 107] Other studies associated with pH indicators,[108] solar cell dyes,[109, 110] nonlinear optical chromophores,[111, 112] and colorimetric sensors[113-115] were also developed over the past few decades. In addition, due to the rigid and planar conjugation structure, aggregation behavior is usually observed for squaraine dyes, while related physical properties[116-121] have also been investigated.

Since two electron-donating groups can be conjugated to the oxocyclobutenolate core, symmetrical and unsymmetrical squaraines can be yielded. The synthesis of symmetrical squarianes is quite straightforward, in which two equivalents of electron-rich aromatic or

heterocyclic compounds and one equivalent of squaric acid are involved and a relative high yield can be obtained.

However, more complicated synthetic routes are expected for unsymmetrical squaraines with different electron-donating groups on each side. Generally speaking, two synthetic routes can afford unsymmetrical squaraine dyes, but both of them require synthesis and separation of the semi-squaraine intermediate. Starting from squaric acid, one of the strategies is conversion of the hydroxyl groups to chlorides, while the other one is generating esters from hydroxyl groups. For the first route, one equivalent of activated electron donor can be conjugated to the core after conversion by nucleophilic attack, followed by hydrolysis of the semi-squaraine. Then the obtained compound is allowed to react with another donor to yield the final structure.

For the second route, more reactive N-alkylated heterocyclic structures function as donors for unsymmetrical squaraine dyes. After converting hydroxyl groups to ester groups, squaric acid derivatives react with activated heterocyclic compounds in a 1:1 molar ratio, resulting in the semi-squaraine. Then another half heterocyclic moiety can be introduced, finally yielding the unsymmetrical product after laborious isolation and purification. [122-125]

Merits are gained when developing near-IR probes. For example, photodamage and phototoxicity caused by UV and visible light excitation can be circumvented. By adjusting donor moieties and increasing π-conjugation systems, optimized squaraines can cover absorption wavelengths from 550 to 850 nm,[112, 126] with high molar extinction coefficients ($\varepsilon > 10^5$ L

mol^{-1} cm^{-1}).[127] In addition, squaraine dyes possess moderate fluorescent quantum yields (Φ_f) in organic solvents in the wavelength range of 650 - 850 nm[128] and a Stokes shift of 10–30 nm.

Squaraines are also potential candidates for two-photon absorption (2PA) research. After a 5000 GM (Goppert-Mayer units, 1×10^{-50} cm^4 s $photon^{-1}$ $molecules^{-1}$)[129] two-photon absorption cross-section (δ_{2PA}) was reported, scientists discovered that increased δ_{2PA} of squaraines can be achieved by extending the π-conjugation. Indeed, Marder *et al*. reported δ2PA values as high as 30,000 GM in THF by adding more pyrrole and benzene derivatives to the structure.[130] Our interest lies in application of squaraine dyes in advanced photonic materials. An example of a squaraine we have developed is shown in Figure 21, along with its linear and nonlinear absorption spectra. As a pyrrolium squaraine dye, **SQ 1** gains extended π-conjugation, and ~20,000 GM δ2PA value in DMSO was obtained.[99]

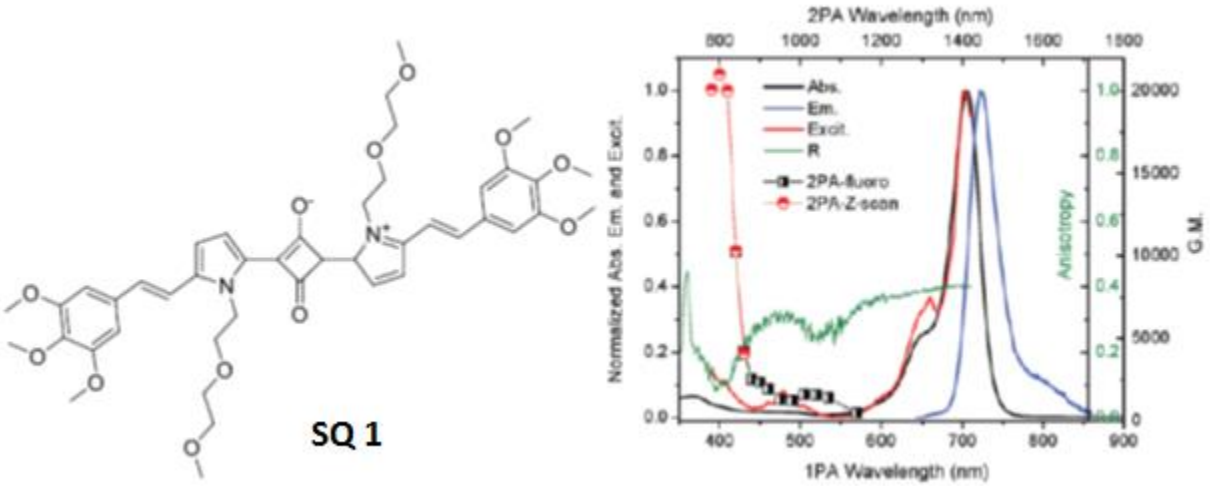

Figure 21. Structure of **SQ 1** and it is linear and nonlinear absorption spectra. Ref 99, copyright 2011 American Chemical Society.

Herein, we report a newly designed squaraine dye **SQ3**. Unlike two unsymmetrical squaraine synthetic routes mentioned above, we employed a one-pot synthesis so that the separation of the semi-squaraine can be avoided. Two different activated heterocyclic compounds were added to the condensation reaction in a 1:1 ratio, and a 10% yield was obtained after purification. Photophyscial characterization was conducted in various solvents. In DMSO, an absorption maximum at 678 nm was observed. Upon excitation, a 692 nm emission maximum was obtained and the calculated fluorescence quantum yield was determined to be 0.32. Near-IR absorption and emission suggest this new compound *SQ3* is favorable for *in vitro* and *in vivo* study, which was later confirmed by *in vitro* bioimaging.

3.2 Materials and Methods

3.2.1 Synthesis

Synthetic reagents and solvents were used as received from commercial suppliers. All chemicals were purchased from Sigma-Aldrich or Fisher. ^{1}H and ^{13}C NMR spectra were recorded on a Bruker Avance 400 NMR spectrometer at 400 and 101 MHz, respectively. High-resolution mass spectrometry analysis was performed at the Department of Chemistry, University of Florida.

3-(4-Iodobutyl)-2-methylbenzothiazol-3-ium iodide (**1**) was prepared as previously reported.[131] A mixture of 2-methylbenzothiazole (0.27 mL, 2.18 mmol) and 1,4-diiodobutane (0.57 mL, 4.36 mmol) in 5 mL acetonitrile was added to a 15-ml microwave vial. The mixture was heated in microwave reactor (CEM Discover model) at 140 ℃ for 2.5 hours. A pale yellow solid was

obtained after precipitation with diethyl ether, filtered off, and washed with isopropyl alcohol and diethyl ether. The yield was 0.47 g (47%): mp 196−198 °C (dec.); ^{1}H NMR (DMSO-d6, 500 MHz) δ: 8.45 (d, 1H), 8.34 (d, 1H), 7.92 (td, 1H), 7.80 (td, 1H), 4.77 (t, 2H), 3.33 (t, 2H), 3.20 (s, 3H), 1.95 (m, 4H).

3-Octadecyl-2-methylbenzothiazol-3-ium iodide (**2**) was prepared by a literature method.[132-134] 1-Iodooctadecane (1.00 g, 2.63 mmol) and 2-methylbenzothiazole (0.17 mL, 1.31 mmol) in 5 ml acetonitrile was added to a 15-ml microwave vial. The mixture was heated in microwave reactor (CEM Discover model) at 140 ℃ for 4 hours. The white precipitate was filtered after the reaction and recrystallized with acetonitrile twice. The yield was 0.24 g (35%): mp 129-131 ℃ (liter. m.p. 116-118^{o}C) [3]; ^{1}H NMR ($CDCl_3$, 500 MHz) δ: 8.34 (d, 1H), 8.00 (d, 1H), 7.85 (td, 1H), 7.71 (td, 1H), 4.85 (t, 2H), 3.48 (s, 3H), 1.96 (m, 2H), 1.49 (m, 2H), 1.25 (m, 30H), 0.88(t, 3H). ^{13}C NMR ($CDCl_3$, 500 MHz) δ: 175.04, 140.98, 129.95, 129.15, 128.64, 124.84, 116.46, 51.57, 33.59, 31.93, 30.52, 29.7, 29.67, 29.62, 29.59, 29.55, 29.5, 29.43, 29.37, 29.17, 28.73, 28.55, 26.85, 22.7, 19.86, 14.13.

2-((3-Octadecylbenzothiazol-2(3H)-ylidene)methyl)-3-oxo-4-((3-(4-(pyridinium-1-yl)butyl)benzothiazol-3-ium-2-yl)methylene)cyclobut-1-enolate iodide (**SQ3**) was prepared by a one-pot synthesis. In a 50-ml round-bottom flask, added 3-(4-Iodobutyl)-2-methylbenzothiazol-3-ium iodide (1) (0.25g, 0.54 mmol) and 3-Octadecyl-2-methylbenzothiazol-3-ium iodide (2) (0.29g, 0.54 mmol) with 3,4-diethoxycyclobutane-1,2-dione (0.08ml, 0.54 mmol) in 24 ml of n-butanol and 6 ml pyridine. The mixture was refluxed with a Dean-Stark apparatus for 12 hours.

The solvent was evaporated under reduced pressure and crude product was purified by column chromatography using a mixture of methanol and dichloromethane (1:20) as an eluent. The yield was 0.05 g (10%): mp 249-250 ℃ (decomposed); ^{1}H NMR (DMSO-d6, 500 MHz) δ: 9.11(d, 2H), 8.61(t, 1H), 8.17(t, 2H), 7.86(q, 2H), 7.58(d, 1H), 7.52(d, 1H), 7.46(m, 2H), 7.28(m, 2H), 5.79(s, 2H), 4.69(t, 2H), 4.29(q, 4H), 2.10(t, 2H), 1.71(q, 4H), 1.31(t, 2H), 1.21(m, 30H), 0.84(t, 3H).^{13}C NMR (DMSO-d6, 500 MHz) δ: 176.17, 175.33, 159.02,158.33, 146.08, 145.23, 141.46, 141.41, 128.66,128.00, 124.46, 124.29, 122.93, 113.11, 112.72, 85.63, 85.48, 60.69, 45.95, 45.03, 39.99, 39.83, 39.66, 39.49, 31.74, 29.48, 29.34, 29.15, 28.23, 27.35, 26.42, 23.88, 22.54, 14.41. HRMS (ESI) for $C_{47}H_{60}N_3O_2S_2$ theoretical *m/z* [M^+]= 762.4121, found [M^+]=762.4132.

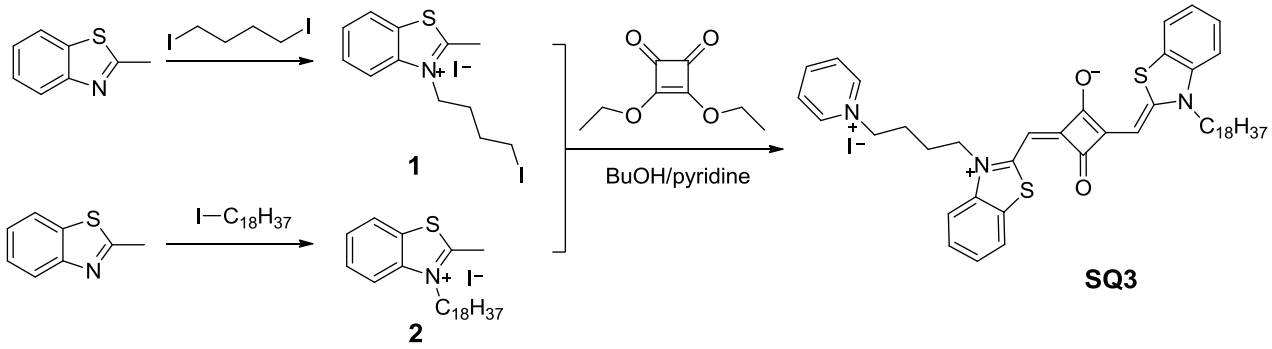

Scheme 3. Synthetic route of **SQ3**.

3.2.2 Linear Photophysical and Photochemical Characterization

The linear absorption spectra were obtained using an Agilent 8453 UV−vis spectrophotometer in 10 mm path length quartz cuvettes in varying. The steady-state fluorescence was measured with a PTI QuantaMaster spectrofluorimeter using 10 mm spectrofluorometric quartz cuvettes. The

correction for the spectral response of the PTI detection system was performed for all fluorescence spectra. The fluorescence quantum yields, Φ_f, were obtained by a standard method [47] relative to cresyl violet in methanol.

3.2.3 *In Vitro* Cell Imaging

Hela cells (ATCC®) were seeded on poly-D-lysine coated coverslips placed into 24-well glass plates (500000 cells per well) and incubated for 48 hours. **SQ3** stock solution in DMSO was then diluted to 20 μM with MEM medium (Corning, Cellgro®) and added into cells. Cells were co-incubated with diluted **SQ3** for 30 min and then fixed with 3.7% formaldehyde. $NaBH_4$ (1 mg/mL) was added twice for 5 min to eliminate auto-fluorescence. The coverslips were then washed with PBS (phosphate buffer saline, Corning, Cellgro®) and mounted on microscope slides with ProLong Gold® antifade reagent (Invitrogen™).

Cell slides were imaged with Olympus IX70 DSU microscope. Tex-Red filter cube (Ex 562/40, DM 593, Em 624/40) was employed to excite **SQ3** and collect the fluorescence at the optimize wavelength range.

3.3 Results and Discussion

3.3.1 Synthesis

A one-pot synthesis was employed as the last step to yield **SQ3** so that purification of the semi-squaraine was avoided. With the goal of developing a near-IR dye, requirements of the extended π-conjugation system were fulfilled by the double bonds formed after the condensation reaction and the benzothiazole part (Scheme 3). Based on the structure, positive charged pyridine derivative was introduced for better cell uptake.

3.3.2 Linear Photophysical and Photochemical Characterization

In Figure 22, absorption and emission spectra of **SQ3** are shown in various solvents. With absorption maxima from 646 nm (dichloromethane) to 678 nm (DMSO), upon excitation, emission maxima varied from 656 nm (dichloromethane) to 692 nm (DMSO) and fluorescence quantum yields were calculated to vary from 0.08 (dichloromethane) to 0.32 (DMSO), together with Stokes shifts drawing in the range of 10-14 nm (Table 3). We believe that aggregation occurred in solvents except DMSO, which leads to decreased fluorescence quantum yields.

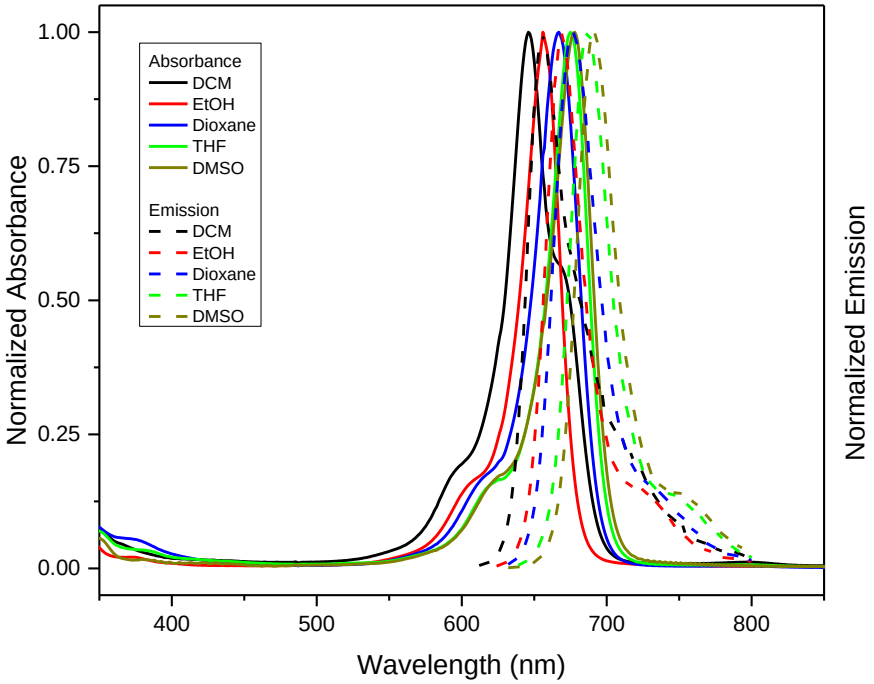

Figure 22. Normalized absorption and emission spectra of *SQ3* in solvents of dichloromethane, ethanol, dioxane, THF, and DMSO.

Table 3. Absorption and Emission Maxima, Fluorescence Quantum Yields and Stokes Shift of SQ3 in Different Solvents

Solvent	λ_{abs} (nm) [a]	λ_{em} (nm) [b]	Φ_f [c]	Stokes shift (nm)
Dichloromethane	670	678	0.08	8
Ethanol	656	669	0.17	13
Dioxane	667	681	0.18	14
THF	674	687	0.16	13
DMSO	678	691	0.32	13

a. maximum absorption peak; b. maximum emission peak; c. fluorescence quantum yield

3.3.3 *In Vitro* Cell Imaging

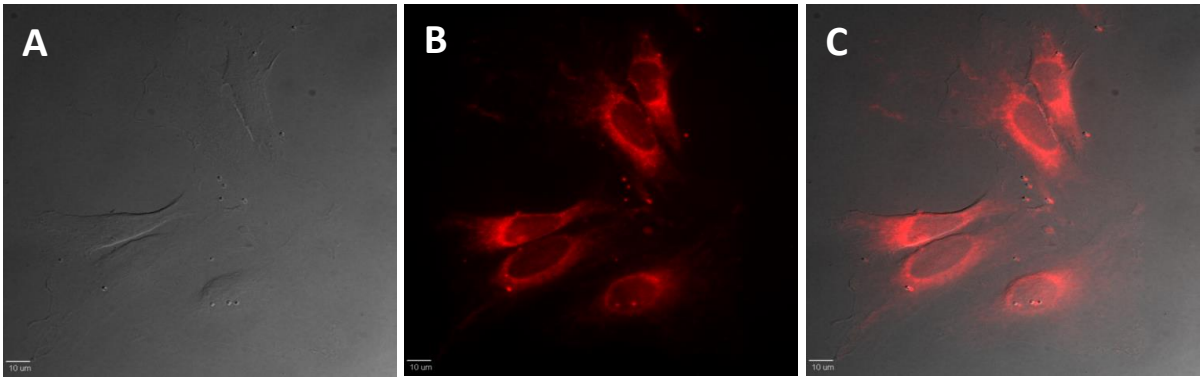

Figure 23. HeLa cells were incubated with **SQ3** (20 μM, 30 min). DIC image (A) indicates healthy morphology of HeLa cells. (B) **SQ3** fluoresence image. Overlay image of **SQ3** fluorescence and DIC (C) indicates effective uptake of **SQ3**. Scale bar shows 10 μm.

Since near-IR absorption and emission were observed for **SQ3**, an *in vitro* study was conducted to demonstrate whether this compound is applicable for bioimaging. After incubation with HeLa cells for 30 min, **SQ3** appeared to readily enter the cells and remarkably clear fluorescence images were obtained (Figure 23). This result suggests that compound **SQ3** is indeed capable of functioning as a near-IR probe.

3.4 Conclusion and Future Work

In summary, a new near-IR unsymmetrical squaraine dye, **SQ3**, was been synthesized by a one-pot synthesis and a 10% yield was obtained after purification. Photophyscial and photochemical characterization was conducted in various solvents to explore possible solvatochromic effects. In DMSO, an absorption maximum at 678 nm was observed, and, upon excitation, a 692 nm

emission maximum was obtained. Fluorescence was relatively efficient with a fluorescence quantum yield of 0.32. The observed near-IR absorption and emission suggested that **SQ3** may be favorable for *in vitro* and *in vivo* study. This was confirmed through incubation with HeLa cells and subsequent *in vitro* imaging, resulting in good apparent cell penetration, little to no interference from autofluorescence, and good contrast, suggesting the future potential in cell and tissue imaging of this novel probe.

Several experiments could be performed and various applications developed in the future. First of all a cell membrane targeting probe can be considered. This requires chemical modification such as introducing longer alkyl chains or farnesyl groups to the structure. Also as mentioned previously, δ2PA is a value worth measuring. With desirable δ2PA, bioimaging can be conducted under 2PA conditions to avoid possible photodamage caused by 1PA experiments and achieve greater depths on tissue.

Another aspect for further development of this newly designed squaraine dye is consideration of its potential as a near-IR viscosity sensor. Since the benzothiazole moiety in the structure plays a typical electron acceptor role in viscosity sensors, if electron donors such as dimethylamine derivatives can be involved in the design, a promising squaraine-based near-IR viscosity sensor will be yielded. Recently, we reported a squaraine-based viscosity sensor utilizing the deoxyuridine as a building block,[43] both TICT and aggregation effects of the squaraine dye yielded a 300-fold fluorescence intensity increase at high viscosity. With cell images being

captured during different stages of mitosis, this new dye comprehensively demonstrated intercellular viscosity was dependent on microtubules (MTs) cross-linking and density.

APPENDIX A: ^{1}H AND ^{13}C, AND MASS SPECTRA OF MOLECULES IN CHAPTER 1

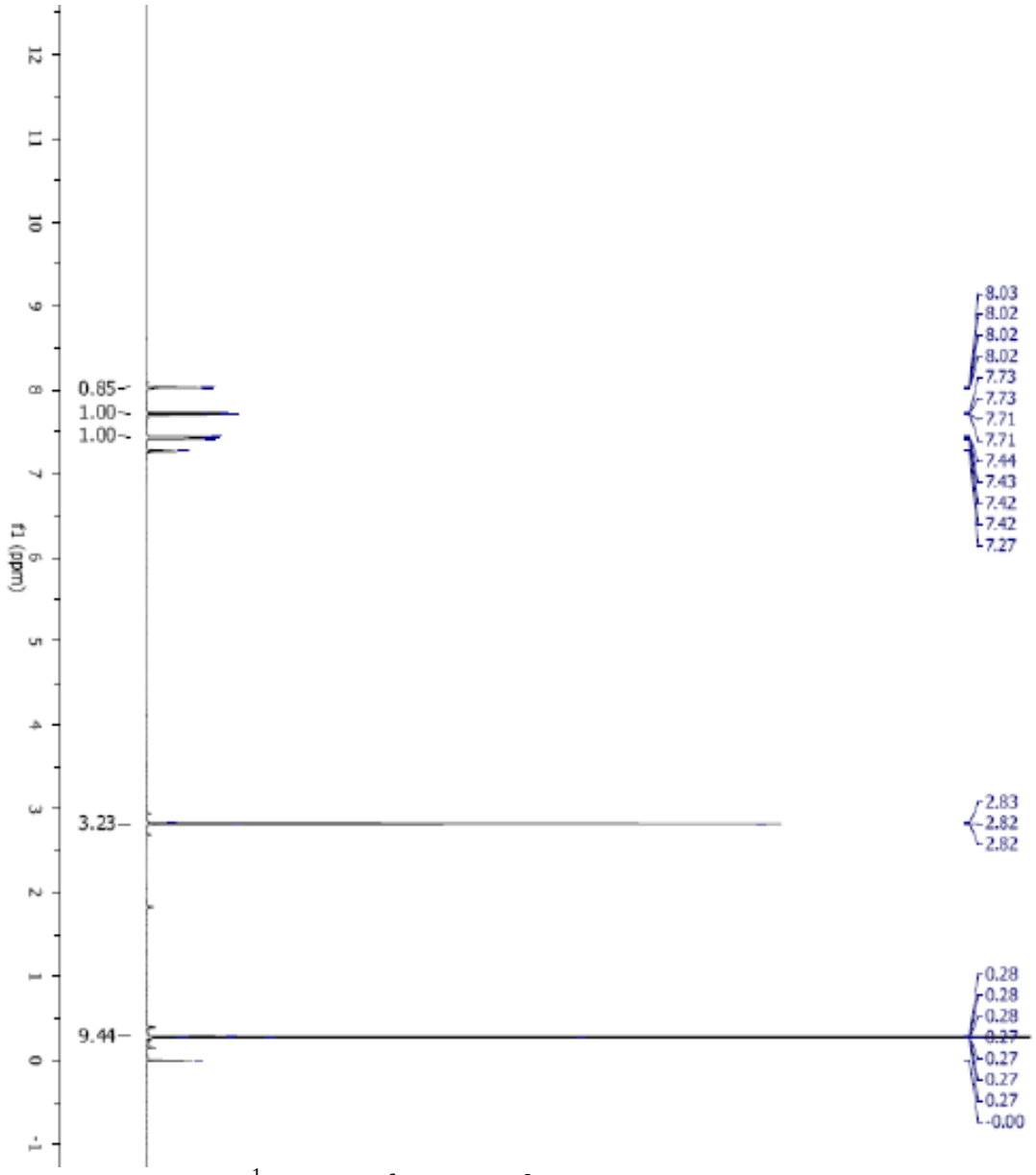

^{1}H NMR of compound **1**

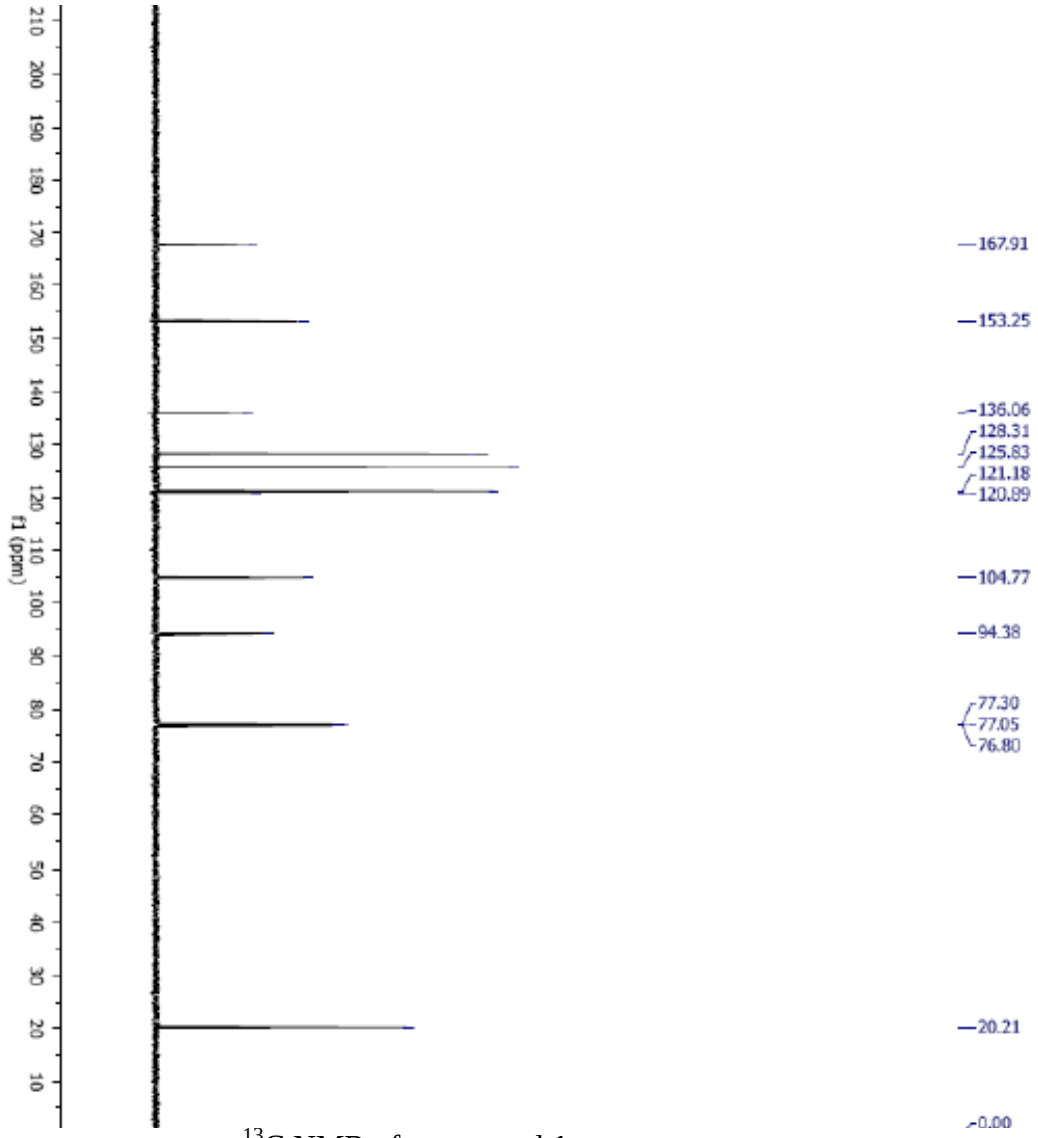

^{13}C NMR of compound **1**

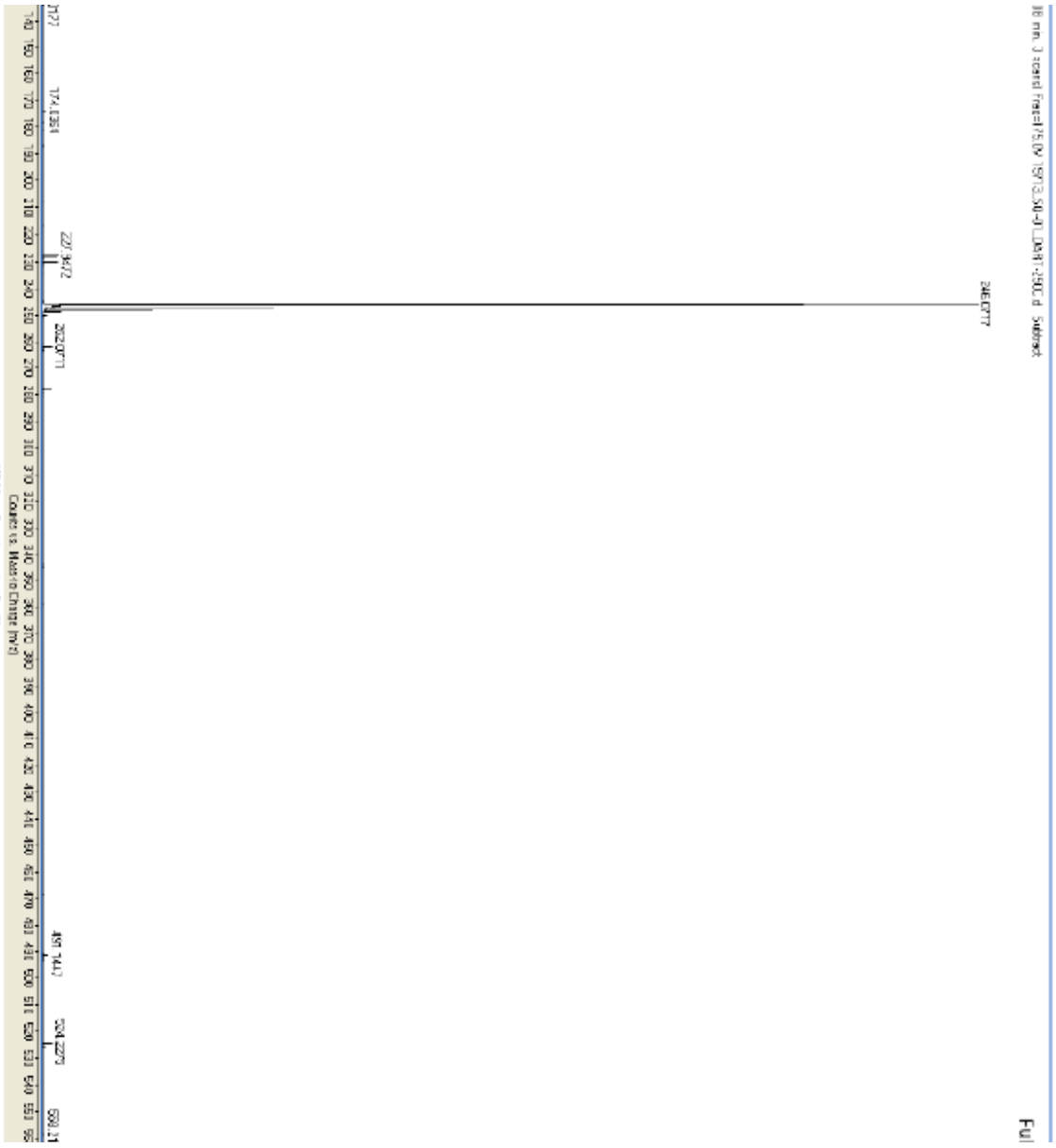

HR MS of compound **1**

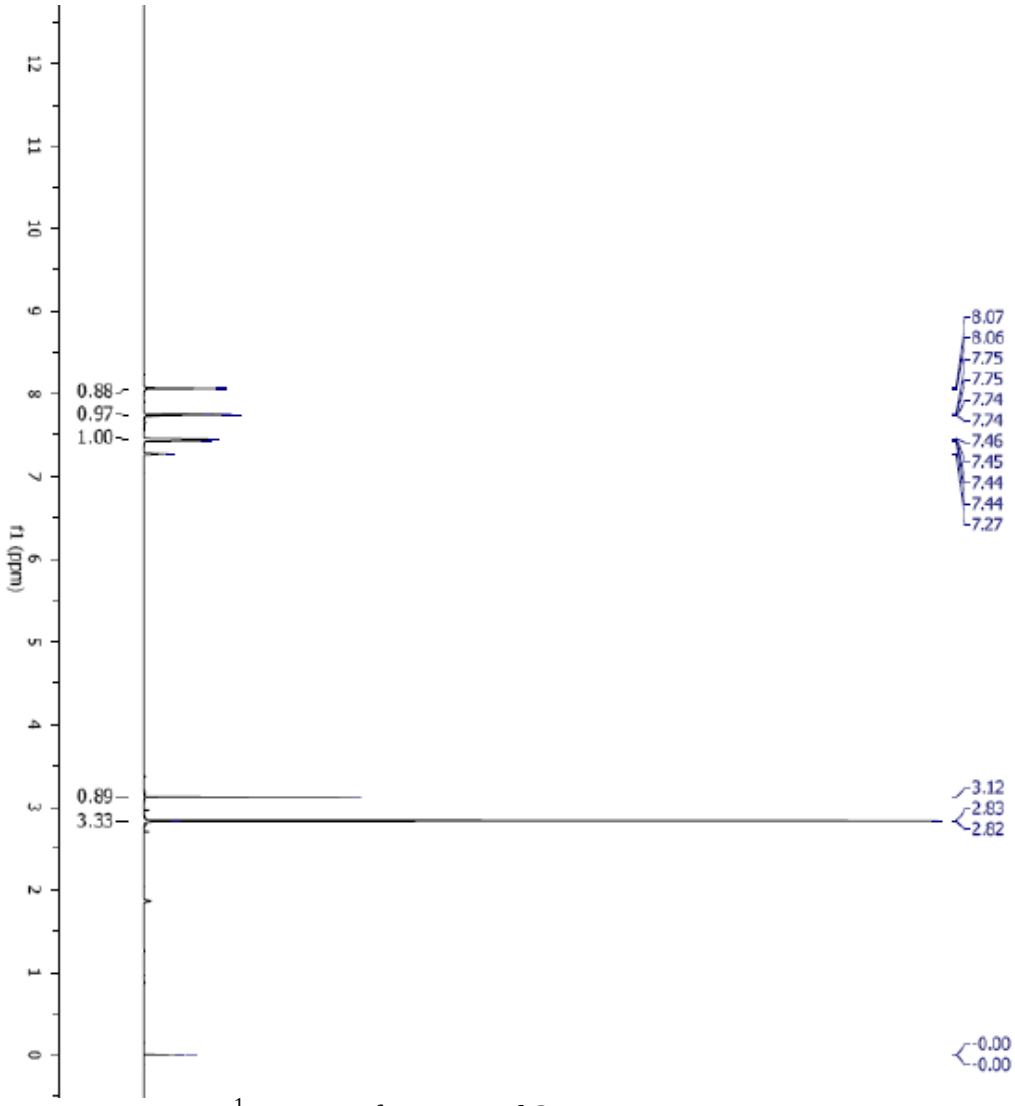

^{1}H NMR of compound **2**

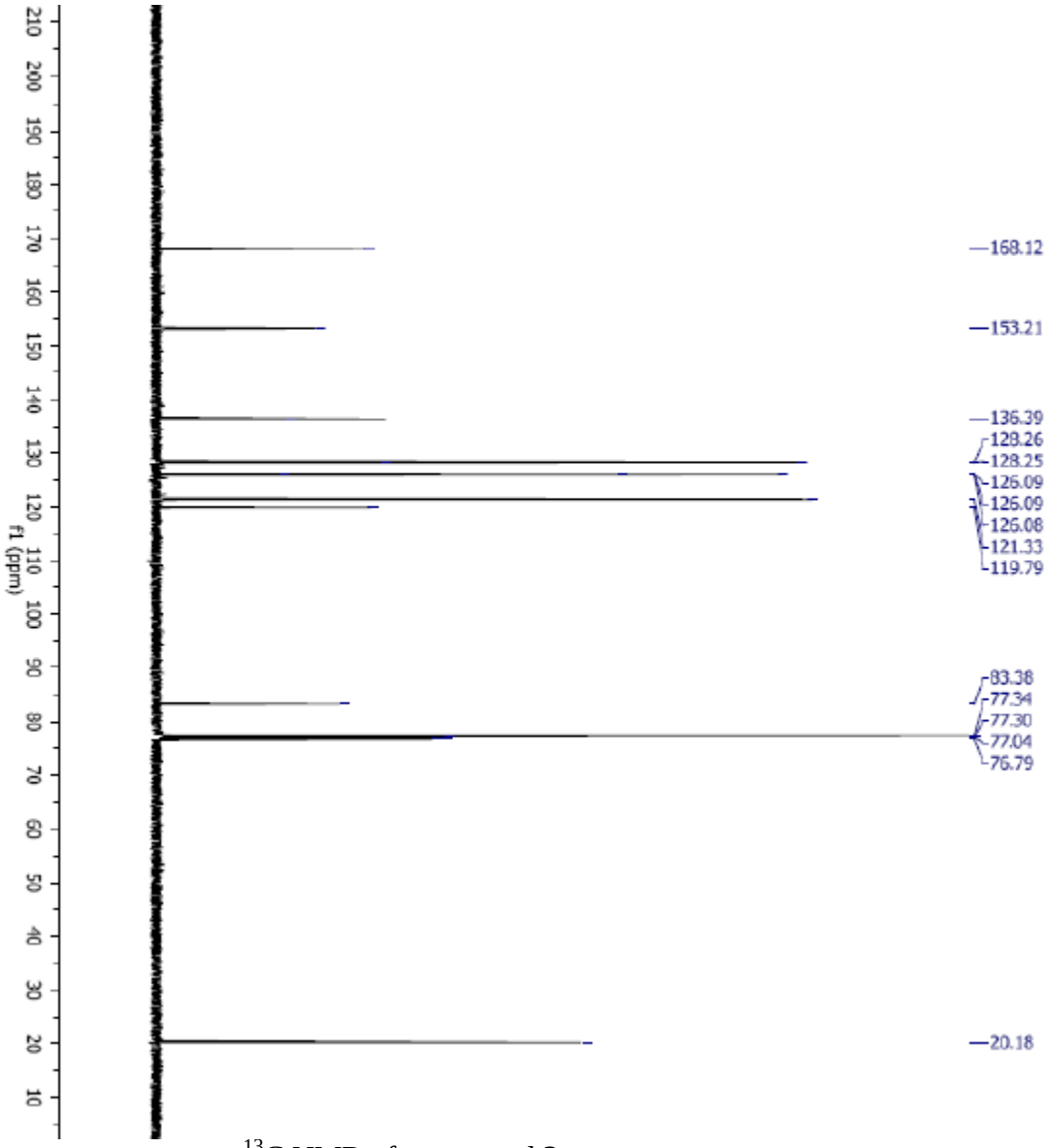

^{13}C NMR of compound **2**

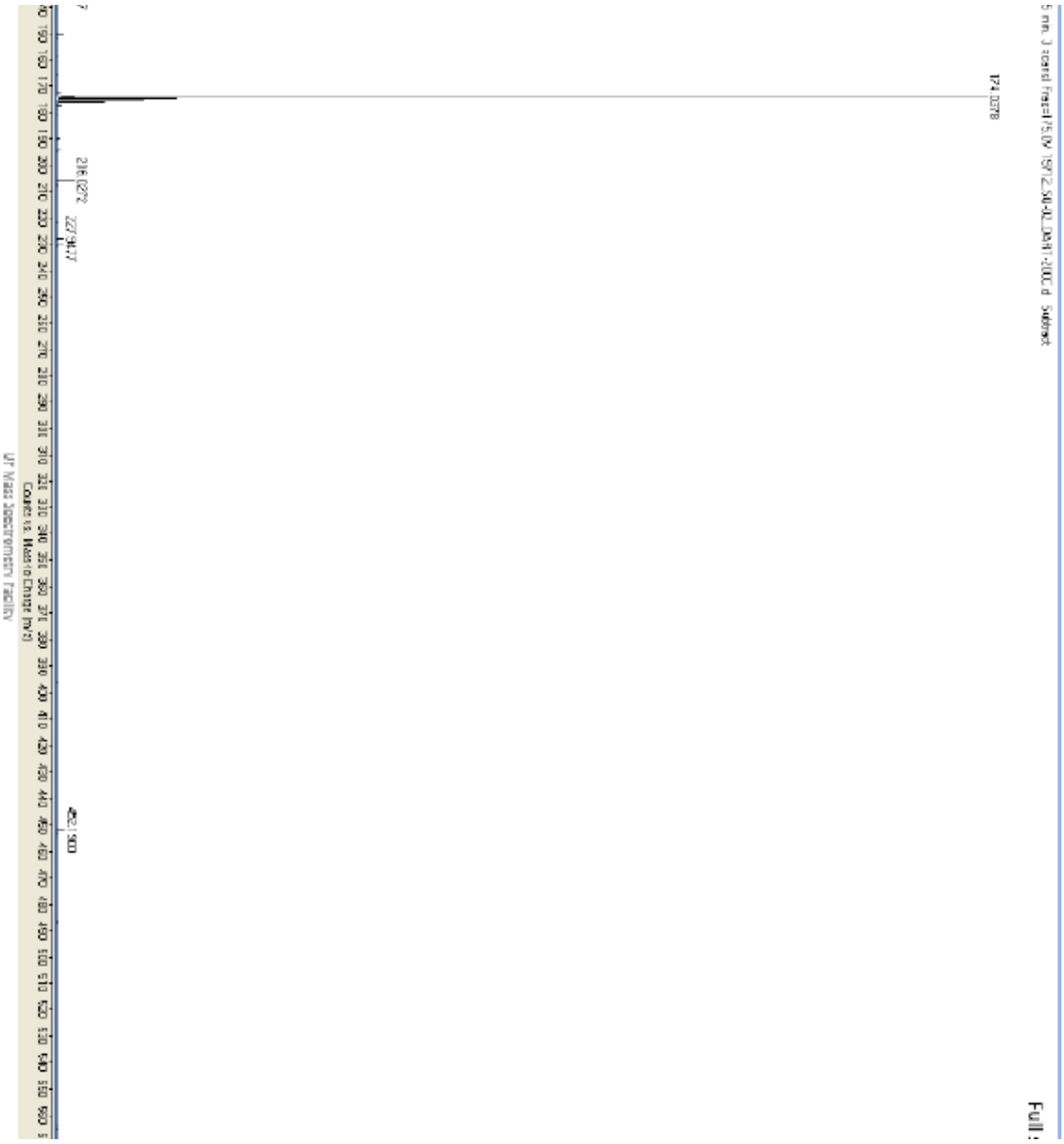

HR MS of compound **2**

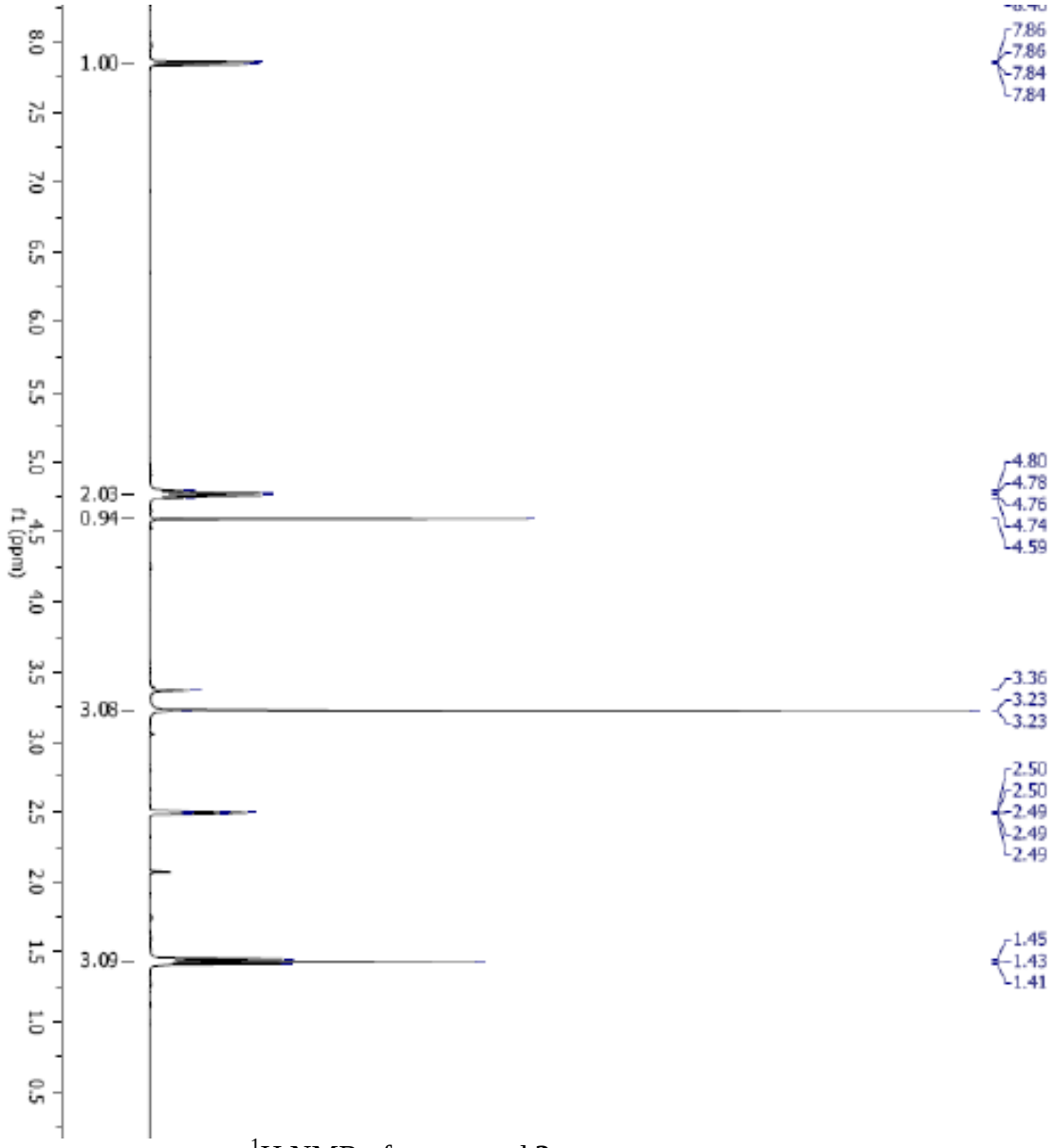

^{1}H NMR of compound **3**

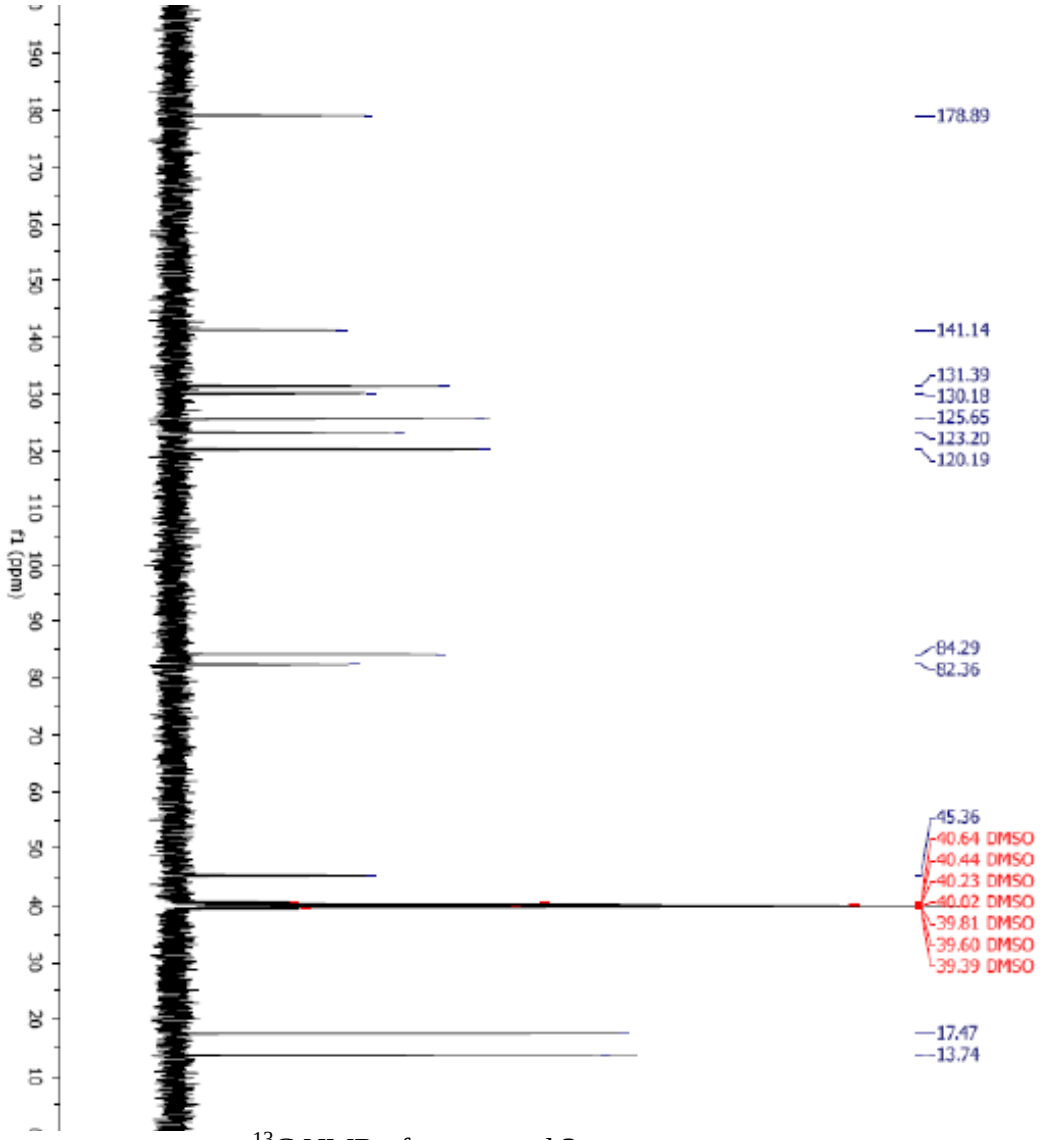

^{13}C NMR of compound **3**

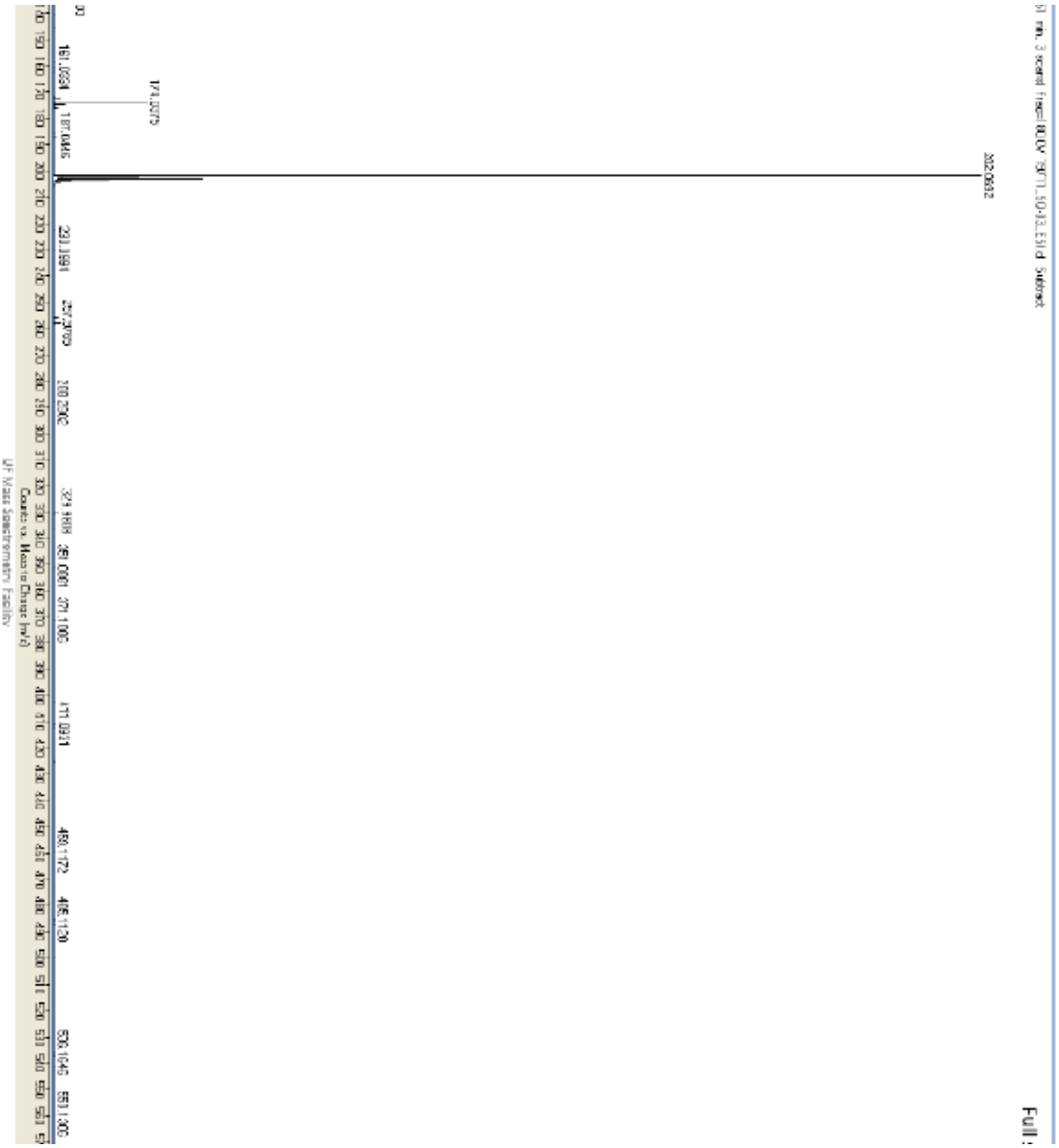

HR MS of compound **3**

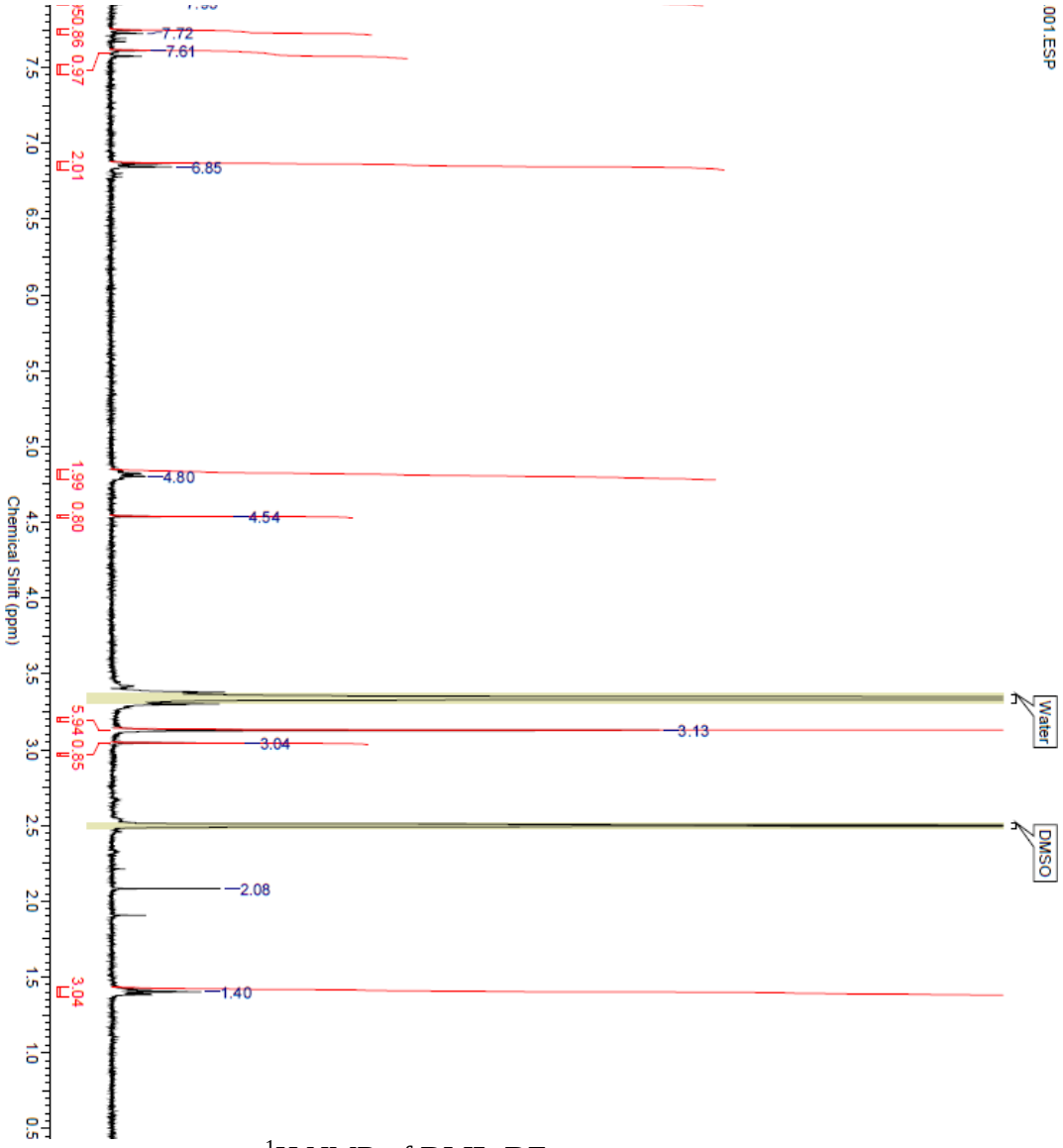

^{1}H NMR of **DML-BZ**

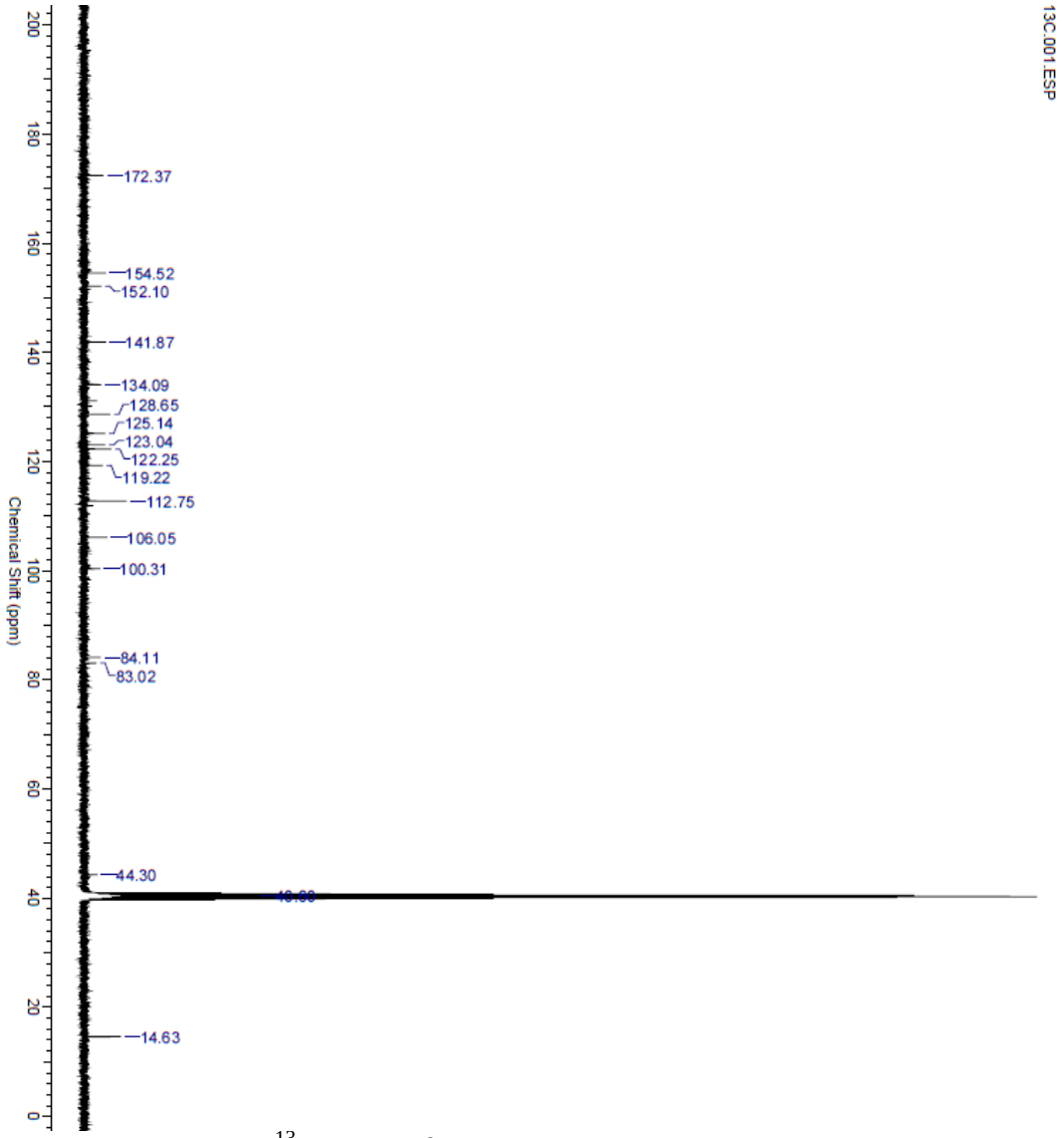

^{13}C NMR of **DML-BZ**

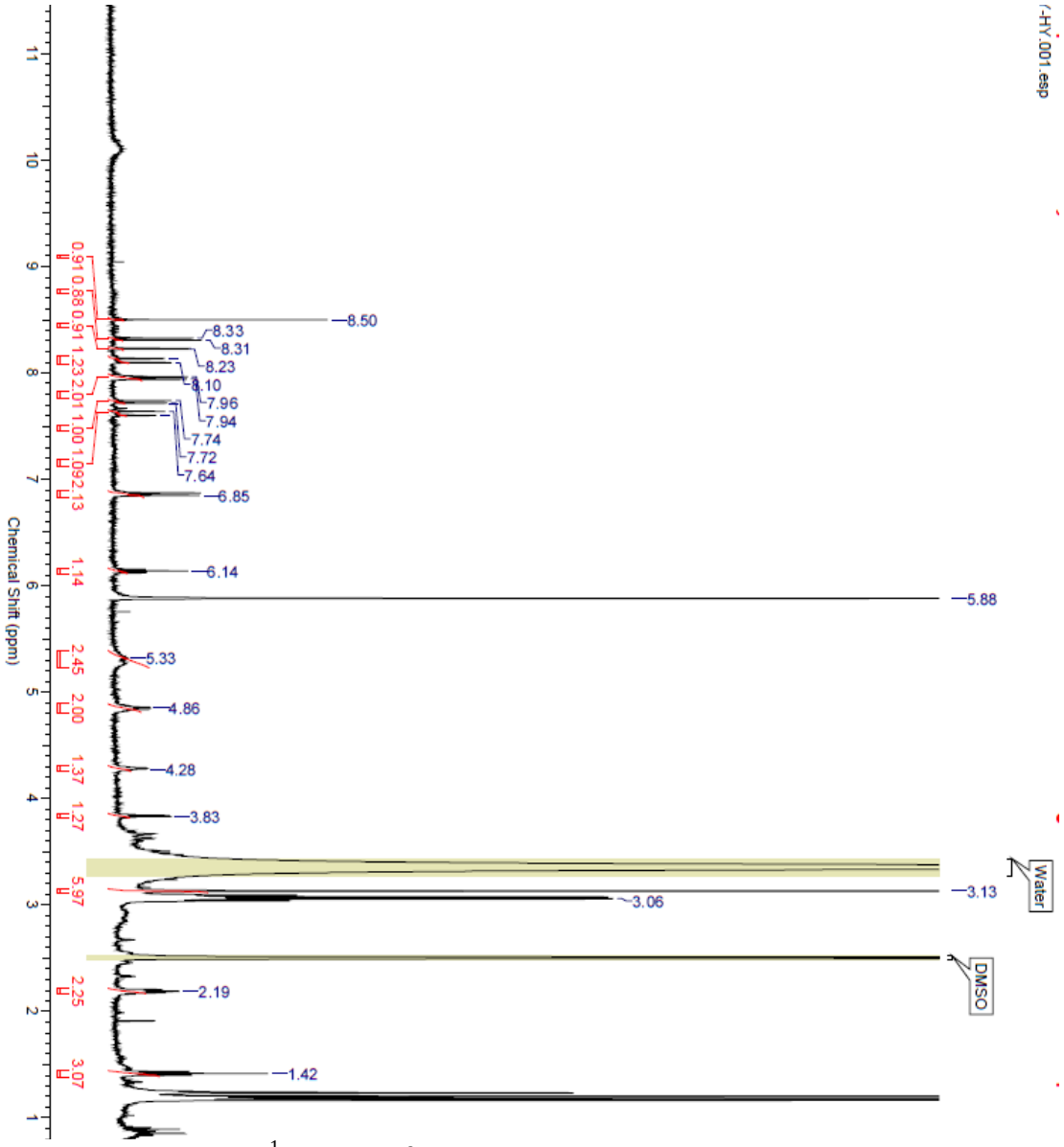

^{1}H NMR of **dU-BZ**

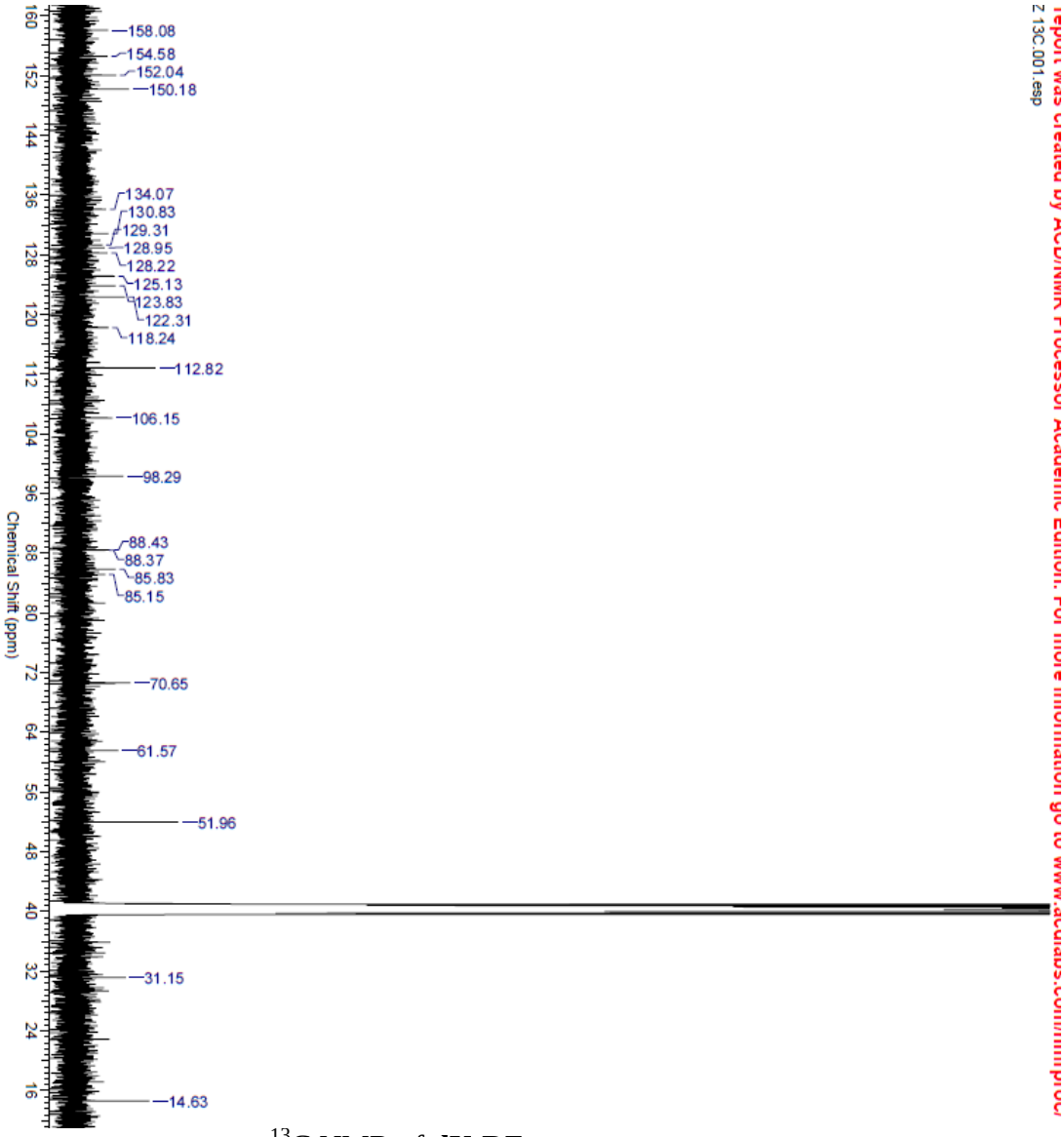

^{13}C NMR of **dU-BZ**

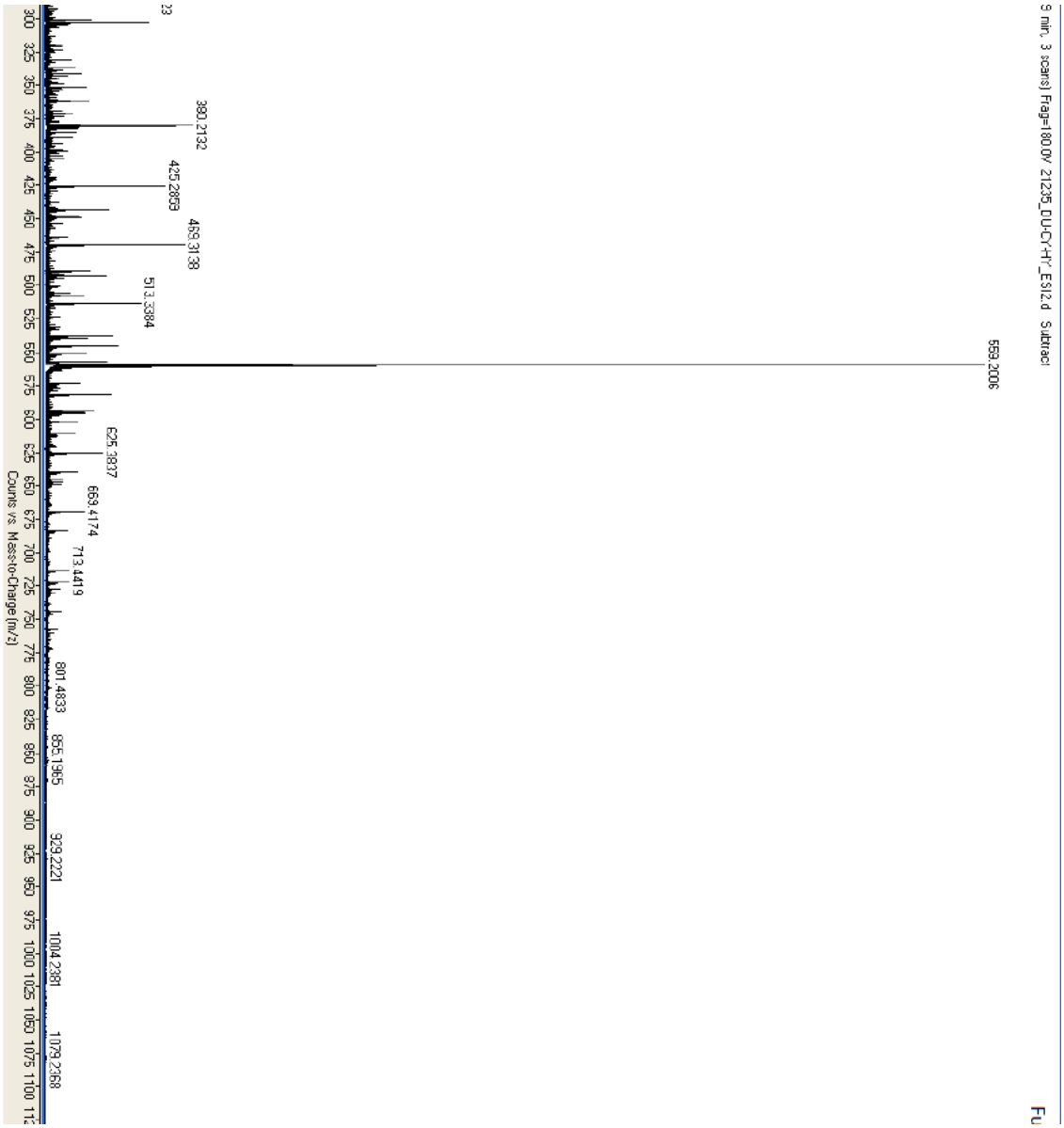
S min, 3 scans) Frag=180.0V 21235_DU-CY-HY_ESI2.d Subtract
559.2006
380.2132
425.2859
469.3138
513.3384
625.3837
663.4174
713.4419
801.4833
855.1965
929.2221
1004.2381
1079.2368
Counts vs. Mass-to-Charge (m/z)

HRMS of **dU-BZ**

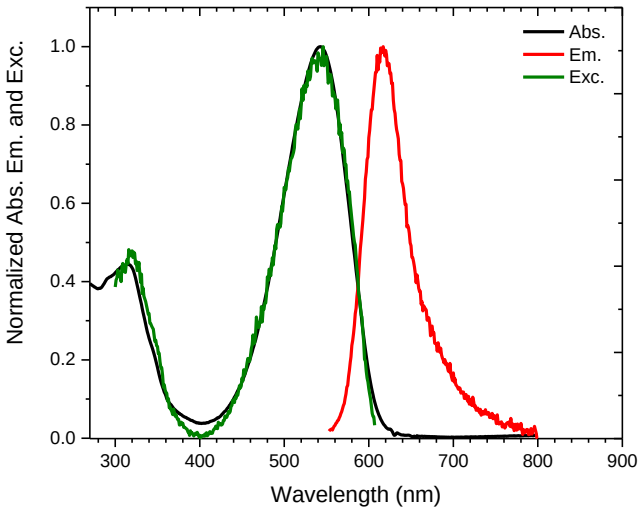

Figure. Absorption, emission and excitation spectra of **dU-BZ** in DMSO

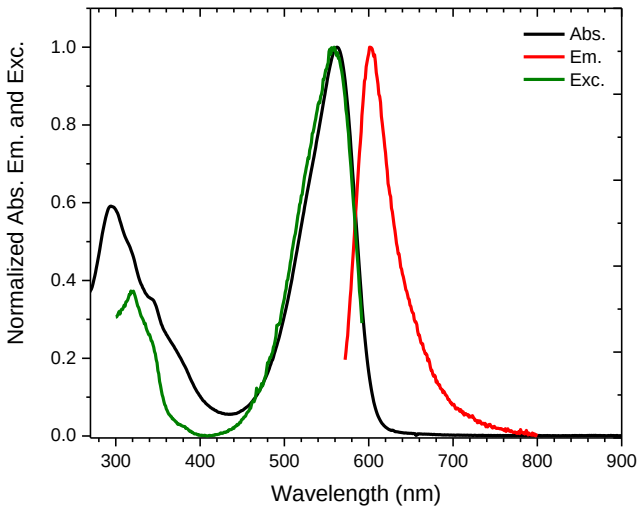

Figure. Absorption, emission and excitation spectra of **dU-BZ** in DCM

Table. Maximum wavelengths of absorption and emission and quantum yields of **dU-BZ** in DMSO and DCM

	dU-BZ	
Solvent	DMSO	DCM
λ_{Abs} (nm)	543 ± 1	562 ± 1
λ_{Em} (nm)	617 ± 1	601 ± 1
Φ_{FL}	0.02 ± 0.002	0.04 ± 0.006

APPENDIX B: ^{1}H AND ^{13}C, AND MASS SPECTRA OF MOLECULES IN CHAPTER 2

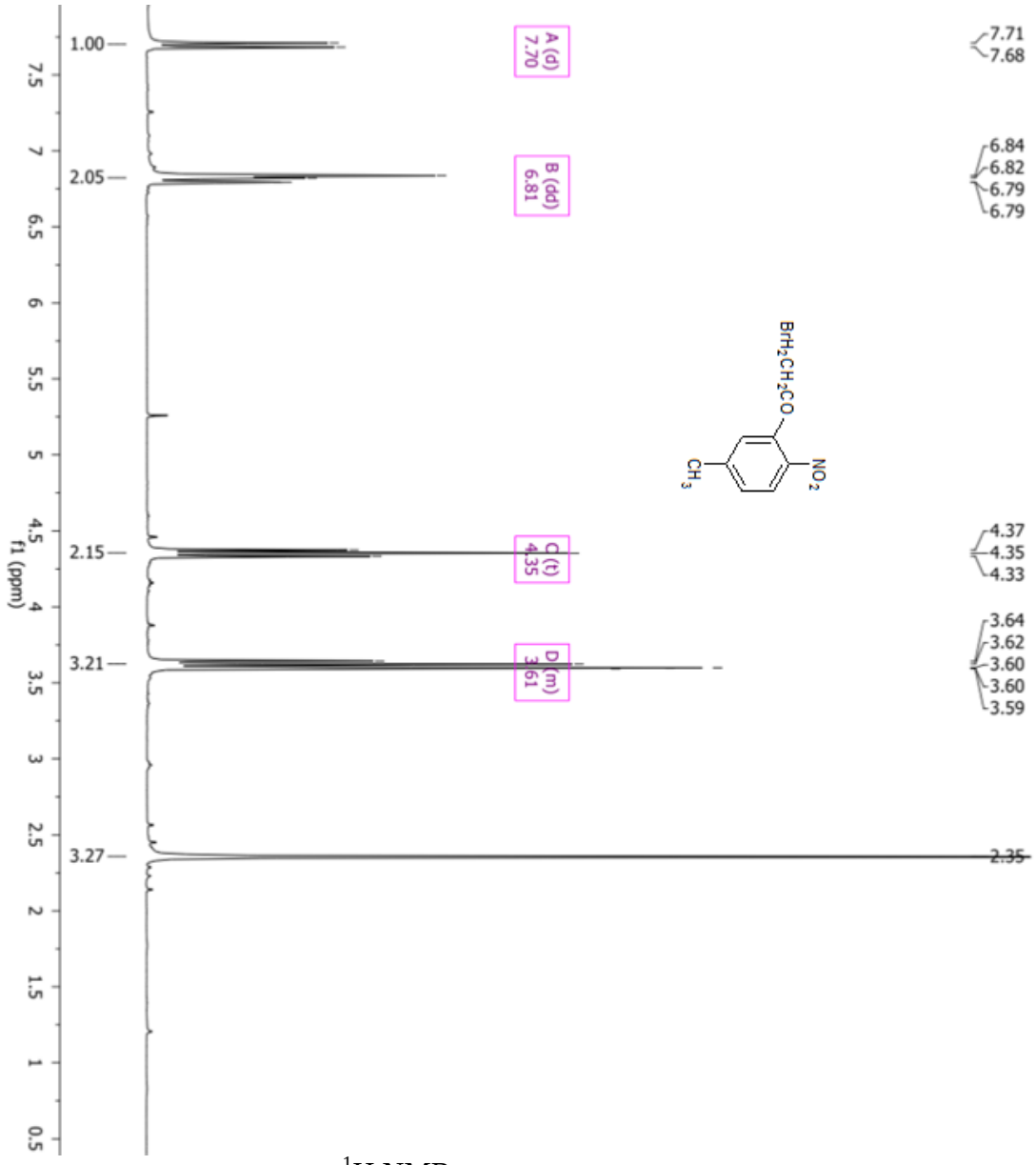
1.00
2.05
2.15
3.21
3.27
A (d) 7.70
B (dd) 6.81
C (t) 4.35
D (m) 3.61
7.71
7.68
6.84
6.82
6.79
6.79
4.37
4.35
4.33
3.64
3.62
3.60
3.60
3.59
2.35
BrH2CH2CO
CH3
NO2
f1 (ppm)

^{1}H NMR

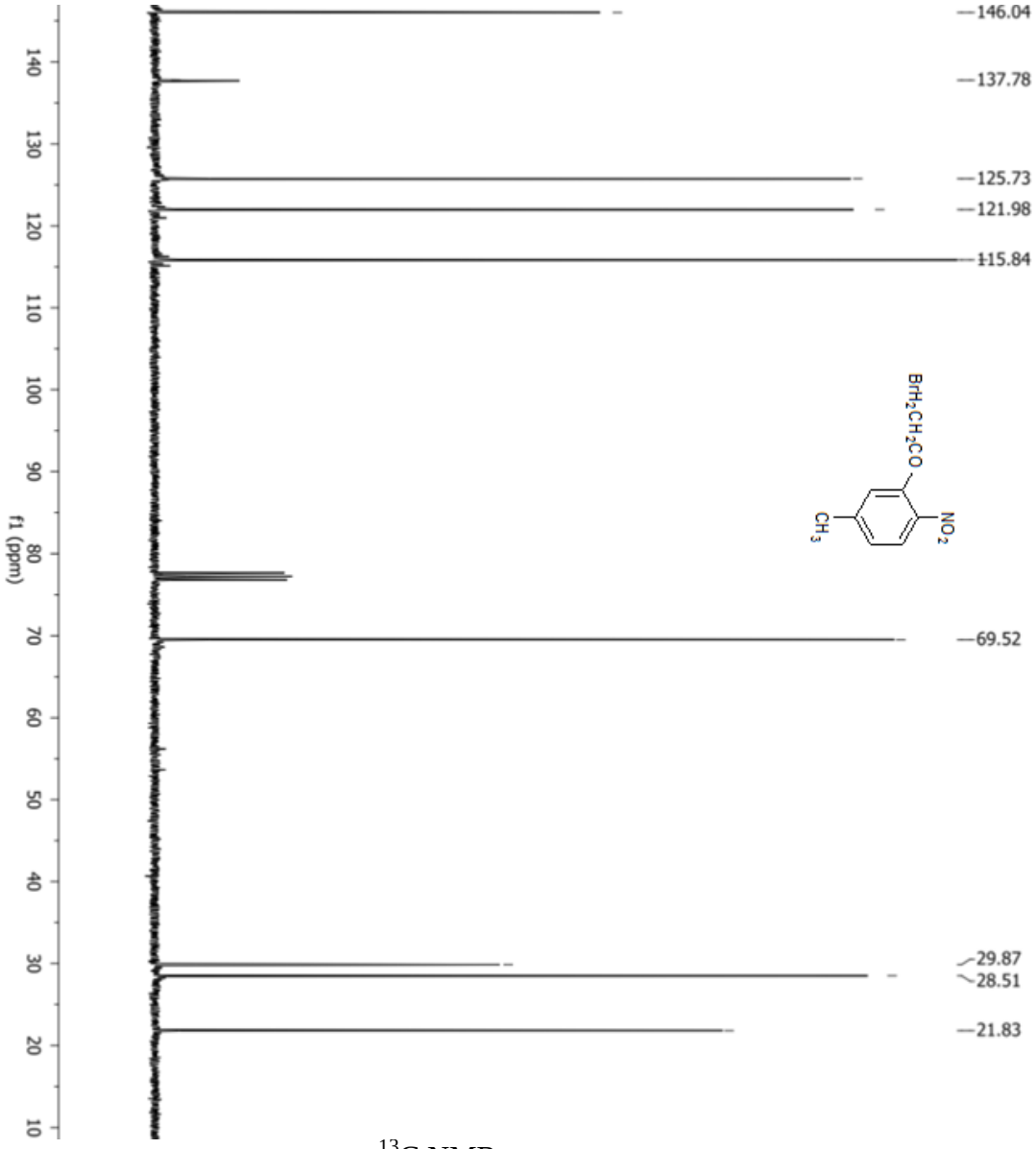
146.04
137.78
125.73
121.98
115.84
69.52
29.87
28.51
21.83
f1 (ppm)
BrH2CH2CO
CH3
NO2

^{13}C NMR

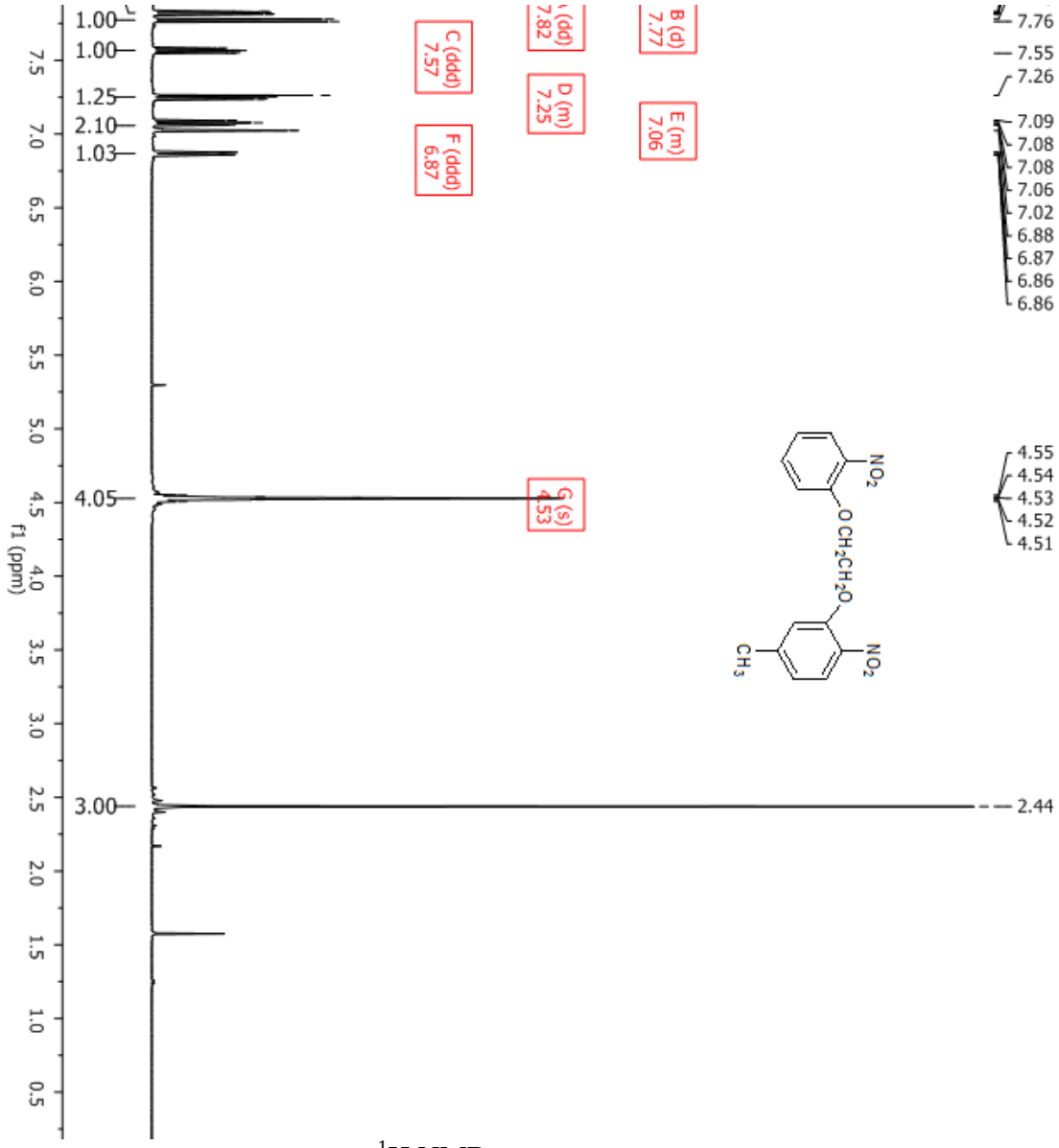
1.00
1.00
1.25
2.10
1.03
4.05
3.00
C (ddd) 7.57
F (ddd) 6.87
D (m) 7.25
G (s) 4.53
B (d) 7.77
E (m) 7.06
7.76
7.55
7.26
7.09
7.08
7.08
7.06
7.02
6.88
6.87
6.86
6.86
4.55
4.54
4.53
4.52
4.51
2.44
NO2
O CH2CH2 O
CH3
NO2
f1 (ppm)

^{1}H NMR

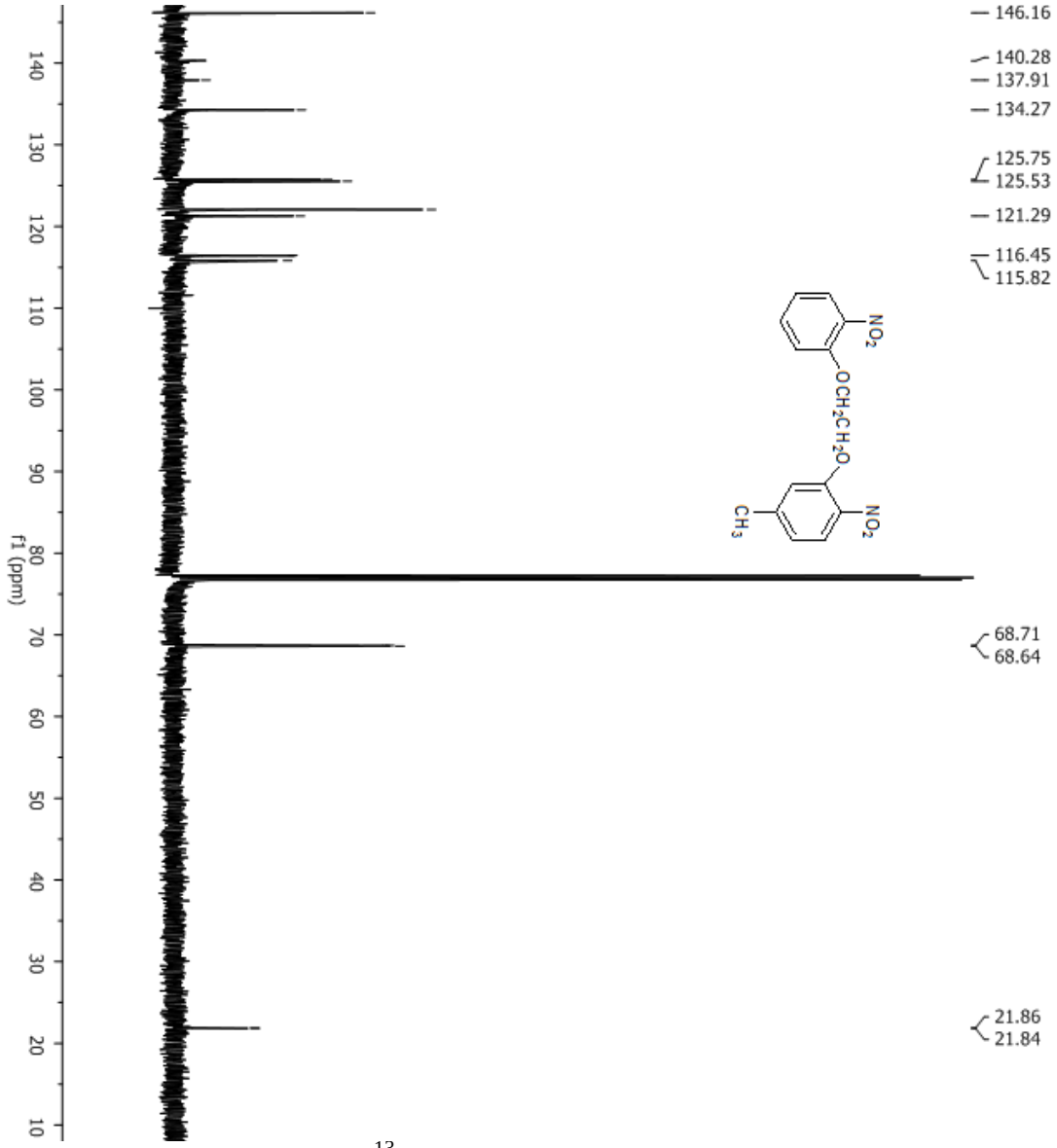
146.16
140.28
137.91
134.27
125.75
125.53
121.29
116.45
115.82
68.71
68.64
21.86
21.84
f1 (ppm)
NO2
OCH2CH2O
CH3
NO2

^{13}C NMR

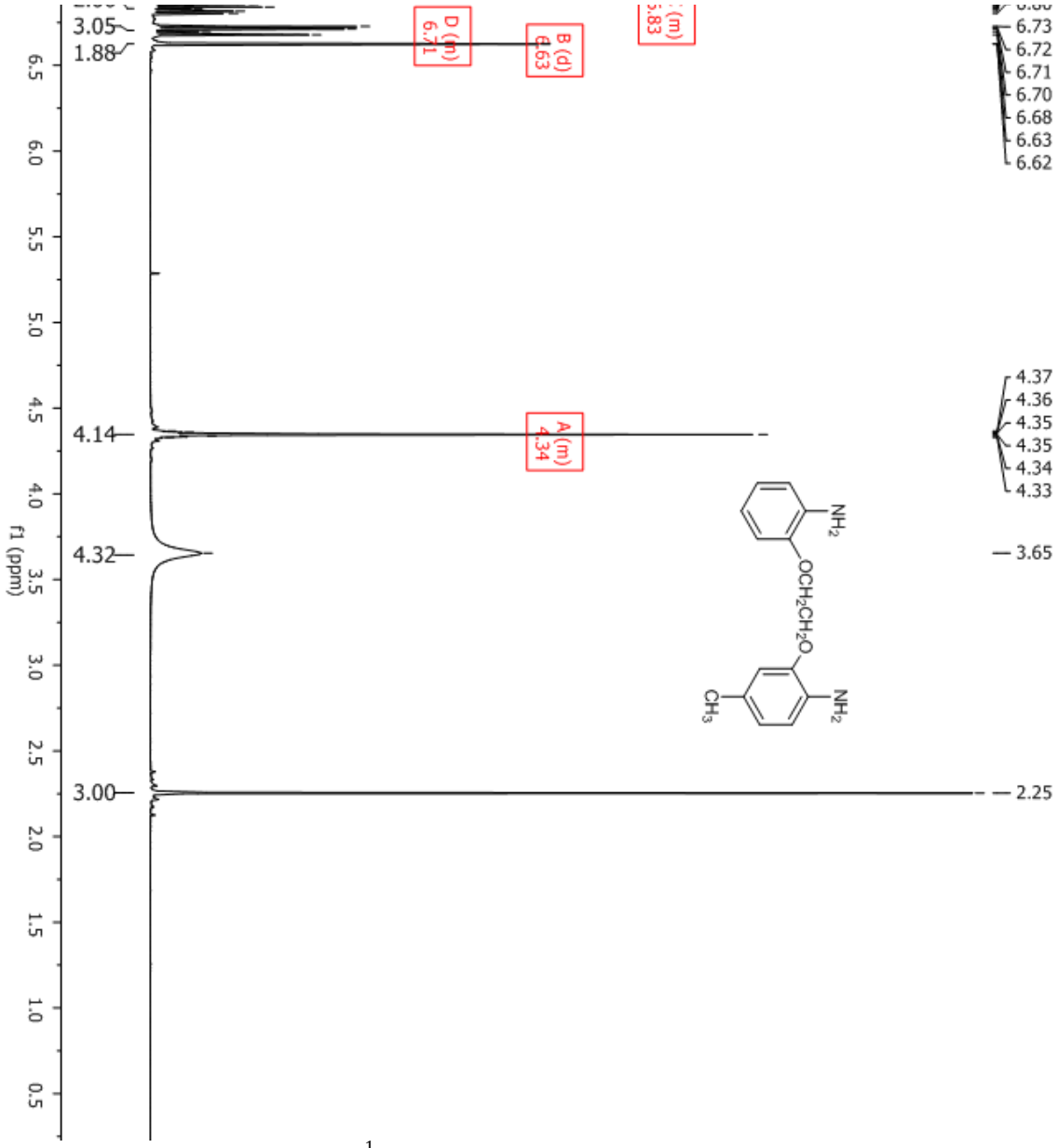
3.05
1.88
4.14
4.32
3.00
f1 (ppm)
D (m) 6.71
B (d) 4.63
A (m) 4.34
6.73
6.72
6.71
6.70
6.68
6.63
6.62
4.37
4.36
4.35
4.35
4.34
4.33
3.65
2.25
NH2
OCH2CH2O
CH3
NH2

^{1}H NMR

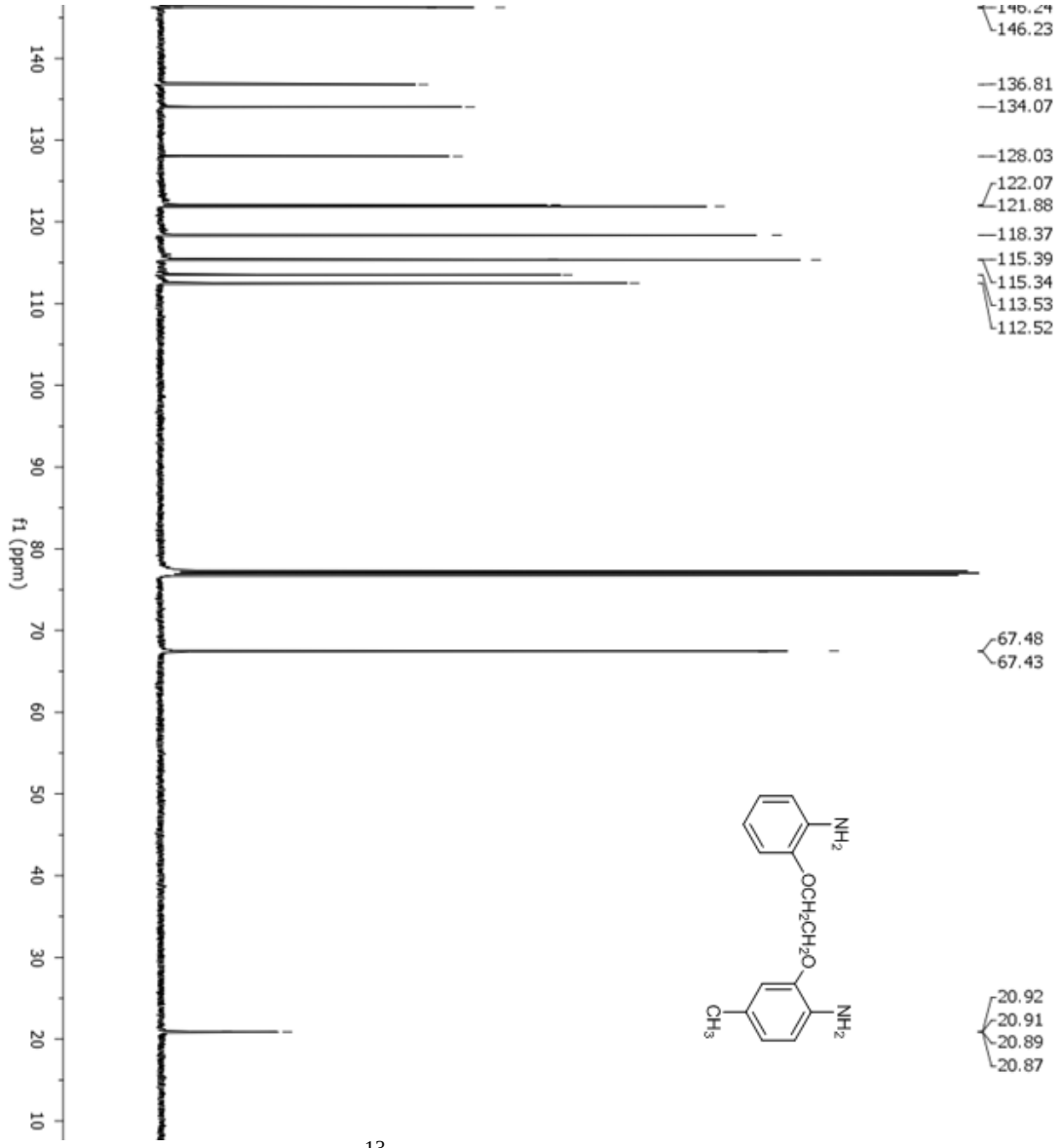
f1 (ppm)
146.24
146.23
136.81
134.07
128.03
122.07
121.88
118.37
115.39
115.34
113.53
112.52
67.48
67.43
20.92
20.91
20.89
20.87
NH2
OCH2CH2O
CH3
NH2

^{13}C NMR

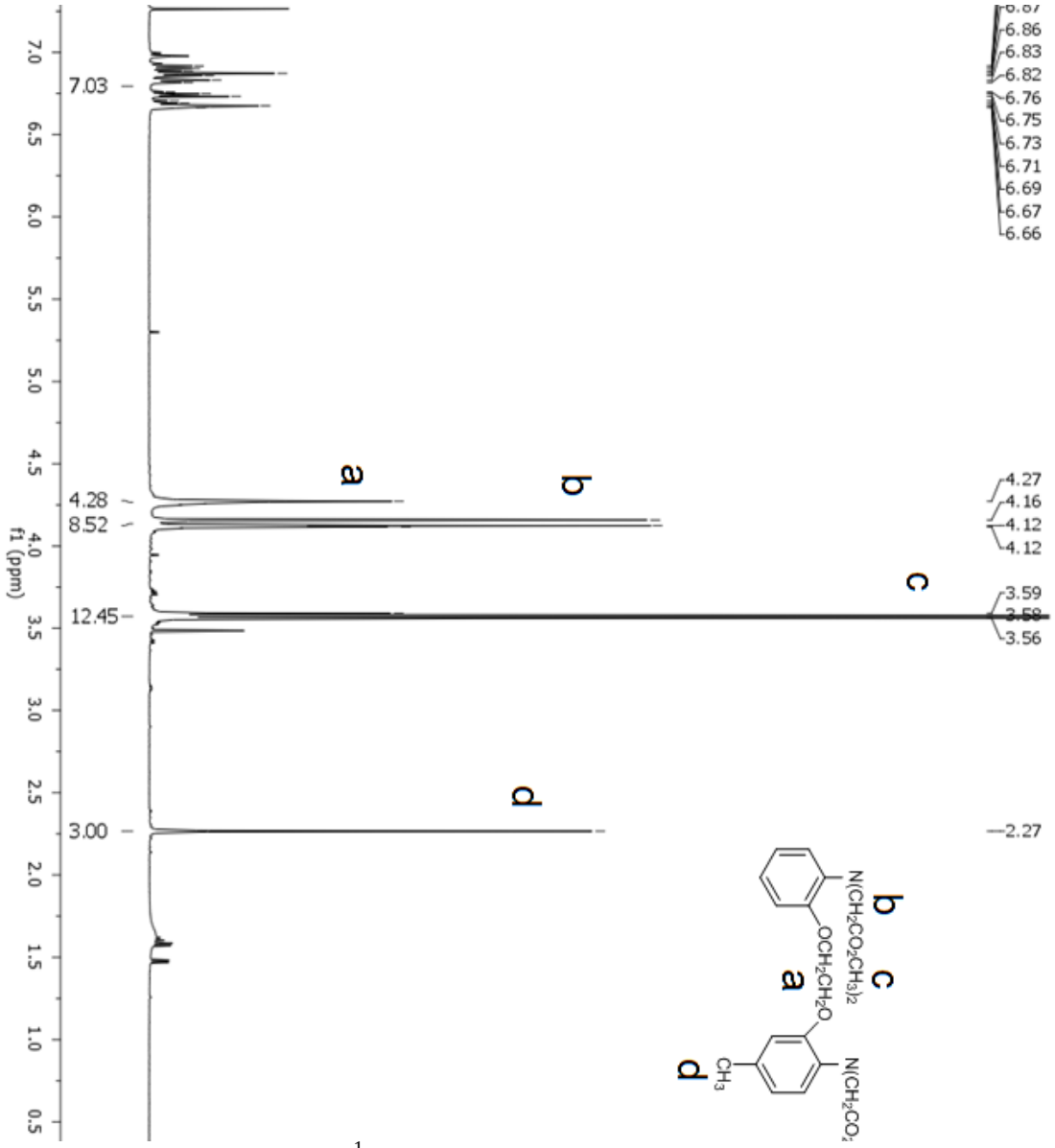
7.03
4.28
8.52
12.45
3.00
a
b
c
d
6.86
6.83
6.82
6.76
6.75
6.73
6.71
6.69
6.67
6.66
4.27
4.16
4.12
4.12
3.59
3.58
3.56
2.27
f1 (ppm)
N(CH2CO2CH3)2
OCH2CH2O
CH3
N(CH2CO2

^{1}H NMR

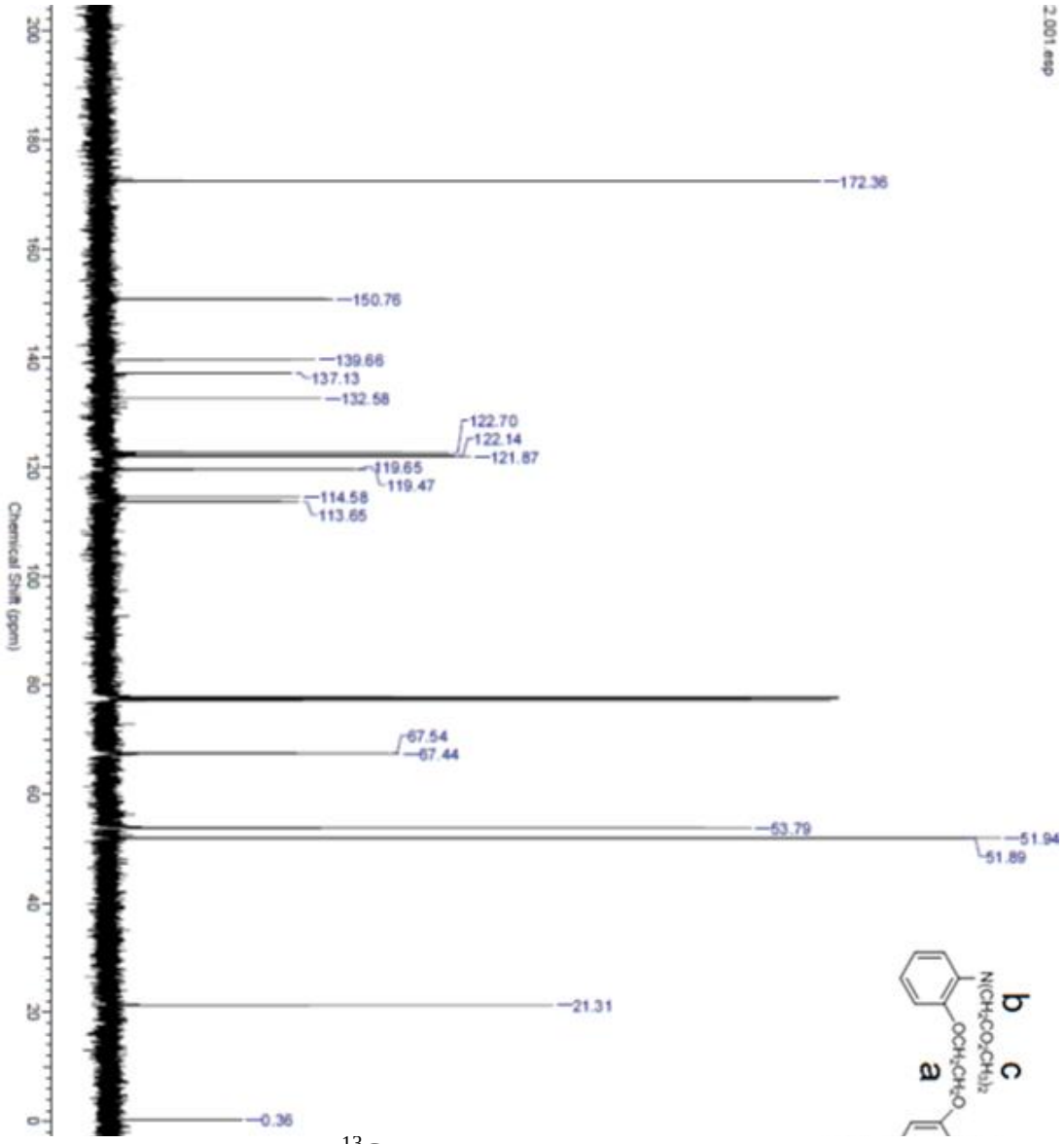
2.001.esp
Chemical Shift (ppm)
172.36
150.76
139.66
137.13
132.58
122.70
122.14
121.87
119.65
119.47
114.58
113.65
67.54
67.44
53.79
51.94
51.89
21.31
0.36
b
c
a
N(CH2CO2CH3)2
OCH2CH2O

^{13}C NMR

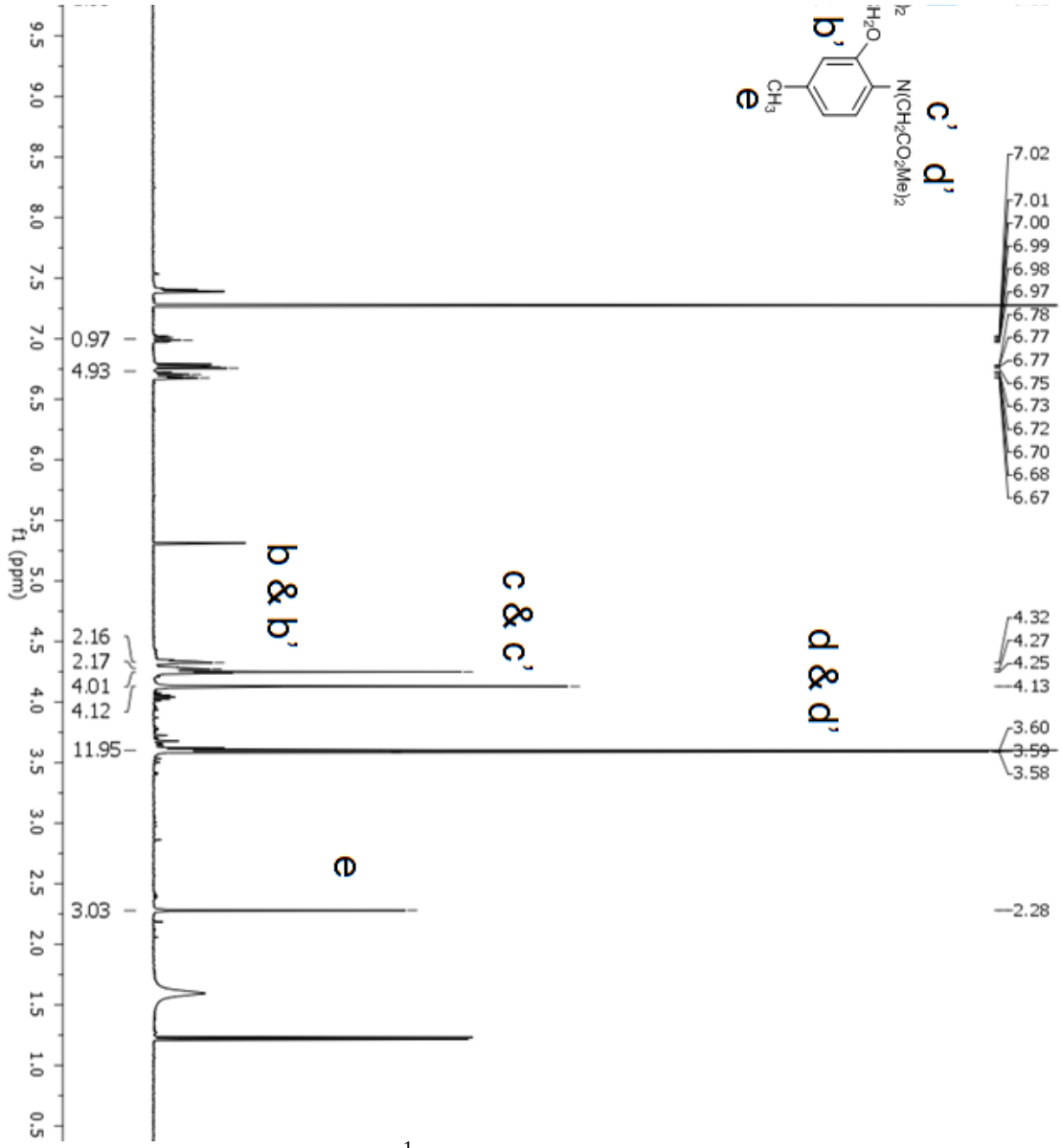
b'
e
c' d'
N(CH2CO2Me)2
7.02
7.01
7.00
6.99
6.98
6.97
6.78
6.77
6.77
6.75
6.73
6.72
6.70
6.68
6.67
0.97
4.93
b & b'
c & c'
d & d'
2.16
2.17
4.01
4.12
11.95
4.32
4.27
4.25
4.13
3.60
3.59
3.58
e
3.03
2.28
f1 (ppm)

BAPTA ^{1}H NMR

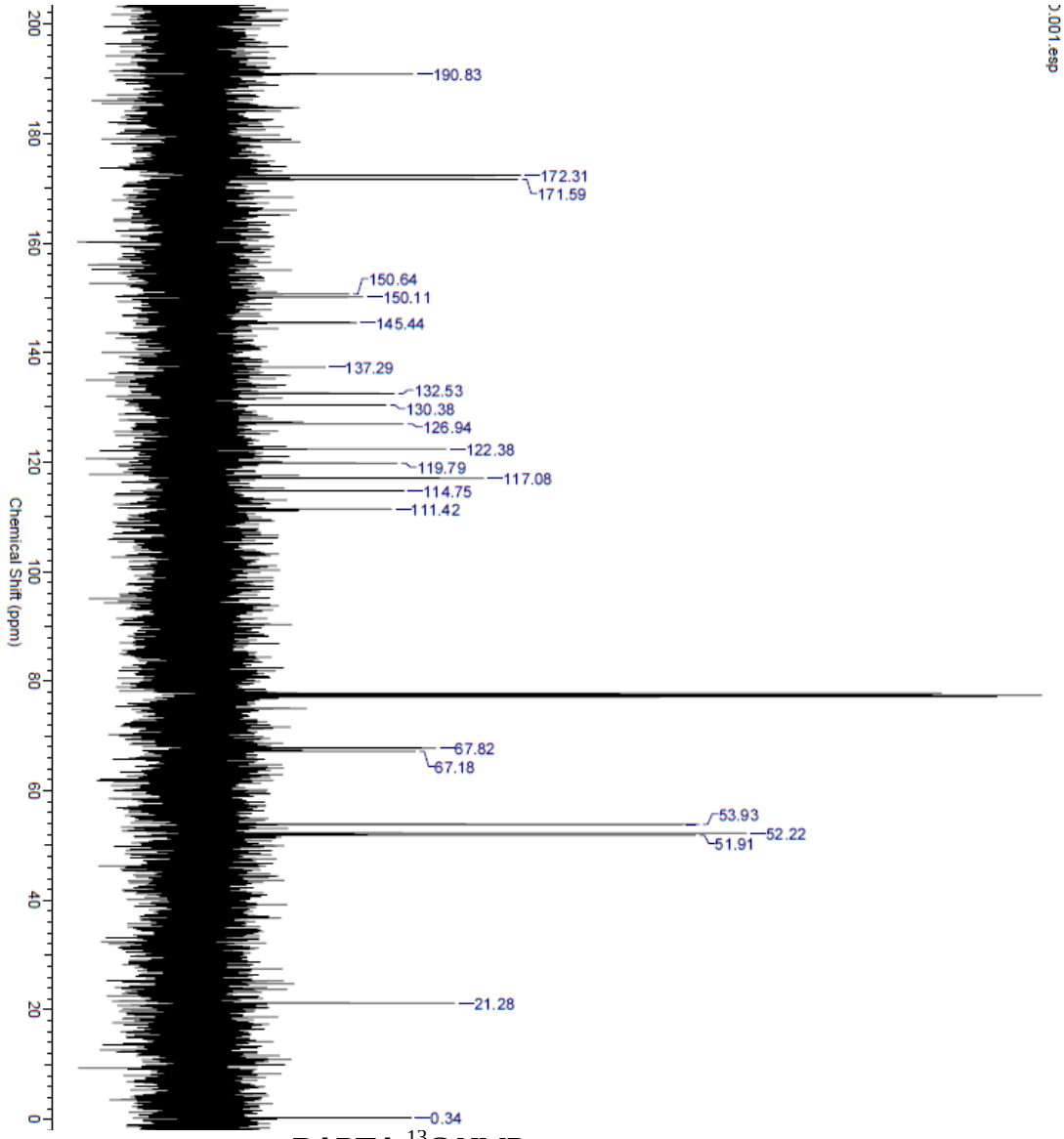

BAPTA ^{13}C NMR

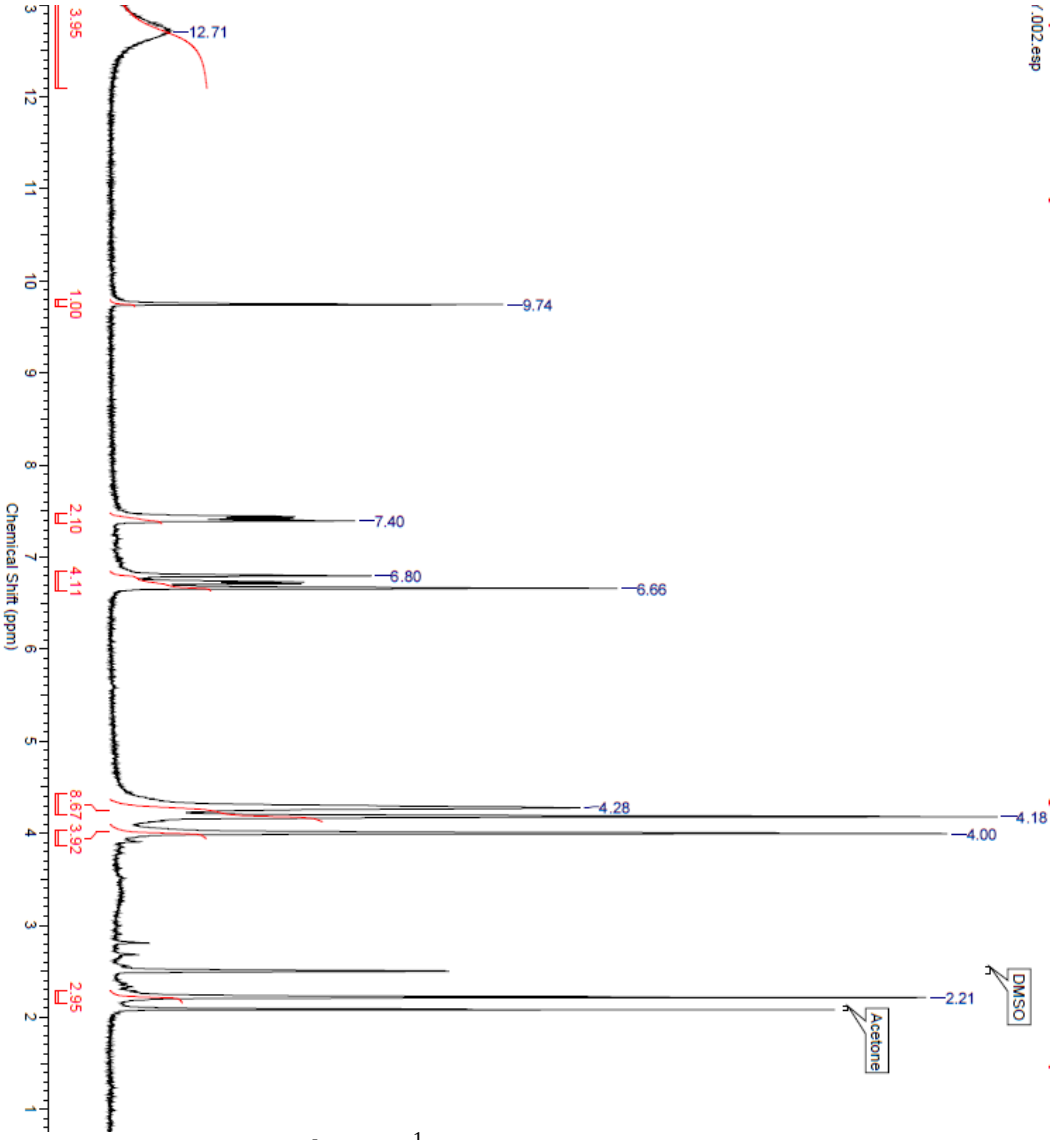
12.71
9.74
7.40
6.80
6.66
4.28
4.18
4.00
2.21
DMSO
Acetone
3.95
1.00
2.10
4.11
8.67
3.92
2.95
Chemical Shift (ppm)

BAP-HY ^{1}H NMR

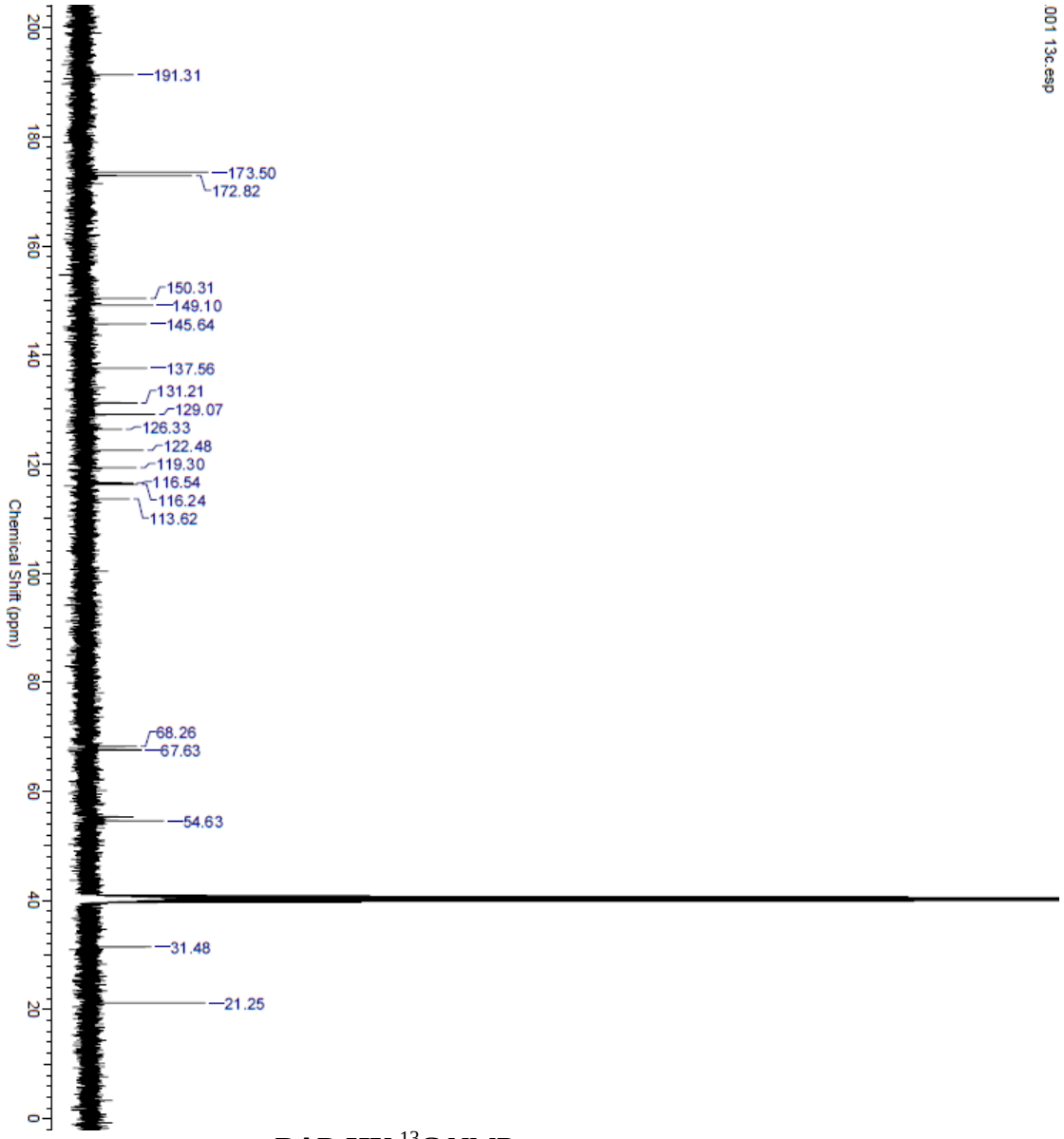

BAP-HY ^{13}C NMR

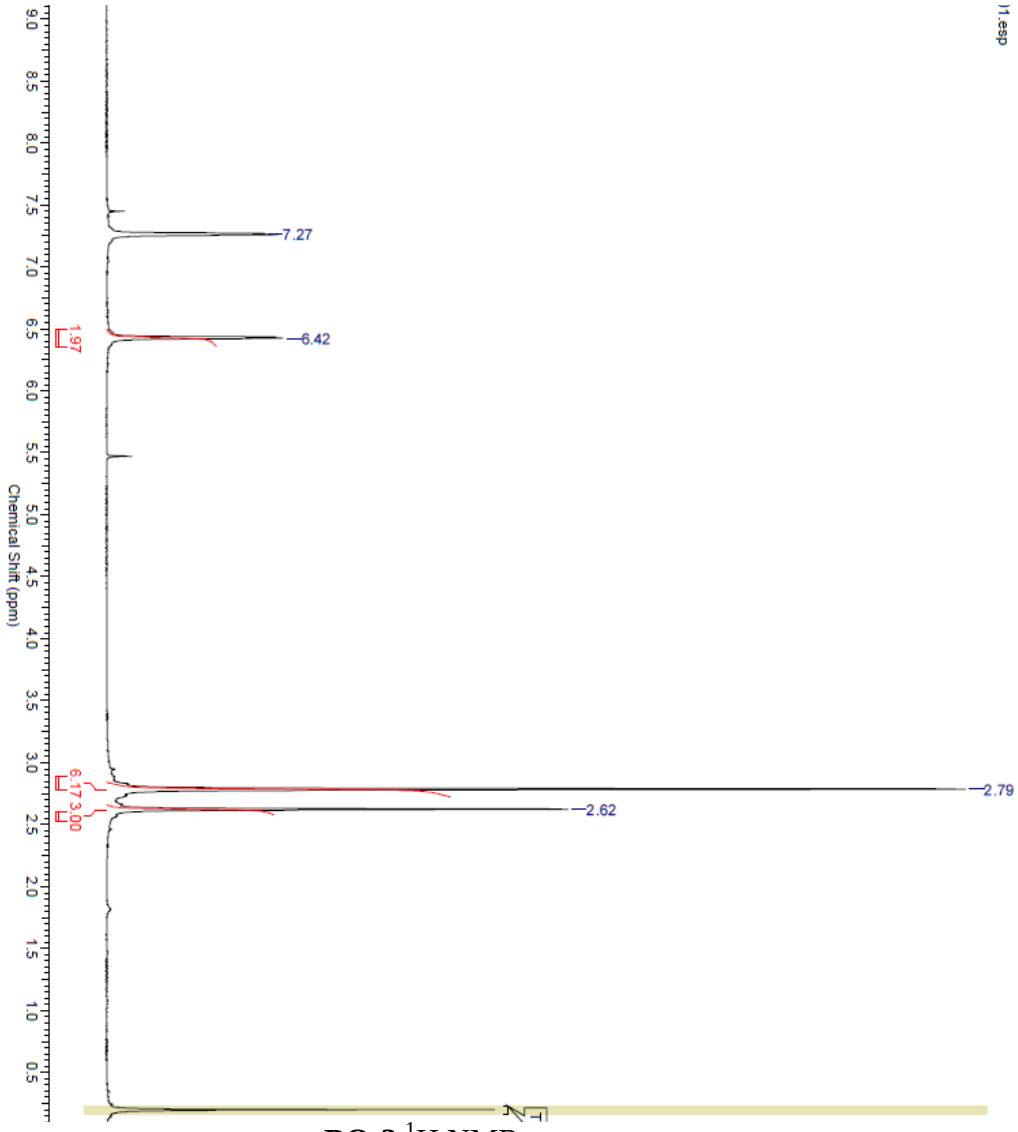

BO-3 ^{1}H NMR

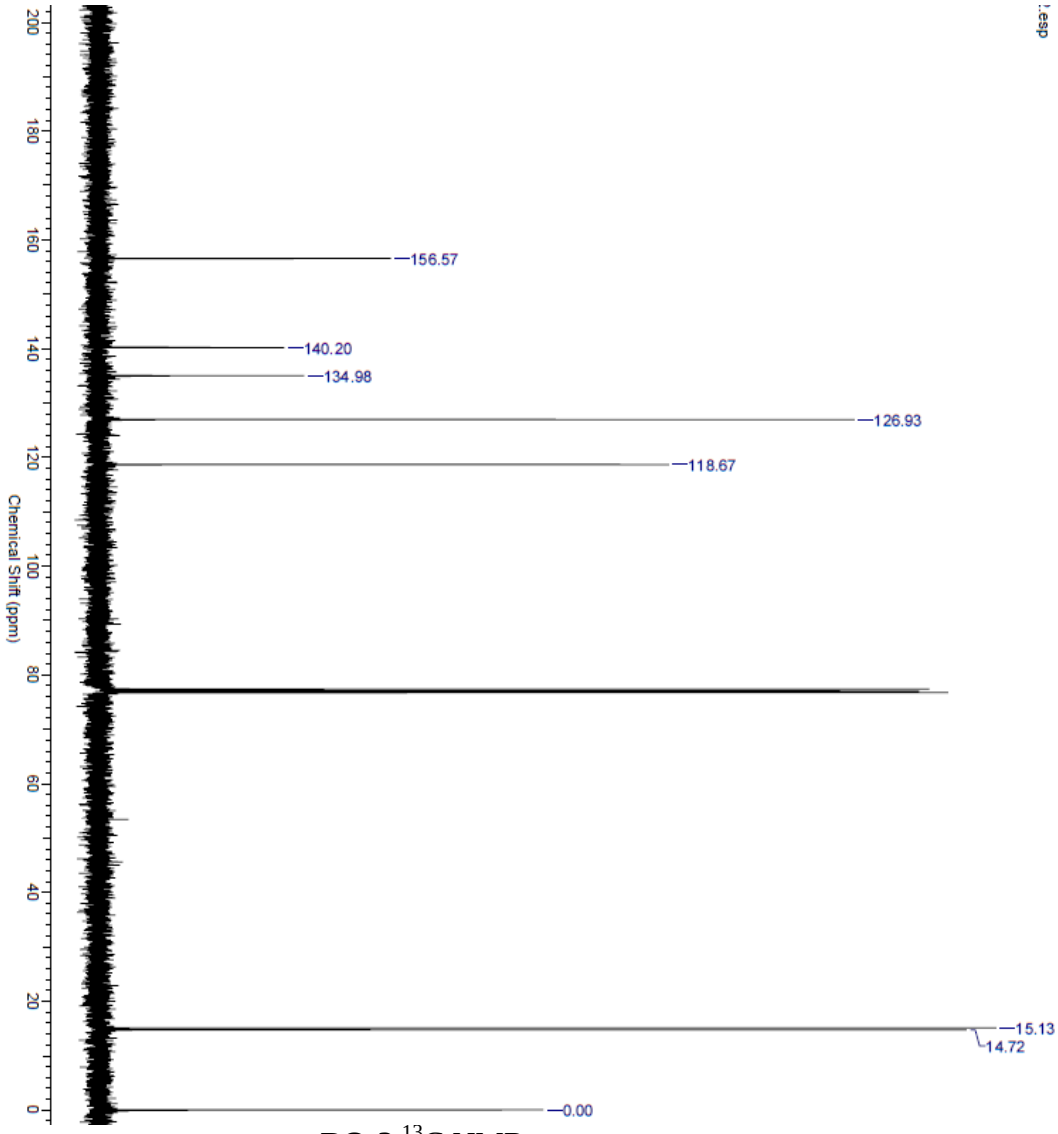
Chemical Shift (ppm)
200
180
160
140
120
100
80
60
40
20
0
156.57
140.20
134.98
126.93
118.67
15.13
14.72
0.00

BO-3 ^{13}C NMR

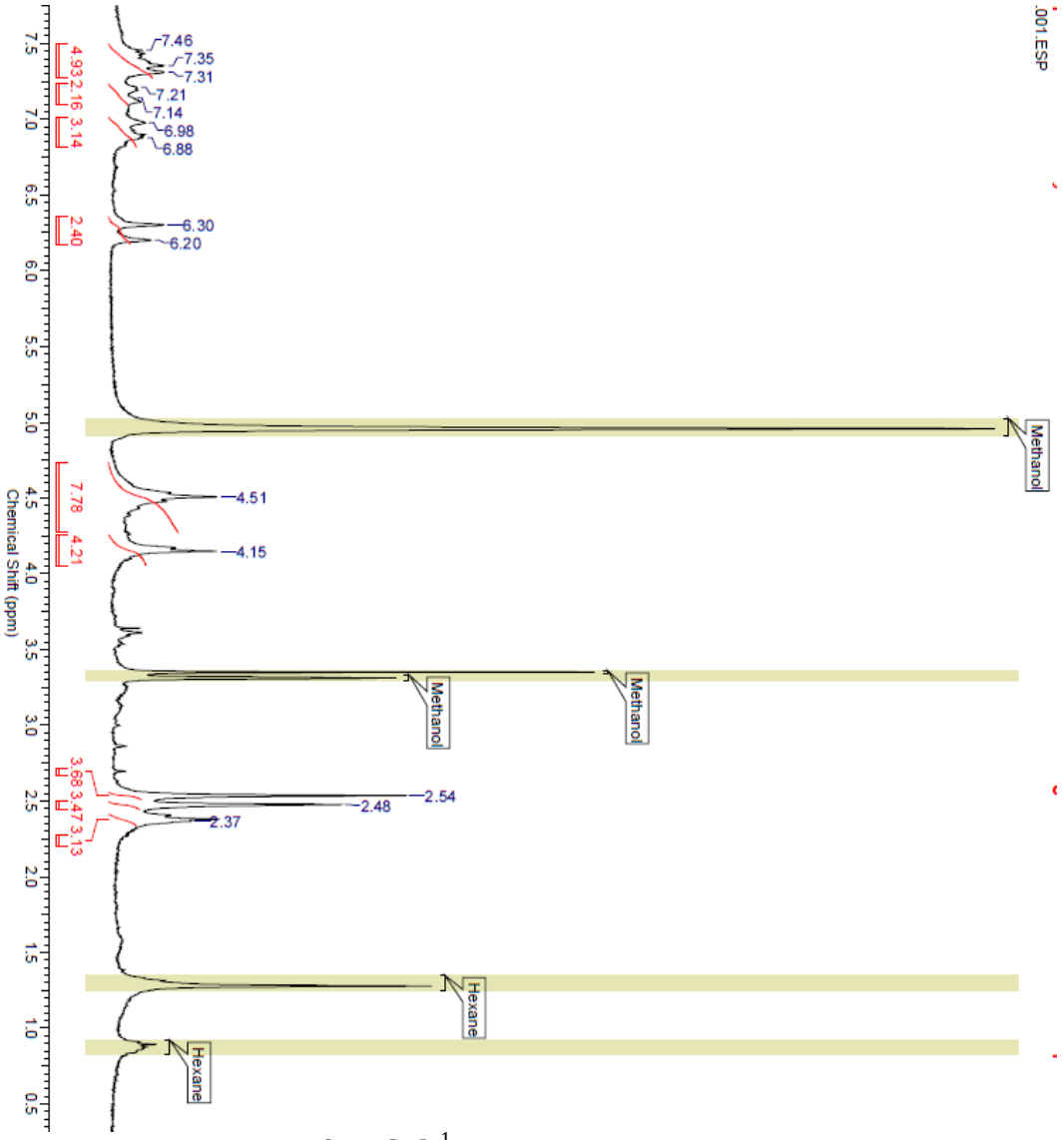

BAPBO-3 ^{1}H NMR

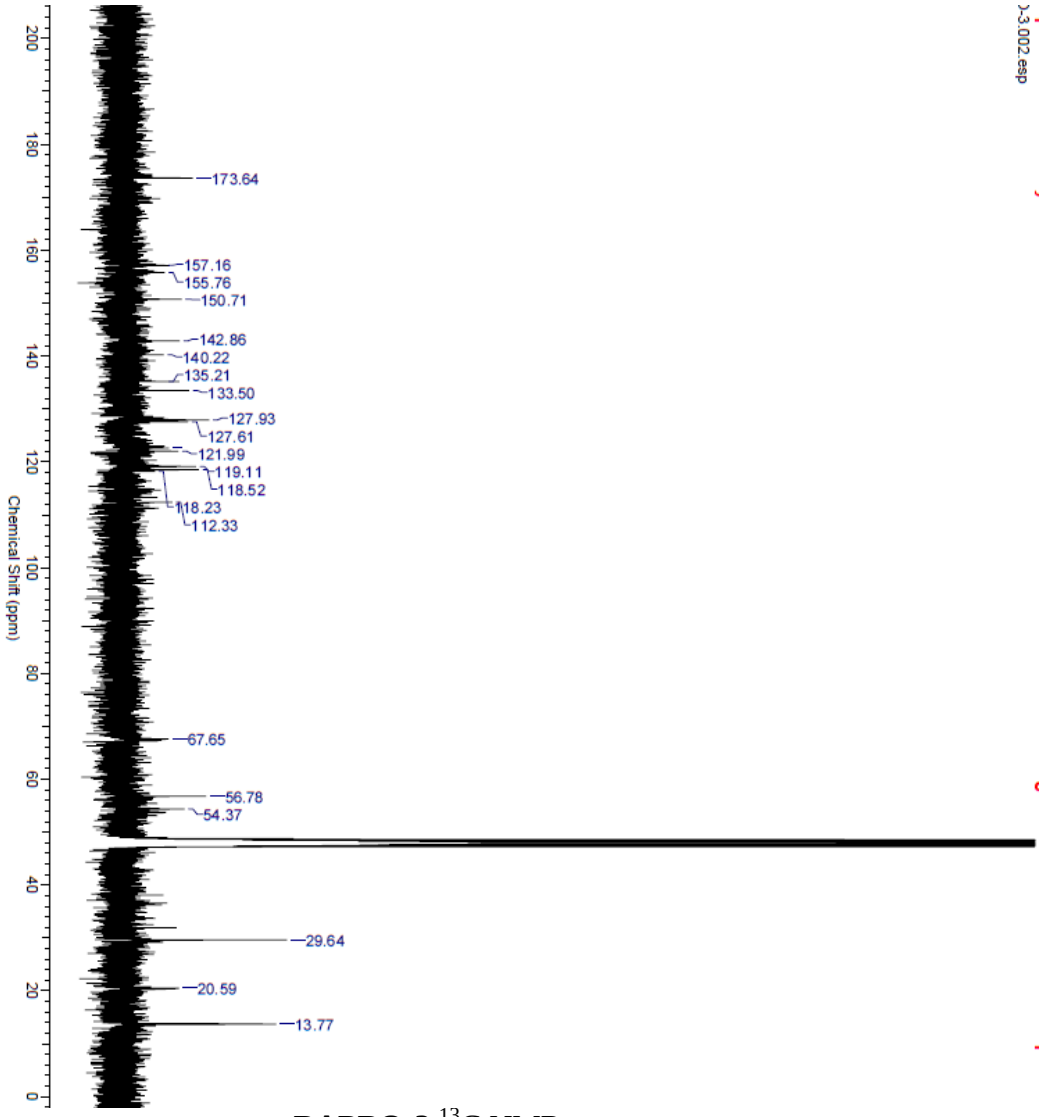

BAPBO-3 ^{13}C NMR

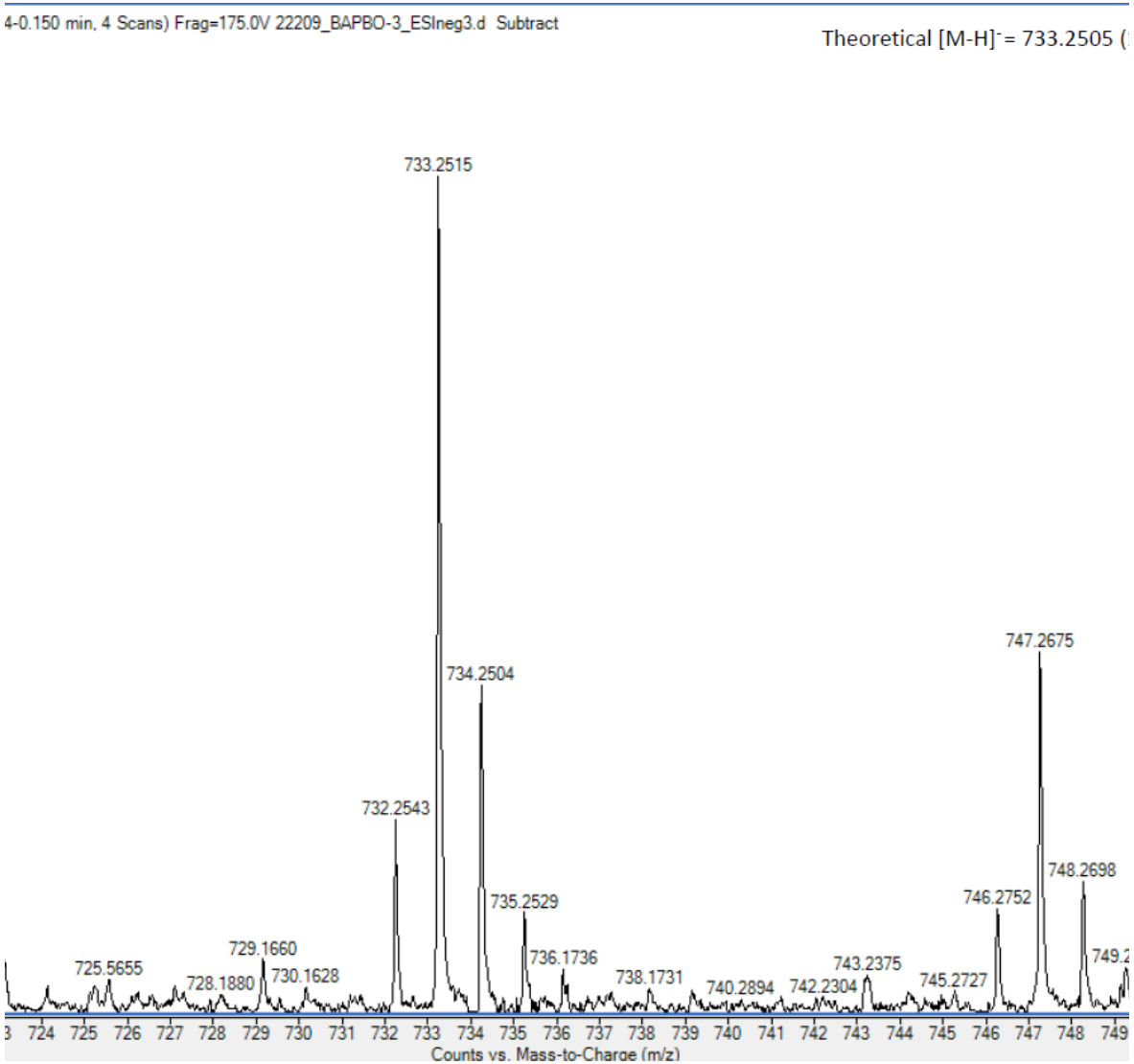
4-0.150 min, 4 Scans) Frag=175.0V 22209_BAPBO-3_ESIneg3.d Subtract
Theoretical [M-H]⁻= 733.2505 (
733.2515
734.2504
732.2543
735.2529
747.2675
748.2698
746.2752
729.1660
736.1736
725.5655
728.1880
730.1628
738.1731
740.2894
742.2304
743.2375
745.2727
724 725 726 727 728 729 730 731 732 733 734 735 736 737 738 739 740 741 742 743 744 745 746 747 748 749
Counts vs. Mass-to-Charge (m/z)

BAPBO-3 HRMS

APPENDIX C: ^{1}H AND ^{13}C, AND MASS SPECTRA OF MOLECULES IN CHAPTER 3

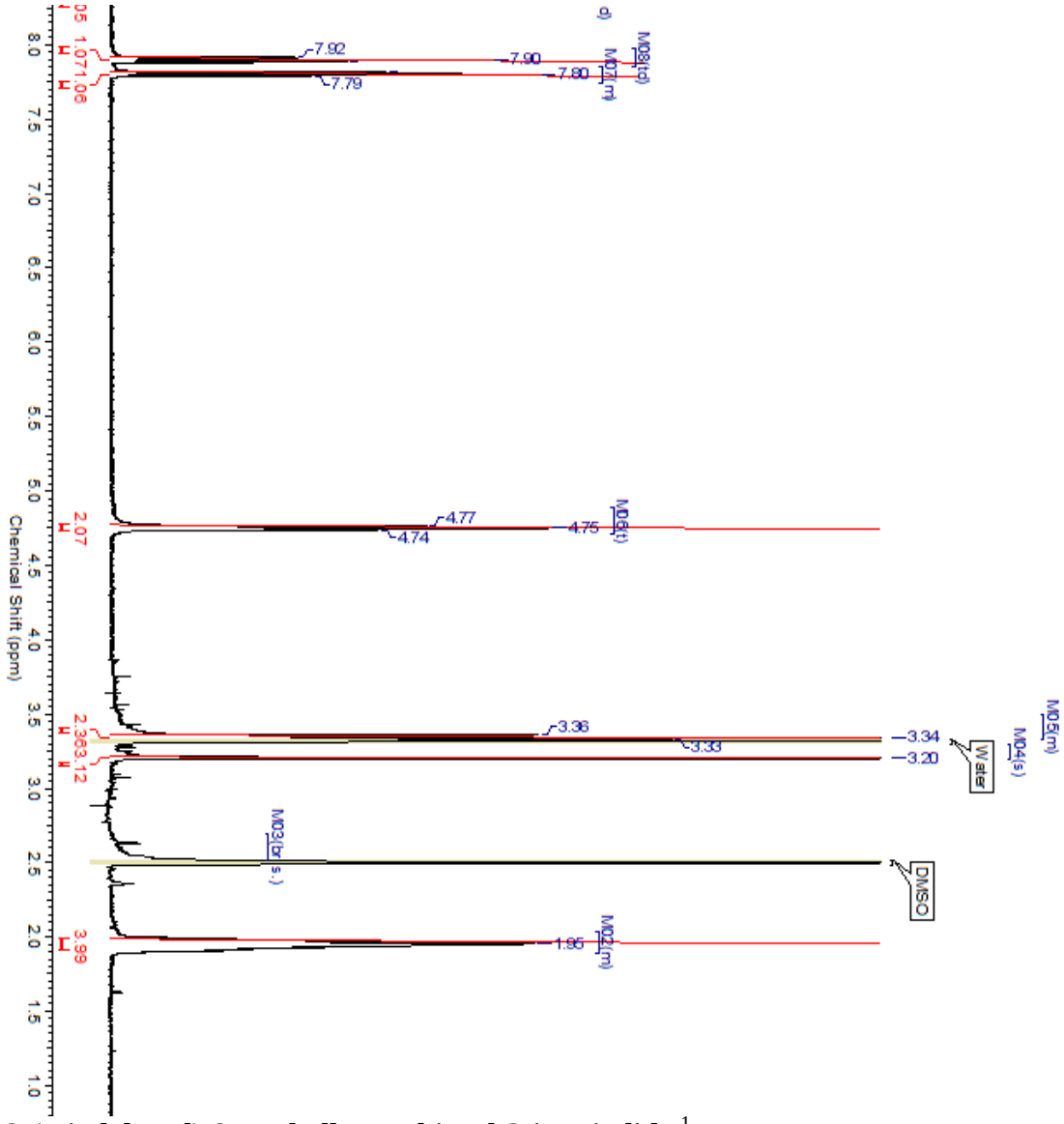

3-(4-iodobutyl)-2-methylbenzothiazol-3-ium iodide ^{1}H NMR

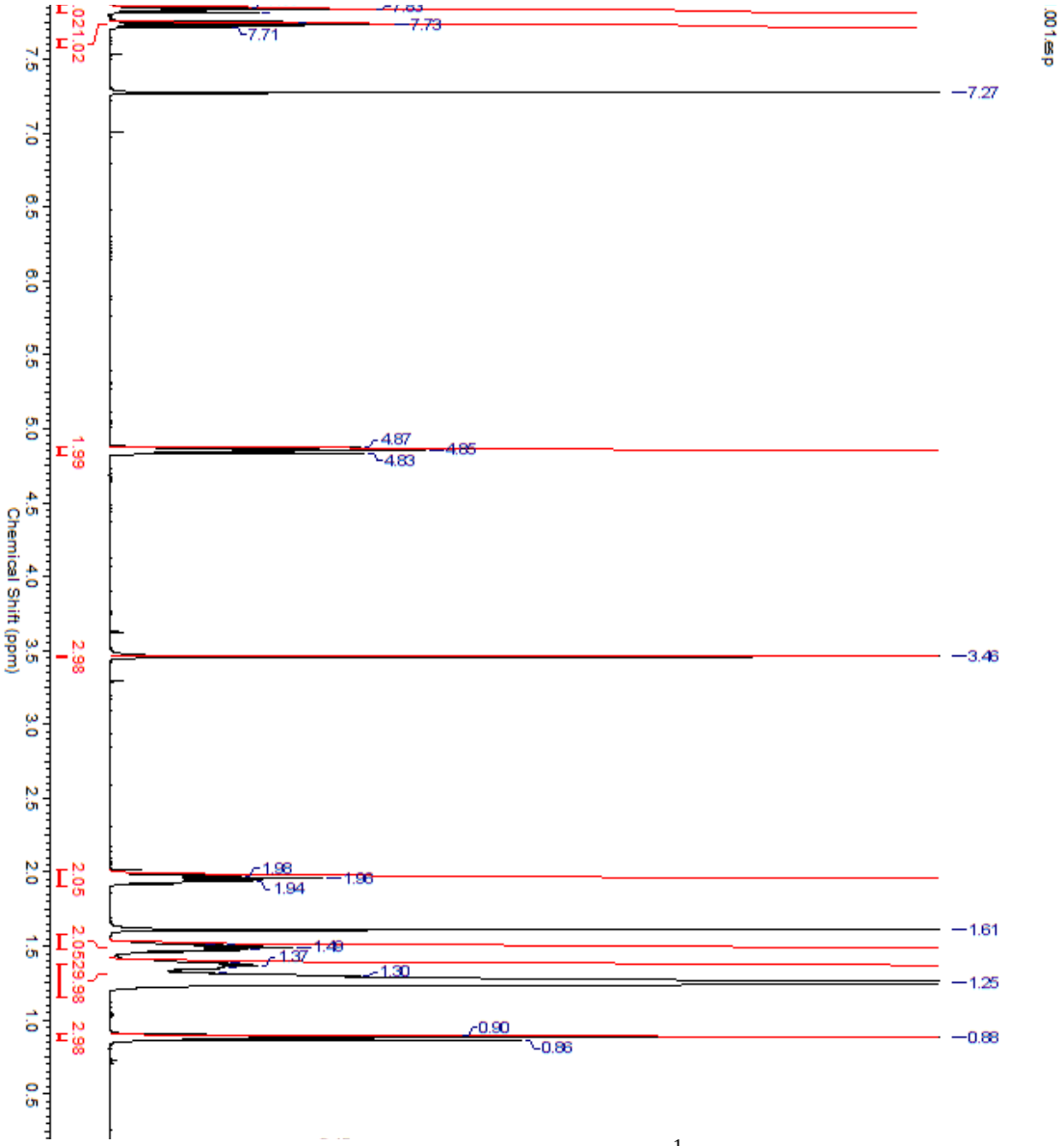

3-Octadecyl-2-methylbenzothiazol-3-ium iodide ^{1}H NMR

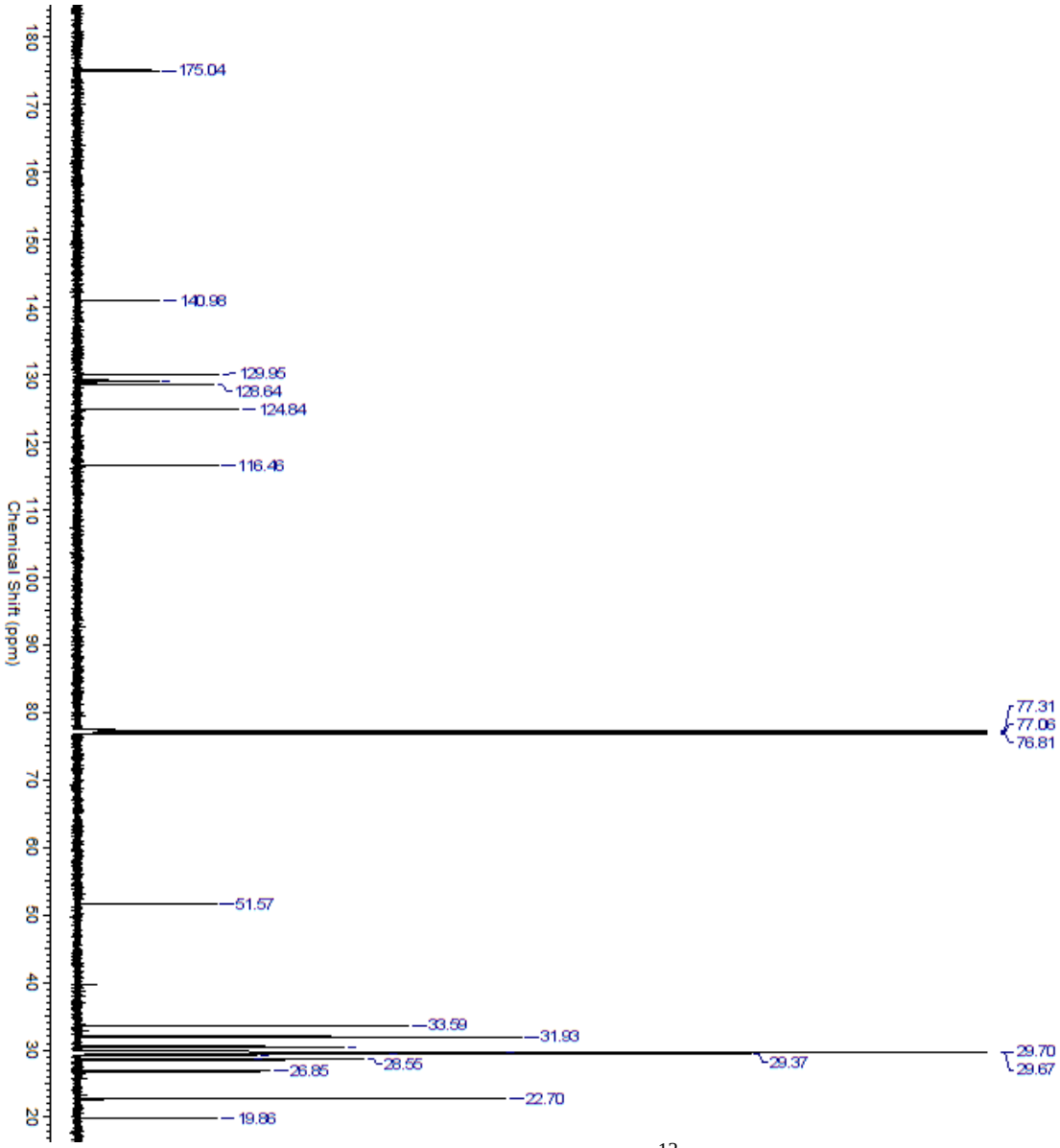

3-Octadecyl-2-methylbenzothiazol-3-ium iodide ^{13}C NMR

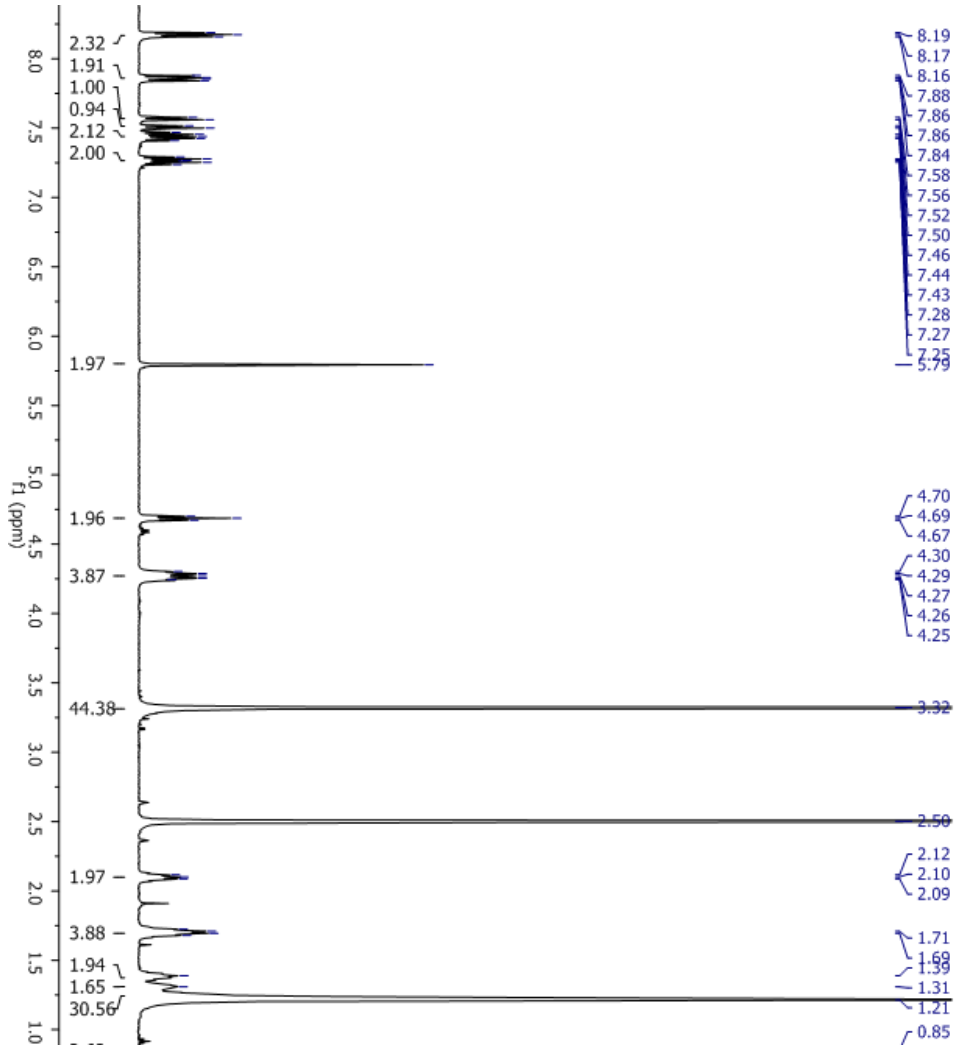

2-((3-octadecylbenzothiazol-2(3H)-ylidene)methyl)-3-oxo-4-((3-(4-(pyridinium-1-yl)butyl)benzothiazol-3-ium-2-yl)methylene)cyclobut-1-enolate iodide ^{1}H NMR

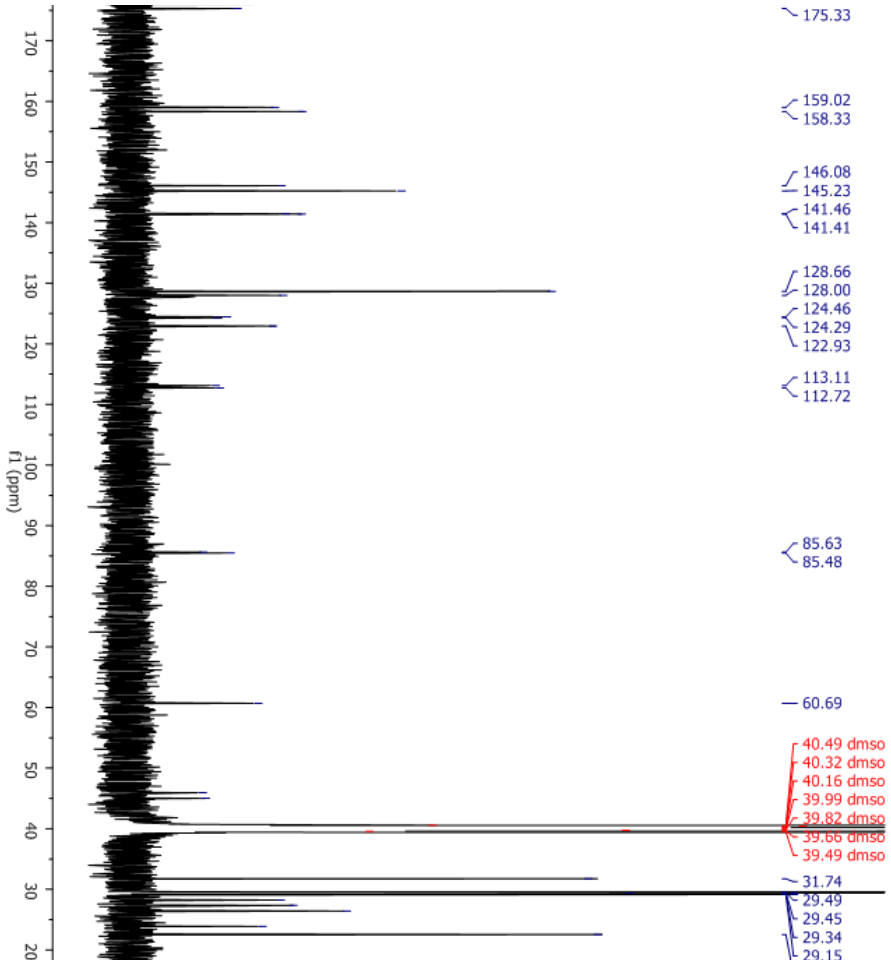

2-((3-octadecylbenzothiazol-2(3H)-ylidene)methyl)-3-oxo-4-((3-(4-(pyridinium-1-yl)butyl)benzothiazol-3-ium-2-yl)methylene)cyclobut-1-enolate iodide ^{13}C NMR

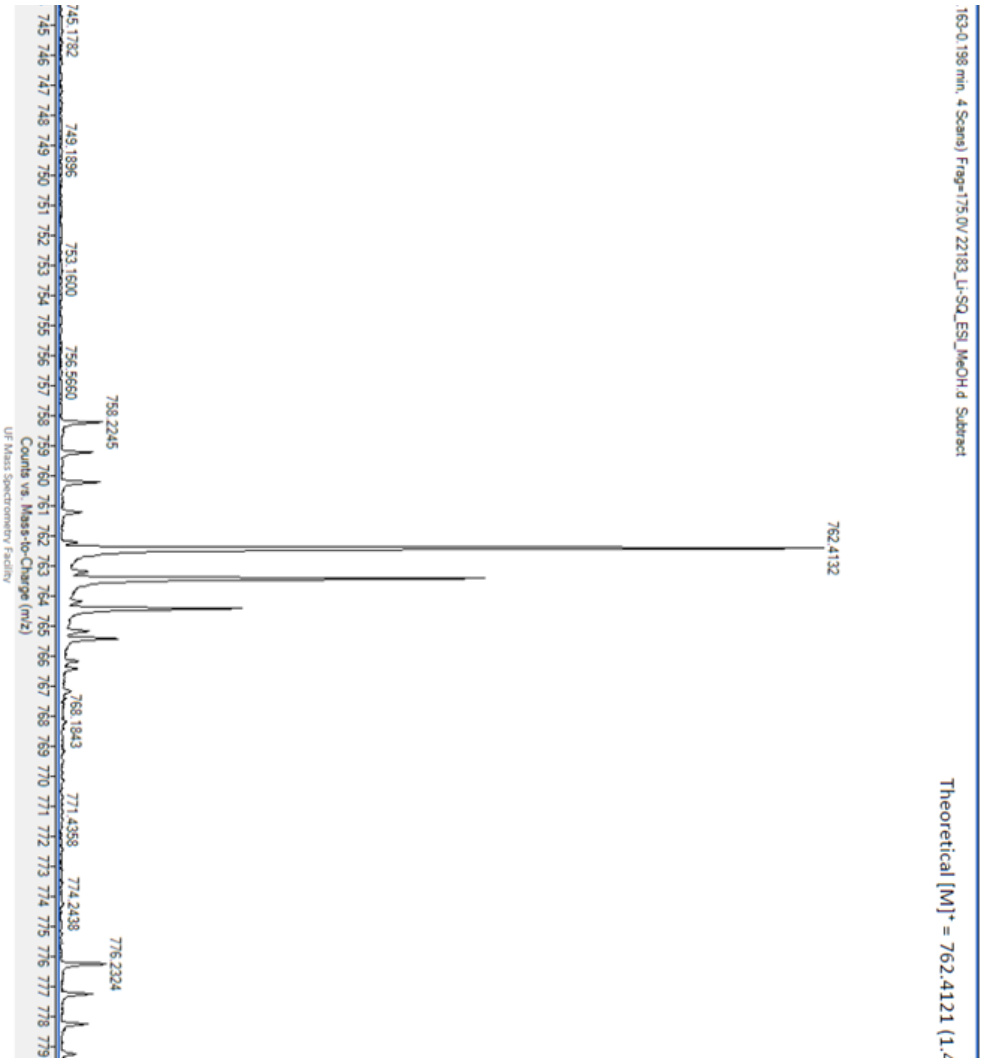

2-((3-octadecylbenzothiazol-2(3H)-ylidene)methyl)-3-oxo-4-((3-(4-(pyridinium-1-yl)butyl)benzothiazol-3-ium-2-yl)methylene)cyclobut-1-enolate iodide HRMS

LIST OF REFERENCES

1. Polyak, K.; Haviv, I.; Campbell, I. G., Co-evolution of tumor cells and their microenvironment. *Trends Genet*, **2009**, 25(1), 30-38.
2. Aleardi, A. M.; Benard, G.; Augereau, O.; Malgat, M.; Talbot, J. C.; Mazat, J. P.; Letellier, T.; Dachary-Prigent, J.; Solaini, G. C.; Rossignol, R., Gradual alteration of mitochondrial structure and function by beta-amyloids: importance of membrane viscosity changes, energy deprivation, reactive oxygen species production, and cytochrome c release. *J Bioenerg Biomembr*, **2005**, 37(4), 207-225.
3. Kaliviotis, E.; Yianneskis, M., On the effect of dynamic flow conditions on blood microstructure investigated with optical shearing microscopy and rheometry. *Proc Inst Mech Eng H*, **2007**, 221(8), 887-897.
4. Shul'man, Z. P. M., V. A., Determination of the Rheological Properties of Whole Blood by the Nonstationary Method of Pulsed Changing of the Rate of Shear. *Journal of Engineering Physics and Thermophysics*, **2005**, 78(5), 1018-1021.
5. Kuimova, M. K.; Botchway, S. W.; Parker, A. W.; Balaz, M.; Collins, H. A.; Anderson, H. L.; Suhling, K.; Ogilby, P. R., Imaging intracellular viscosity of a single cell during photoinduced cell death. *Nat Chem*, **2009**, 1(1), 69-73.
6. Haidekker, M. A.; Theodorakis, E. A., Molecular rotors--fluorescent biosensors for viscosity and flow. *Org Biomol Chem*, **2007**, 5(11), 1669-1678.
7. Grabowski, Z. R. R., K.; Siemiarczuk, A.; Cowley, D. J.; Baumann, W., Twisted Intramolecular Charge Transfer States (TICT). A New Class of Excited States with a Full Charge Separation. *Nouveau Journal de Chimie*, **1979**, 3(7), 443-454.

8. Haidekker, M. A., Nipper, M., Mustafic, A., Lichlyter, D., Dakanali, M., and Theodorakis, E.A. , Dyes with Segmental Mobility: Molecular Rotors. *Advanced Fluorescence Reporters in Chemistry and Biology I: Fundamentals and Molecular Design*, **2010**, 8, 267–308.

9. Kwok, W. M.; Ma, C.; Matousek, P.; Parker, A. W.; Phillips, D.; Toner, W. T.; Towrie, M.; Umapathy, S., A determination of the structure of the intramolecular charge transfer state of 4-dimethylaminobenzonitrile (DMABN) by time-resolved resonance Raman spectroscopy. *Journal of Physical Chemistry A*, **2001**, 105(6), 984-990.

10. Sahoo, S. K.; Umapathy, S.; Parker, A. W., Time-Resolved Resonance Raman Spectroscopy: Exploring Reactive Intermediates. *Applied Spectroscopy*, **2011**, 65(10), 1087-1115.

11. Jin, H.; Liang, M.; Arzhantsev, S.; Li, X.; Maroncelli, M., Photophysical Characterization of Benzylidene Malononitriles as Probes of Solvent Friction. *Journal of Physical Chemistry B*, **2010**, 114(22), 7565-7578.

12. Swalina, C.; Maroncelli, M., Nonradiative Deactivation in Benzylidene Malononitriles. *Journal of Physical Chemistry C*, **2010**, 114(12), 5602-5610.

13. Strehmel, B.; Seifert, H.; Rettig, W., Photophysical properties of fluorescence probes .2. A model of multiple fluorescence for stilbazolium dyes studied by global analysis and quantum chemical calculations. *Journal of Physical Chemistry B*, **1997**, 101(12), 2232-2243.

14. Cao, X.; Tolbert, R. W.; McHale, J. L.; Edwards, W. D., Theoretical study of solvent effects on the intramolecular charge transfer of a hemicyanine dye. *Journal of Physical Chemistry A*, **1998**, 102(17), 2739-2748.

15. Pillai, Z. S.; Sudeep, P. K.; Thomas, K. G., Effect of viscosity on the singlet-excited state dynamics of some hemicyanine dyes. *Research on Chemical Intermediates*, **2003**, 29(3), 293-305.

16. Ghiso, J.; Frangione, B., Amyloidosis and Alzheimer's disease. *Adv Drug Deliv Rev*, **2002**, 54(12), 1539-1551.

17. Khurana, R.; Coleman, C.; Ionescu-Zanetti, C.; Carter, S. A.; Krishna, V.; Grover, R. K.; Roy, R.; Singh, S., Mechanism of thioflavin T binding to amyloid fibrils. *J Struct Biol*, **2005**, 151(3), 229-238.

18. Naik, L. R.; Naik, A. B.; Pal, H., Steady-state and time-resolved emission studies of Thioflavin-T. *Journal of Photochemistry and Photobiology a-Chemistry*, **2009**, 204(2-3), 161-167.

19. Kumar, S.; Singh, A. K.; Krishnamoorthy, G.; Swaminathan, R., Thioflavin T Displays Enhanced Fluorescence Selectively Inside Anionic Micelles and Mammalian Cells. *Journal of Fluorescence*, **2008**, 18(6), 1199-1205.

20. Khurana, R.; Coleman, C.; Ionescu-Zanetti, C.; Carter, S. A.; Krishna, V.; Grover, R. K.; Roy, R.; Singh, S., Mechanism of thioflavin T binding to amyloid fibrils. *Journal of Structural Biology*, **2005**, 151(3), 229-238.

21. Haidekker, M. A.; Brady, T.; Wen, K.; Okada, C.; Stevens, H. Y.; Snell, J. M.; Frangos, J. A.; Theodorakis, E. A., Phospholipid-bound molecular rotors: synthesis and characterization. *Bioorg Med Chem*, **2002**, 10(11), 3627-3636.

22. Kung, C. E.; Reed, J. K., Microviscosity Measurements of Phospholipid-Bilayers Using Fluorescent Dyes That Undergo Torsional Relaxation. *Biochemistry*, **1986**, 25(20), 6114-6121.

23. Nipper, M. E.; Dakanali, M.; Theodorakis, E.; Haidekker, M. A., Detection of liposome membrane viscosity perturbations with ratiometric molecular rotors. *Biochimie*, **2011**, 93(6), 988-994.

24. Kung, C. E.; Reed, J. K., Fluorescent Molecular Rotors - a New Class of Probes for Tubulin Structure and Assembly. *Biochemistry*, **1989**, 28(16), 6678-6686.

25. Sawada, S.; Iio, T.; Hayashi, Y.; Takahashi, S., Fluorescent Rotors and Their Applications to the Study of G-F Transformation of Actin. *Analytical Biochemistry*, **1992**, 204(1), 110-117.

26. Loutfy, R. O., Arnold, B.A., Effect of Viscosity and Temperature on Torsional Relaxation of Molecular Rotors *Phys. Chem.*, **1982**, 86(21), 4205-4211.

27. Fischer, D.; Theodorakis, E. A.; Haidekker, M. A., Synthesis and use of an in-solution ratiometric fluorescent viscosity sensor. *Nat Protoc*, **2007**, 2(1), 227-236.

28. Yang, Z.; He, Y.; Lee, J. H.; Park, N.; Suh, M.; Chae, W. S.; Cao, J.; Peng, X.; Jung, H.; Kang, C.; Kim, J. S., A self-calibrating bipartite viscosity sensor for mitochondria. *J Am Chem Soc*, **2013**, 135(24), 9181-9185.

29. Wang, L.; Xiao, Y.; Tian, W.; Deng, L., Activatable rotor for quantifying lysosomal viscosity in living cells. *J Am Chem Soc*, **2013**, 135(8), 2903-2906.

30. Luby-Phelps, K.; Mujumdar, S.; Mujumdar, R. B.; Ernst, L. A.; Galbraith, W.; Waggoner, A. S., A novel fluorescence ratiometric method confirms the low solvent viscosity of the cytoplasm. *Biophys J*, **1993**, 65(1), 236-242.

31. Haidekker, M. A.; Brady, T. P.; Lichlyter, D.; Theodorakis, E. A., A ratiometric fluorescent viscosity sensor. *J Am Chem Soc*, **2006**, 128(2), 398-399.

32. Peng, X.; Yang, Z.; Wang, J.; Fan, J.; He, Y.; Song, F.; Wang, B.; Sun, S.; Qu, J.; Qi, J.; Yan, M., Fluorescence ratiometry and fluorescence lifetime imaging: using a single molecular sensor for dual mode imaging of cellular viscosity. *J Am Chem Soc*, **2011**, 133(17), 6626-6635.

33. Lopez-Duarte, I.; Vu, T. T.; Izquierdo, M. A.; Bull, J. A.; Kuimova, M. K., A molecular rotor for measuring viscosity in plasma membranes of live cells. *Chem Commun (Camb)*, **2014**, 50(40), 5282-5284.

34. Kuimova, M. K.; Yahioglu, G.; Levitt, J. A.; Suhling, K., Molecular rotor measures viscosity of live cells via fluorescence lifetime imaging. *Journal of the American Chemical Society*, **2008**, 130(21), 6672-+.

35. Goncalves, M. S., Fluorescent labeling of biomolecules with organic probes. *Chem Rev*, **2009**, 109(1), 190-212.

36. Ahn, H. Y.; Yao, S.; Wang, X.; Belfield, K. D., Near-infrared-emitting squaraine dyes with high 2PA cross-sections for multiphoton fluorescence imaging. *ACS Appl Mater Interfaces*, **2012**, 4(6), 2847-2854.

37. Zhang, Y.; Yue, X.; Kim, B.; Yao, S.; Bondar, M. V.; Belfield, K. D., Bovine serum albumin nanoparticles with fluorogenic near-IR-emitting squaraine dyes. *ACS Appl Mater Interfaces*, **2013**, 5(17), 8710-8717.

38. Cristofoli, W. A.; Wiebe, L. I.; De Clercq, E.; Andrei, G.; Snoeck, R.; Balzarini, J.; Knaus, E. E., 5-alkynyl analogs of arabinouridine and 2'-deoxyuridine: cytostatic activity against herpes simplex virus and varicella-zoster thymidine kinase gene-transfected cells. *J Med Chem*, **2007**, 50(12), 2851-2857.

39. Sinkeldam, R. W.; Greco, N. J.; Tor, Y., Fluorescent analogs of biomolecular building blocks: design, properties, and applications. *Chem Rev*, **2010**, 110(5), 2579-2619.

40. Srivatsan, S. G.; Tor, Y., Fluorescent pyrimidine ribonucleotide: synthesis, enzymatic incorporation, and utilization. *J Am Chem Soc*, **2007**, 129(7), 2044-2053.

41. Yamakoshi, H.; Dodo, K.; Palonpon, A.; Ando, J.; Fujita, K.; Kawata, S.; Sodeoka, M., Alkyne-tag Raman imaging for visualization of mobile small molecules in live cells. *J Am Chem Soc*, **2012**, 134(51), 20681-20689.

42. Herdewijn, P., Modified Nucleosides, in: Biochemistry Biotechnology and Medicine, **2008**, Wiley-VCH: Weinheim.

43. Zhang, Y.; Yue, X.; Kim, B.; Yao, S.; Belfield, K. D., Deoxyribonucleoside-modified squaraines as near-IR viscosity sensors. *Chemistry*, **2014**, 20(24), 7249-7253.

44. Teo, Y. N.; Kool, E. T., DNA-multichromophore systems. *Chem Rev*, **2012**, 112(7), 4221-4245.

45. Kovacs, A. J., Applicability of the Free Volume Concept on Relaxation Phenomena in the Glass Transition Range. *Rheologica Aeta*, **1966**, 5(4), 262-269.

46. Förester, T., Hoffmann, G. Z. , The viscosity dependence of fluorescence quantum yields of some dye systems. *Phys. Chem.*, **1971**, 75, 63.

47. Lakowicz, J. R., *Principles of Fluorescence Spectroscopy*. **1999**, New York: Kluwer.

48. O'Connor, D. V. P., D., *Time-Correlated Single-Photon Counting*. **1984**, London: Academic Press.

49. Becker, W., *AdVanced Time-Correlated Single Photon Counting Techniques*. **2005**, Berlin: Springer.

50. Valeur, B., *Molecular Fluorescence*. **2002**, Weinheim: Wiley-VCH.

51. Levitt, J. A.; Chung, P. H.; Kuimova, M. K.; Yahioglu, G.; Wang, Y.; Qu, J.; Suhling, K., Fluorescence anisotropy of molecular rotors. *Chemphyschem*, **2011**, 12(3), 662-672.

52. Maczek, C.; Bock, G.; Jurgens, G.; Schonitzer, D.; Dietrich, H.; Wick, G., Environmental influence on age-related changes of human lymphocyte membrane viscosity using severe combined immunodeficiency mice as an in vivo model. *Experimental Gerontology*, **1998**, 33(5), 485-498.

53. Shiraishi, K.; Matsuzaki, S.; Ishida, H.; Nakazawa, H., Impaired Erythrocyte Deformability and Membrane Fluidity in Alcoholic Liver-Disease - Participation in Disturbed Hepatic Microcirculation. *Alcohol and Alcoholism*, **1993**, 28, 59-64.

54. Zubenko, G. S.; Kopp, U.; Seto, T.; Firestone, L. L., Platelet membrane fluidity individuals at risk for Alzheimer's disease: a comparison of results from fluorescence spectroscopy and electron spin resonance spectroscopy. *Psychopharmacology*, **1999**, 145(2), 175-180.

55. Osterode, W.; Holler, C.; Ulberth, F., Nutritional antioxidants, red cell membrane fluidity and blood viscosity in Type 1 (insulin dependent) diabetes mellitus. *Diabetic Medicine*, **1996**, 13(12), 1044-1050.

56. Nadiv, O.; Shinitzky, M.; Manu, H.; Hecht, D.; Roberts, C. T.; Leroith, D.; Zick, Y., Elevated Protein-Tyrosine-Phosphatase Activity and Increased Membrane Viscosity Are Associated with Impaired Activation of the Insulin-Receptor Kinase in Old Rats. *Biochemical Journal*, **1994**, 298, 443-450.

57. Levitt, J. A.; Kuimova, M. K.; Yahioglu, G.; Chung, P. H.; Suhling, K.; Phillips, D., Membrane-Bound Molecular Rotors Measure Viscosity in Live Cells via Fluorescence Lifetime Imaging. *Journal of Physical Chemistry C*, **2009**, 113(27), 11634-11642.

58. Haidekker, M. A.; L'Heureux, N.; Frangos, J. A., Fluid shear stress increases membrane fluidity in endothelial cells: a study with DCVJ fluorescence. *American Journal of Physiology-Heart and Circulatory Physiology*, **2000**, 278(4), H1401-H1406.

59. Morales, A. R.; Yanez, C. O.; Zhang, Y. W.; Wang, X. H.; Biswas, S.; Urakami, T.; Komatsu, M.; Belfield, K. D., Small molecule fluorophore and copolymer RGD peptide conjugates for ex vivo two-photon fluorescence tumor vasculature imaging. *Biomaterials*, **2012**, 33(33), 8477-8485.

60. Clapham, D. E., Calcium signaling. *Cell*, **1995**, 80(2), 259-268.

61. Berridge, M. J.; Lipp, P.; Bootman, M. D., The versatility and universality of calcium signalling. *Nat Rev Mol Cell Biol*, **2000**, 1(1), 11-21.

62. Tsien, R. Y., New Calcium Indicators and Buffers with High Selectivity against Magnesium and Protons - Design, Synthesis, and Properties of Prototype Structures. *Biochemistry*, **1980**, 19(11), 2396-2404.

63. Grynkiewicz, G.; Poenie, M.; Tsien, R. Y., A new generation of Ca2+ indicators with greatly improved fluorescence properties. *J Biol Chem*, **1985**, 260(6), 3440-3450.

64. Lakowicz, J. R.; Szmacinski, H.; Nowaczyk, K.; Johnson, M. L., Fluorescence lifetime imaging of calcium using Quin-2. *Cell Calcium*, **1992**, 13(3), 131-147.

65. Becker, P. L.; Fay, F. S., Photobleaching of fura-2 and its effect on determination of calcium concentrations. *Am J Physiol*, **1987**, 253(4 Pt 1), C613-618.

66. Scanlon, M.; Williams, D. A.; Fay, F. S., A Ca2+-insensitive form of fura-2 associated with polymorphonuclear leukocytes. Assessment and accurate Ca2+ measurement. *J Biol Chem*, **1987**, 262(13), 6308-6312.

67. Patterson, G. H.; Piston, D. W., Photobleaching in two-photon excitation microscopy. *Biophys J*, **2000**, 78(4), 2159-2162.

68. Helmchen, F.; Denk, W., Deep tissue two-photon microscopy. *Nat Methods*, **2005**, 2(12), 932-940.

69. Roussakis, E.; Liepouri, F.; Nifli, A. P.; Castanas, E.; Deligeorgiev, T. G.; Katerinopoulos, H. E., ICPBC and C12-ICPBC: two new red emitting, fluorescent Ca2+ indicators excited with visible light. *Cell Calcium*, **2006**, 39(1), 3-11.

70. Ozmen, B., Akkaya, E. U., Infrared Fluorescence Sensing of Submicromolar Calcium: Pushing the Limits of Photoinduced Electron Transfer. *Tetrahedron Lett.*, **2000**, 41, 9185-9188.

71. Akkaya, E. U.; Turkyilmaz, S., A squaraine-based near IR fluorescent chemosensor for calcium. *Tetrahedron Letters*, **1997**, 38(25), 4513-4516.

72. Zhu, B. C.; Jia, H. Y.; Zhang, X. L.; Chen, Y.; Liu, H. P.; Tan, W. H., Engineering a subcellular targetable, red-emitting, and ratiometric fluorescent probe for Ca2+ and its bioimaging applications. *Analytical and Bioanalytical Chemistry*, **2010**, 397(3), 1245-1250.

73. Karolin, J.; Johansson, L. B. A.; Strandberg, L.; Ny, T., Fluorescence and Absorption Spectroscopic Properties of Dipyrrometheneboron Difluoride (Bodipy) Derivatives in Liquids, Lipid-Membranes, and Proteins. *Journal of the American Chemical Society*, **1994**, 116(17), 7801-7806.

74. Wittmershaus, B. P.; Skibicki, J. J.; McLafferty, J. B.; Zhang, Y. Z.; Swan, S., Spectral properties of single BODIPY dyes in polystyrene microspheres and in solutions. *Journal of Fluorescence*, **2001**, 11(2), 119-128.

75. Boens, N.; Leen, V.; Dehaen, W., Fluorescent indicators based on BODIPY. *Chemical Society Reviews*, **2012**, 41(3), 1130-1172.

76. Basaric, N.; Baruah, M.; Qin, W. W.; Metten, B.; Smet, M.; Dehaen, W.; Boens, N., Synthesis and spectroscopic characterisation of BODIPY (R) based fluorescent off-on indicators with low affinity for calcium. *Organic & Biomolecular Chemistry*, **2005**, 3(15), 2755-2761.

77. Kim, H. J.; Kim, J. S., BODIPY appended cone-calix[4]arene: selective fluorescence changes upon Ca2+ binding. *Tetrahedron Letters*, **2006**, 47(39), 7051-7055.

78. Gee, K. R.; Rukavishnikov, A.; Rothe, A., New Ca2+ fluoroionophores based on the BODIPY fluorophore. *Combinatorial Chemistry & High Throughput Screening*, **2003**, 6(4), 363-366.

79. Kamiya, M.; Johnsson, K., Localizable and Highly Sensitive Calcium Indicator Based on a BODIPY Fluorophore. *Analytical Chemistry*, **2010**, 82(15), 6472-6479.

80. Matsui, A.; Umezawa, K.; Shindo, Y.; Fujii, T.; Citterio, D.; Oka, K.; Suzuki, K., A near-infrared fluorescent calcium probe: a new tool for intracellular multicolour Ca2+ imaging. *Chemical Communications*, **2011**, 47(37), 10407-10409.

81. Zhu, B.; Jia, H.; Zhang, X.; Chen, Y.; Liu, H.; Tan, W., Engineering a subcellular targetable, red-emitting, and ratiometric fluorescent probe for Ca2+ and its bioimaging applications. *Anal Bioanal Chem*, **2010**, 397(3), 1245-1250.

82. Palao, E.; Agarrabeitia, A. R.; Banuelos-Prieto, J.; Lopez, T. A.; Lopez-Arbeloa, I.; Armesto, D.; Ortiz, M. J., 8-Functionalization of alkyl-substituted-3,8-dimethyl BODIPYs by Knoevenagel condensation. *Org Lett*, **2013**, 15(17), 4454-4457.

83. Grynkiewicz, G., Poenie, M., Tsien, R. Y., A New Generation of Ca2+ Indicators with Greatly Improved Fluorescence Properties. *J Bio Chem*, **1986**, 260(6), 3440-3450.

84. Kollmannsberger, M.; Gareis, T.; Heinl, S.; Breu, J.; Daub, J., Electrogenerated chemiluminescence and proton-dependent switching of fluorescence: Functionalized difluoroboradiaza-s-indacenes. *Angewandte Chemie-International Edition in English*, **1997**, 36(12), 1333-1335.

85. Gabe, Y.; Urano, Y.; Kikuchi, K.; Kojima, H.; Nagano, T., Highly sensitive fluorescence probes for nitric oxide based on boron dipyrromethene chromophore-rational design of

potentially useful bioimaging fluorescence probe. *Journal of the American Chemical Society*, **2004**, 126(10), 3357-3367.

86. Cielen, E.; Tahri, A.; Heyen, K. V.; Hoornaert, G. J.; De Schryver, F. C.; Boens, N., Synthesis and spectroscopic characterisation of fluorescent indicators for Na+ and K+. *Journal of the Chemical Society-Perkin Transactions 2*, **1998**(7), 1573-1580.

87. Connors, K. A., *Binding Constants. The Measurement of Molecular Complex Stability*. **1987**, New York: J. Wiley & Sons.

88. Tribs, A., Jacob, K., Cyclotrimethine Dyes Derived from Squaric Acid. *Angew. Chem. Int. Ed. Engl.*, **1965**, 4, 694.

89. Schmidt, H. A., Reaktionen von Quadratsäure und Quadratsäure-Derivaten. *Synthesis*, **1980**, 12, 961-994.

90. Chen, H. J.; Farahat, M. S.; Law, K. Y.; Whitten, D. G., Aggregation of surfactant squaraine dyes in aqueous solution and microheterogeneous media: Correlation of aggregation behavior with molecular structure. *Journal of the American Chemical Society*, **1996**, 118(11), 2584-2594.

91. Liang, K. N.; Farahat, M. S.; Perlstein, J.; Law, K. Y.; Whitten, D. G., Exciton interactions in nonconjugated squaraine dimers. Mechanisms for coupling and consequences for photophysics and photochemistry. *Journal of the American Chemical Society*, **1997**, 119(4), 830-831.

92. Law, K. Y., Squaraine Chemistry - Design, Synthesis, and Xerographic Properties of a Highly Sensitive Unsymmetrical Fluorinated Squaraine. *Chemistry of Materials*, **1992**, 4(3), 605-611.

93. Gassensmith, J. J.; Arunkumar, E.; Barr, L.; Baumes, J. M.; DiVittorio, K. M.; Johnson, J. R.; Noll, B. C.; Smith, B. D., Self-assembly of fluorescent inclusion complexes in competitive media including the interior of living cells. *Journal of the American Chemical Society*, **2007**, 129(48), 15054-15059.

94. Wang, W. H.; Fu, A.; Lan, J. B.; Gao, G.; You, J. S.; Chen, L. J., Rational Design of Fluorescent Bioimaging Probes by Controlling the Aggregation Behavior of Squaraines: A Special Effect of Ionic Liquid Pendants. *Chemistry-a European Journal*, **2010**, 16(17), 5129-5137.

95. Sreejith, S.; Ma, X.; Zhao, Y. L., Graphene Oxide Wrapping on Squaraine-Loaded Mesoporous Silica Nanoparticles for Bioimaging. *Journal of the American Chemical Society*, **2012**, 134(42), 17346-17349.

96. Beverina, L.; Crippa, M.; Landenna, M.; Ruffo, R.; Salice, P.; Silvestri, F.; Versari, S.; Villa, A.; Ciaffoni, L.; Collini, E.; Ferrante, C.; Bradamante, S.; Mari, C. M.; Bozio, R.; Pagani, G. A., Assessment of water-soluble pi-extended squaraines as one- and two-photon singlet oxygen photosensitizers: Design, synthesis, and characterization. *Journal of the American Chemical Society*, **2008**, 130(6), 1894-1902.

97. Oushiki, D.; Kojima, H.; Takahashi, Y.; Komatsu, T.; Terai, T.; Hanaoka, K.; Nishikawa, M.; Takakura, Y.; Nagano, T., Near-Infrared Fluorescence Probes for Enzymes Based on Binding Affinity Modulation of Squarylium Dye Scaffold. *Analytical Chemistry*, **2012**, 84(10), 4404-4410.

98. Xu, Y. Q.; Liu, Q.; Li, X. P.; Wesdemiotis, C.; Pang, Y., A zwitterionic squaraine dye with a large Stokes shift for in vivo and site-selective protein sensing. *Chemical Communications*, **2012**, 48(92), 11313-11315.

99. Ahn, H. Y.; Yao, S.; Wang, X.; Belfield, K. D., Near-Infrared-Emitting Squaraine Dyes with High 2PA Cross-Sections for Multiphoton Fluorescence Imaging. *Acs Applied Materials & Interfaces*, **2012**, 4(6), 2847-2854.

100. Johnson, J. R.; Fu, N.; Arunkumar, E.; Leevy, W. M.; Gammon, S. T.; Piwnica-Worms, D.; Smith, B. D., Squaraine rotaxanes: Superior substitutes for Cy-5 in molecular probes for near-infrared fluorescence cell imaging. *Angewandte Chemie-International Edition*, **2007**, 46(29), 5528-5531.

101. Thomas, J.; Sherman, D. B.; Amiss, T. J.; Andaluz, S. A.; Pitner, J. B., Synthesis and biosensor performance of a Near-IR thiol-reactive fluorophore based on benzothiazolium squaraine. *Bioconjugate Chemistry*, **2007**, 18(6), 1841-1846.

102. Oswald, B.; Patsenker, L.; Duschl, J.; Szmacinski, H.; Wolfbeis, O. S.; Terpetschnig, E., Synthesis, spectral properties, and detection limits of reactive squaraine dyes, a new class of diode laser compatible fluorescent protein labels. *Bioconjugate Chemistry*, **1999**, 10(6), 925-931.

103. Patonay, G.; Salon, J.; Sowell, J.; Strekowski, L., Noncovalent labeling of biomolecules with red and near-infrared dyes. *Molecules*, **2004**, 9(3), 40-49.

104. Ioffe, V. M.; Gorbenko, G. P.; Domanov, Y. A.; Tatarets, A. L.; Patsenker, L. D.; Terpetsching, E. A.; Dyubko, T. S., A new fluorescent squaraine probe for the measurement of membrane polarity. *Journal of Fluorescence*, **2006**, 16(1), 47-52.

105. Reddington, M. V., Synthesis and properties of phosphonic acid containing cyanine and squaraine dyes for use as fluorescent labels. *Bioconjugate Chemistry*, **2007**, 18(6), 2178-2190.

106. Jisha, V. S.; Arun, K. T.; Hariharan, M.; Ramaiah, D., Site-selective binding and dual mode recognition of serum albumin by a squaraine dye. *Journal of the American Chemical Society*, **2006**, 128(18), 6024-6025.

107. Ramaiah, D.; Eckert, I.; Arun, K. T.; Weidenfeller, L.; Epe, B., Squaraine dyes for photodynamic therapy: Study of their cytotoxicity and genotoxicity in bacteria and mammalian cells. *Photochemistry and Photobiology*, **2002**, 76(6), 672-677.

108. Snee, P. T.; Somers, R. C.; Nair, G.; Zimmer, J. P.; Bawendi, M. G.; Nocera, D. G., A ratiometric CdSe/ZnS nanocrystal pH sensor. *Journal of the American Chemical Society*, **2006**, 128(41), 13320-13321.

109. Morel, D. L., Stogryn, E. L., Ghosh, A. K.; Feng, T., Purwin, P. E., Shaw, R. F., Fishman, C., Bird, G. R., Piechowski, A. P., Organic Photovoltaic Cells. Correlation Between Cell Performance and Molecular Structure. *J. Phys. Chem.*, **1984**, 88, 923-933.

110. Alex, S.; Santhosh, U.; Das, S., Dye sensitization of nanocrystalline TiO2: enhanced efficiency of unsymmetrical versus symmetrical squaraine dyes. *Journal of Photochemistry and Photobiology a-Chemistry*, **2005**, 172(1), 63-71.

111. Odom, S. A.; Webster, S.; Padilha, L. A.; Peceli, D.; Hu, H.; Nootz, G.; Chung, S. J.; Ohira, S.; Matichak, J. D.; Przhonska, O. V.; Kachkovski, A. D.; Barlow, S.; Bredas, J. L.; Anderson, H. L.; Hagan, D. J.; Van Stryland, E. W.; Marder, S. R., Synthesis and Two-

Photon Spectrum of a Bis(Porphyrin)-Substituted Squaraine. *Journal of the American Chemical Society*, **2009**, 131(22), 7510-+.

112. Chen, C. T.; Marder, S. R.; Cheng, L. T., Syntheses and Linear and Nonlinear-Optical Properties of Unsymmetrical Squaraines with Extended Conjugation. *Journal of the American Chemical Society*, **1994**, 116(7), 3117-3118.

113. Wallace, K. J.; Gray, M.; Zhong, Z. L.; Lynch, V. M.; Anslyn, E. V., An artificial siderophore for the detection of iron(III). *Dalton Transactions*, **2005**(14), 2436-2441.

114. Wang, W. D.; Fu, A.; You, J. S.; Gao, G.; Lan, J. B.; Chen, L. J., Squaraine-based colorimetric and fluorescent sensors for Cu2+-specific detection and fluorescence imaging in living cells. *Tetrahedron*, **2010**, 66(21), 3695-3701.

115. Shafeekh, K. M.; Rahim, M. K. A.; Basheer, M. C.; Suresh, C. H.; Das, S., Highly selective and sensitive colourimetric detection of Hg2+ ions by unsymmetrical squaraine dyes. *Dyes and Pigments*, **2013**, 96(3), 714-721.

116. Stoll, R. S.; Severin, N.; Rabe, J. P.; Hecht, S., Synthesis of a novel chiral squaraine dye and its unique aggregation behavior in solution and in self-assembled monolayers. *Advanced Materials*, **2006**, 18(10), 1271-1275.

117. Ajayaghosh, A.; Chithra, P.; Varghese, R.; Divya, K. P., Controlled self-assembly of squaraines to 1D supramolecular architectures with high molar absorptivity. *Chemical Communications*, **2008**(8), 969-971.

118. Chen, H. J.; Herkstroeter, W. G.; Perlstein, J.; Law, K. Y.; Whitten, D. G., Aggregation of a Surfactant Squaraine in Langmuir-Blodgett-Films, Solids, and Solution. *Journal of Physical Chemistry*, **1994**, 98(19), 5138-5146.

119. Chen, H. J.; Law, K. Y.; Whitten, D. G., Aggregation of amphiphilic squaraines at the air-water interface and in Langmuir-Blodgett films. *Journal of Physical Chemistry*, **1996**, 100(14), 5949-5955.

120. Liang, K. N.; Law, K. Y.; Whitten, D. G., Multiple Aggregation of Surfactant Squaraines in Langmuir-Blodgett-Films and in Dmso Water Mixtures. *Journal of Physical Chemistry*, **1994**, 98(50), 13379-13384.

121. Dimitriev, O. P.; Dimitriyeva, A. P.; Tolmachev, A. I.; Kurdyukov, V. V., Solvent-induced organization of squaraine dyes in solution capillary layers and adsorbed films. *Journal of Physical Chemistry B*, **2005**, 109(10), 4561-4567.

122. Block, M. A. B.; Khan, A.; Hecht, S., Avenues into the synthesis of illusive poly(m-phenylene-alt-squaraine)s: Polycondensation of m-phenylenediamines with squaric acid intercepted by intermediate semisquaraines of exceptionally low reactivity. *Journal of Organic Chemistry*, **2004**, 69(1), 184-187.

123. Ohno, M.; Yamamoto, Y.; Shirasaki, Y.; Eguchi, S., Synthesis of Squaric Acid-Derivatives by Lewis Acid-Catalyzed Reaction of Its Dichloride, Methyl-Ester Chloride, Diethylamide Chloride, and Ethyl Diester with Unsaturated Organosilanes - New Method for C-C Bond Formation on Cyclobutenedione. *Journal of the Chemical Society-Perkin Transactions 1*, **1993**(2), 263-271.

124. Lunelli, B., New, optimized preparation of 1,2-dichlorocyclobuten-3,4-dione (C4O2Cl2) from squaric acid and oxalyl chloride. *Tetrahedron Letters*, **2007**, 48(20), 3595-3597.

125. Keil, D.; Hartmann, H., Synthesis and characterization of a new class of unsymmetrical squaraine dyes. *Dyes and Pigments*, **2001**, 49(3), 161-179.

126. Sreejith, S.; Carol, P.; Chithra, P.; Ajayaghosh, A., Squaraine dyes: a mine of molecular materials. *Journal of Materials Chemistry*, **2008**, 18(3), 264-274.

127. He, Y.; Zhou, W. H.; Wu, F. P.; Li, M. Z.; Wang, E. J., Photoreaction and photopolymerization studies on squaraine dyes/iodonium salts combination. *Journal of Photochemistry and Photobiology a-Chemistry*, **2004**, 162(2-3), 463-471.

128. McEwen, J. J.; Wallace, K. J., Squaraine dyes in molecular recognition and self-assembly. *Chemical Communications*, **2009**(42), 6339-6351.

129. Scherer, D.; Dorfler, R.; Feldner, A.; Vogtmann, T.; Schwoerer, M.; Lawrentz, U.; Grahn, W.; Lambert, C., Two-photon states in squaraine monomers and oligomers. *Chemical Physics*, **2002**, 279(2-3), 179-207.

130. Chung, S. J.; Zheng, S. J.; Odani, T.; Beverina, L.; Fu, J.; Padilha, L. A.; Biesso, A.; Hales, J. M.; Zhan, X. W.; Schmidt, K.; Ye, A. J.; Zojer, E.; Barlow, S.; Hagan, D. J.; Van Stryland, E. W.; Yi, Y. P.; Shuai, Z. G.; Pagani, G. A.; Bredas, J. L.; Perry, J. W.; Marder, S. R., Extended squaraine dyes with large two-photon absorption cross-sections. *Journal of the American Chemical Society*, **2006**, 128(45), 14444-14445.

131. Tokar, V. P.; Losytskyy, Y.; Kovalska, V. B.; Kryvorotenko, D. V.; Balanda, A. O.; Prokopets, V. M.; Galak, M. P.; Dmytruk, I. M.; Yashchuk, V. M.; Yarmoluk, S. M., Fluorescence of styryl dyes-DNA complexes induced by single- and two-photon excitation. *Journal of Fluorescence*, **2006**, 16(6), 783-791.

132. Kim, S.; Mor, G. K.; Paulose, M.; Varghese, O. K.; Baik, C.; Grimes, C. A., Molecular Design of Near-IR Harvesting Unsymmetrical Squaraine Dyes. *Langmuir*, **2010**, 26(16), 13486-13492.

133. Das, S.; Thomas, K. G.; Ramanathan, R.; George, M. V.; Kamat, P. V., Photochemistry of Squaraine Dyes .6. Solvent Hydrogen-Bonding Effects on the Photophysical Properties of Bis(Benzothiazolylidene)Squaraines. *Journal of Physical Chemistry*, **1993**, 97(51), 13625-13628.

134. Mills, W. H., Cyanine dyes. IV. Cyanine dyes of the benzothiazole series. *J. Chem. Soc.* , **1922**, 121, 455-466.